NOAA Technical Memorandum ERL PMEL-100

TSUNAMI INUNDATION MODELING WORKSHOP REPORT (NOVEMBER 16-18, 1993)

Eddie N. Bernard
Frank I. Gonzalez

Pacific Marine Environmental Laboratory
Seattle, Washington
January 1994

noaa NATIONAL OCEANIC AND ATMOSPHERIC ADMINISTRATION / Environmental Research Laboratories

NOAA Technical Memorandum ERL PMEL-100

TSUNAMI INUNDATION MODELING WORKSHOP REPORT (NOVEMBER 16-18, 1993)

Eddie N. Bernard
Frank I. Gonzalez

Pacific Marine Environmental Laboratory
Seattle, Washington
January 1994

UNITED STATES DEPARTMENT OF COMMERCE

Ronald H. Brown
Secretary

NATIONAL OCEANIC AND ATMOSPHERIC ADMINISTRATION

D. James Baker
Under Secretary for Oceans and Atmosphere/Administrator

Environmental Research Laboratories

Alan R. Thomas
Director

NOTICE

Mention of a commercial company or product does not constitute an endorsement by NOAA/ERL. Use of information from this publication concerning proprietary products or the tests of such products for publicity or advertising purposes is not authorized.

Contribution No. 1511 from NOAA/Pacific Marine Environmental Laboratory

For sale by the National Technical Information Service, 5285 Port Royal Road
Springfield, VA 22161

CONTENTS

Tsunami Inundation Modeling Workshop Report (November 16–18, 1993)

Eddie N. Bernard and Frank I. Gonzalez

Executive Summary

The discussions during the Tsunami Inundation Modeling Workshop led to the conclusion that the modeling technology exists to produce tsunami inundation maps for emergency preparedness. With this foundation, the members of the Workshop agreed to the following recommendations:

1. A NOAA tsunami mapping/research unit should be established as soon as possible and should be guided by a state users steering group.
2. Tsunami inundation maps and other products of the NOAA mapping/research unit should be used expressly for disaster preparedness and response (i.e., to develop evacuation plans).
3. Products of the NOAA mapping/research unit should include
   a. Inundation maps for distantly and locally generated tsunamis (e.g., for U.S. west coast, likely distant scenario would be an Alaskan earthquake, whereas the local scenario would be a tsunami generated along the Cascadia Subduction Zone). Such maps would (1) be based on "design earthquakes," developed by consensus among experts; (2) include the maximum extent of flooding that could be expected; (3) use historical data, where possible, including inundation measurements and tide gauge data; (4) be at a scale of 1:24,000 (USGS 7.5-min quadrangle maps) or larger; and (5) be archived in a digital/GIS format.
   b. Other important tsunami effects, including maximum currents, maximum drawdown (representing the trough of the tsunami wave), and model animation (video simulation of tsunami runup and inundation).
4. Systematic production of tsunami inundation maps should include the following steps:
   Step 1: site identification/priorities
   Step 2: map scale identification
   Step 3: collection of existing and additional bathymetry and topography of site
   Step 4: development of earthquake scenarios for local and distant tsunamis
   Step 5: formulation and examination of relevant historical tsunami case studies
   Step 6: selection and application of a tsunami inundation model, using steps 4 and 5 to guide specification of input

Step 7: evaluation of accuracy and utility of maps and other products through monitoring future tsunamis

Step 8: periodic review, updating maps, and improvement of the other products

In order to produce these products, the following technical recommendations should be implemented:

- Conduct a stringent comparative study of existing two-dimensional inundation models.
- Choose and appropriately instrument a site to collect data for testing and improving inundation models.
- Define and develop the bathymetric/topographic data base essential to the productive use of inundation models.
- Construct and validate current velocity maps for use in harbors and inundation zones.

I. Introduction

NOAA/PMEL organized this Workshop as part of its efforts to establish an improved tsunami hazard reduction program. Goals are to (1) develop model-based tsunami inundation maps for at-risk communities, (2) improve the tsunami detection/warning system, and (3) conduct research to improve tsunami modeling and data collection (see *Protecting the People, A Tsunami Hazard Reduction Program for the United States* in Appendix A). This Workshop focused on the inundation mapping process including

- presentation/discussion of user needs and desired products
- presentation of five tsunami inundation mapping models, their capabilities and limitations, and sample applications of these models
- development of recommendations by modelers and product users

Twenty-one people participated in the Workshop, including nine emergency specialists (see Appendix B for complete list). The Workshop followed the agenda listed in Appendix C. The first day was spent in learning why inundation maps are important to the users, learning about five existing models that can provide these maps, and learning about specific applications of these models to produce the maps. On the second day, the participants divided into two groups to discuss (1) technical modeling and (2) policy that should guide map production. Each group spent 4 hours discussing the issues and formulating recommendations. These recommendations were presented to the entire group at the end of the second day. On the third day, the whole group discussed these recommendations and modified them into a set of Workshop recommendations. The Workshop was closed by a presentation on the creation of two inundation maps for northern California under the assumption that a Cascadia Subduction Zone earthquake would produce a tsunami. In this report, we will summarize the discussions and describe how the recommendations were formulated.

II. Model Descriptions and Applications

Five models were presented along with an application to a specific site:

A. George Curtis presented the one-dimensional model developed at the University of Hawaii for the inundation/evacuation map project for the State of Hawaii. This project was completed in 1991 and covers about 46 percent of the coastlines. Evacuation maps derived from this model are published in the telephone directory of each island. Details of the model and application are found in Appendix D. This model was verified by Hawaiian Island runup data. One problem identified by Brian Yanagi of Hawaii State Civil Defense is that no monies are available to update the current maps or to expand the coverage.

B. Dennis Moore presented the Mader two-dimensional model developed at the University of Hawaii with some NOAA finanical support. Moore showed application of this model to Hilo, Hawaii, for a 100-m and 10-m grid. Dr. Mader was absent due to medical reasons. Details of the Mader model are found in Appendixes E and F with application to Hilo Bay. This model was verified by comparison with runup data from Hilo, Hawaii, and the Look Laboratory physical model for Hilo.

C. Phil Liu presented the Shuto/Liu two-dimensional model, which uses a different numerical scheme than Mader's model. Details of the model are described in Appendix G with application to Hilo, Hawaii, described in Appendix H. Liu also showed the comparisons between model and analytical solutions. Liu used the Mader 100-m grid to calculate inundation for Hilo, Hawaii, and compared the results with the runup data from the 1960 tsunami that flooded Hilo. An early comparison of the two models showed reasonable results. The differences are attributed to the input wave.

D. Zygmunt Kowalik presented his two-dimensional model with application to Alberni Inlet, British Columbia, Canada. The application of this model was verified with both runup data and time-series data from a tide gauge operating in 1964. Details of the model, verification, and application are found in Appendix I.

E. Vasily Titov described a new, two-dimensional model under development at the University of Southern California. He presented applications to the Nicaragua, Indonesia, and Sea of Japan tsunamis. The details of the model and its application are found in Appendix J.

III. Recommendations from the Technical Modeling Group

1. Background

Descriptions and applications of five inundation models were presented on November 16 and the morning of November 17. Table 1 summarizes some of the characteristics of these models; more detail is provided in the appendixes. The model presentations were followed by a 4-hour meeting of a modeling group composed of George Carrier, Frank González (discussion leader), Zygmunt Kowalik, Philip Liu, William Mass, Dennis Moore, and Vasily Titov. This meeting identified a number of important inundation modeling issues, although time limitations

made a thorough discussion of these issues impossible. The group did, however, reach agreement on six individual recommendations that were then presented to the full Workshop assembly. Subsequently, during open discussion by all Workshop participants on November 18, the six original recommendations were reduced to four; two of the six were consolidated into one, and a third was eliminated on the grounds that it was too general. This short summary report presents the recommendations and briefly discusses some of the more significant issues that arose during the meeting. These issues were identified by the group as being very important considerations in establishing an appropriate context for the recommendations.

2. Recommendations

1. Conduct a stringent, comparative study of existing, two-dimensional inundation models.
2. Choose and appropriately instrument a site to collect data for testing and improving inundation models.
3. Define and develop the bathymetric/topographic data base essential to the productive use of inundation models.
4. Construct and validate current velocity maps for use in harbors and inundation zones.

3. Discussion

At the start of the meeting, an initial question was posed: "Can the two-dimensional models provide better inundation estimates than the one-dimensional engineering model used by George Curtis to provide inundation maps for Hawaii?" After some discussion, all agreed that two-dimensional models should provide more accurate estimates. It was noted that the one-dimensional approach, while very useful, was somewhat subjective, and the results depended to a great extent on the skill, experience, and judgment of the user. Furthermore, the one-dimensional approach cannot provide estimates of current velocities, which are an important aspect of the tsunami hazard.

A second question was then posed: "Of the two-dimensional models described in the earlier presentations, could one model be recommended by this group for immediate implementation to produce operational inundation maps?" Most present felt this was not possible because no one in the group felt familiar enough with all of the models to competently make such a recommendation. This led directly to the recommendation for a comparative model study (recommendation 1).

Several approaches to conducting a model comparison were mentioned and briefly discussed. Possible procedural variations included the types of test cases that might be used and the issue of who should actually run each model. One major obstacle to comparing models was acknowledged—the lack of field observations for comparison. It was suggested that laboratory data should also be considered as test data for inundation models. However, actual field

observations would be most valuable, and this led to the recommendation to concentrate instrumentation at a selected site to gather such measurements (recommendation 2).

Instrumentation and siting strategy was not discussed in detail, but it was agreed that measurements of both sea level and currents were needed in locations representing at least three regions of the inundation model domain: outer boundaries, interior ocean grid points, and grid points on land. Hilo was generally acknowledged to be a good candidate site for such an effort. This site is characterized by a good quality historical inundation data base and a midocean location, which increases the likelihood of an incident tsunami wave from most potential source areas around the Pacific Rim. During the full Workshop discussion of this recommendation, it was also pointed out that instrument sensitivity and the ratio of signal-to-background-noise level were important issues; for tsunamis with amplitudes on the order of centimeters, these factors may limit the successful measurement of amplitude and currents.

Good-quality bathymetric and topographic data are essential for accurate inundation model results. A systematic effort to define and address this chronic need was recommended (recommendation 3). This effort should include the following activities: establish realistic requirements, based in part on accuracy goals and sensitivity studies; develop an inventory of data available from Federal and state agencies; and identify high-priority regions and communities with inadequate data to support modeling efforts. It was also pointed out that data requirements may be consistent with existing bathymetric measurement capabilities, i.e., the required accuracy and density of coverage may not be as stringent in the deep ocean as in the nearshore region.

A third question was then posed: "Given a 'perfect' inundation model, exactly what model-derived products would be most useful to community officials responsible for hazard mitigation?" This recognized the need to move beyond the traditional notion of a "tsunami inundation map" to that of a more general "tsunami hazards map" that might include current information or take into account such complicating factors as resonance or interactions with tides and other background sea level phenomena. This question led to two separate recommendations regarding the production and validation of current velocity maps, which were later consolidated in the full Workshop dicussion (recommendation 4). A particular issue of concern was the basic assumption of vertically uniform water motion inherent in the two-dimensional models. Specific validation techniques for current velocities derived from two-dimensional models were discussed, and these included the use of field data, laboratory data, and three-dimensional models.

A second, more general, recommendation was also made regarding model-derived products: "Develop procedures and criteria for site-specific tsunami hazard maps, possibly using propagation models, and with careful consideration given to resonance phenomena and background sea level." In the full Workshop discussion, this statement was considered too general and was therefore dropped in favor of the more specific recommendation regarding current velocity maps.

Table 1. Inundation Model Characteristics
(Semicolons separate multiple capabilities or options.)

Model (Modeler)	Governing Equations (Coordinate System)	Numerics (Grid)	Friction	Open Boundary	Moving Boundary	Obstacles	Tests / Applications
JTRE Engineering (G. Curtis)	1-D Channel (Cartesian)	Analytic expression (Variable transects)	Manning; DeChezy	Wave amplitude specified	No time dependence	Not included	Hilo; Crescent City; Eureka; most of Hawaii coastline
U. Alaska (Z. Kowalik)	2-D NL SWLW (Cartesian)	FD; Leapfrog; Euler; Arakawa-C (Square; Nested)	Manning; DeChezy	Wave amplitude specified; radiation condition	Extrapolation; Upwind-downwind form of continuity equation (marker and cell method)	Zero normal flow; wier formula	Parabolic basin; sloping beach; Alberni inlet
Cornell/Tohoku (P. Liu)	2-D NL SWLW (Cartesian)	FD Explicit Leapfrog (Square; Interactive nested)	Manning; DeChezy	Wave amplitude specified; radiation condition	Continuity equation extrapolation	Zero normal flow; wier formula	Hilo; Parabolic basin; 1983 Japan Sea; laboratory data
SWAN (C. Mader)	2-D NL SWLW (Cartesian; quasi-spherical)	FD: Wave and depth cell-centered, velocity cell boundary centered (Square; Nested)	DeChezy	Wave amplitude specified; radiation condition	Upwind-downwind form of continuity equation (marker and cell method)	Zero normal flow	Hilo; Crescent City; Eureka
U.S.C. (V. Titov)	2-D NL SWLW (Cartesian)	FD Splitting method (Variable; Square; Interactive nested)	none	Wave amplitude specified; radiation condition	Extrapolation; sliding shoreline algorithm	Zero normal flow	Laboratory data; Nicaragua; Okushiri

Abbreviations:
NL = nonlinear; SWLW = shallow water long wave; FD = finite difference; 1-D = one-dimensional; 2-D = two-dimensional

The four recommendations of the Workshop Modeling Group thus emphasize specific actions aimed at producing a first version of tsunami hazard mitigation products over a relatively short time period of 1 or 2 years. Nonetheless, the group members wish to emphasize that, if site-specific tsunami hazard products derived from inundation models are to be improved, a number of well-defined scientific and engineering issues must be addressed as part of a longer term research effort.

IV. Recommendations from Policy/Users Group

A. A NOAA tsunami mapping unit, as proposed in Appendix A, but modified to include recommendations of this Workshop, should be established as soon as possible.

B. Tsunami inundation maps and other products of the NOAA research/mapping unit should be used expressly for disaster preparedness and response (i.e., to develop evacuation plans)

C. Products of the NOAA research/mapping unit should include:

1. Inundation maps for distant and locally generated tsunamis (e.g., for U.S. west coast, likely distant scenario would be an Alaskan earthquake, whereas the local scenario would be a tsunami generated along the Cascadia Subduction Zone); such maps would
   (a) be based on "design earthquakes," developed by consensus among experts
   (b) include the maximum extent of flooding that could be expected ("maximum extent" will need further clarification; Workshop participants talked about several possible inundation lines for the distant and local scenario, including tsunami inundation from the "maximum capable" and "maximum probable" earthquake)
   (c) use historical data, where possible, including inundation measurements and tide gauges data. Paleotsunami data may be included to identify areas that have experienced past tsunamis.
   (d) be produced at a scale of 1:24,000 (USGS 7.5-min quadrangle sheets) or larger
   (e) be archived in a digital/GIS format
2. Other important tsunami effects, including maximum currents, maximum drawdown (representing the trough of the tsunami wave), and model animation (video simulation of tsunami runup and inundation, followed by drawdown, and so on, for the several wave cycles expected). Note: Additional tsunami information, particularly the drawdown and currents that could be expected, were deemed by users as very useful products for disaster preparedness and response planning, particularly in harbors and for ports and other water-oriented development. Modelers at the Workshop noted that this information could be provided by available two-dimensional tsunami inundation models, but that verification would be problematic because of a lack of historical data.

D. A systematic process for production of tsunami inundation maps should be developed and should include the following:

Step 1: Site identification/priorities (state responsibility, with priorities based on population, property at risk, and other appropriate criteria)

Step 2: Map scale identification (principally a state decision, based on proposed end uses, but constrained by available bathymetric and topographic information, the cost of new data collection, and the capability of the inundation model being employed)

Step 3: Collection of existing and additional bathymetry and topography of site (NOAA, USGS, FEMA, state, local)

Step 4: Development of earthquake scenarios for local and distant tsunamis (local advisory group with NOAA, USGS, FEMA, state participation)

Step 5: Formulate case studies of historic studies or analogs (NOAA research/mapping unit)

Step 6: Select and apply tsunami inundation model, using steps 4 and 5 to specify inputs (NOAA research/mapping unit)

Step 7: Evaluate accuracy and utility of maps and other products through monitoring of future tsunamis (mini-events as well as larger tsunamis) and new knowledge gained through research and model improvement

Step 8: Periodically review and update maps and other products (state and NOAA research/mapping unit)

E. The group felt that the NOAA mapping unit would be well served by a steering panel comprised of representatives from each of the five states affected by tsunamis (Alaska, California, Hawaii, Oregon, Washington). This steering panel would provide policy guidance on the production of maps to ensure some uniformity.

V. Other Issues

A. NOAA currently does not have funding to carry out this program, which represents a significant expansion of its existing tsunami research. The program is supported in principal at NOAA, but the competition for dollars is at issue. There were informal discussions about building "grass roots" support for the effort.

B. Subsequent Workshops are planned on tsunami warning system improvement (possibly in southern California) and tsunami hazard education (possibly in Oregon with Sea Grant/DOGAMI as hosts)

C. There are several components to the tsunami inundation mapping problem:

Source: First, an accurate estimate of tsunami generator at the source (estimates of sea bottom deformation based on seismological data and calculation of "fault-plane solutions"). Note: Such fault-plane estimates, particularly for larger earthquakes,

have greatly underestimated tsunami wave height and runup when compared to actual tsunami measurements (by factors of 3–10, depending on the event). This problem needs to be solved to get accurate initial conditions for tsunami inundation models.

Propagation: Assuming source inputs are accurate, models of propagation are the most reliable part of the tsunami inundation prediction problem.

Tsunami inundation: Bringing the wave into very shallow water and onshore was the subject of this Workshop. Models are improving, but there have been only a few applications. Much more work needs to be done to improve and verify these models and provide additional information such as current velocities.

D. NOAA/PMEL, in collaboration with the State of California, has modeled a northern California M8.4 Cascadia Subduction Zone earthquake-generated tsunami for Humboldt Bay. Using a fault-plane solution to model seafloor deformation, a 2.8-m tsunami was generated. Given empirical evidence that larger tsunamis can be produced by smaller earthquakes (e.g., The M_s-7.8 earthquake on July 12, 1993, in Japan), the incident tsunami wave was increased to 10 m, and the resultant inundation was mapped. This illustrates the problem discussed in C above.

E. The creation and distribution of evacuation maps derived from inundation maps should be coordinated by NOAA, FEMA, and the respective states.

Program Development Plan for Protecting the People

A Tsunami Hazard Reduction Program for the United States

- Tsunami inundation modeling for better preparedness
- Early tsunami detection and measurement for faster, more accurate warnings
- Research to sustain improvements and incorporate new technologies

Pacific Marine Environmental Laboratory/Office of Oceanic and Atmospheric Research
and
National Weather Service Pacific Region
Request to the

National Oceanic and Atmospheric Administration

U.S. Department of Commerce

February 19, 1993

Overview of the Initiative

What is the Problem?

U.S. coastal communities and Federal agencies are unprepared to react to NOAA's tsunami warnings because of inadequate information on the approaching tsunami and its potential impact on the affected community. The problem arises because tsunami inundation studies have not been conducted for more than 90 percent of the Pacific coastal communities **and** because NOAA's tsunami detection network is unable to provide accurate tsunami measurements in a timely manner. This initiative addresses the problems through a comprehensive program of tsunami hazard preparedness and improved tsunami detection to provide faster, more accurate tsunami warnings.

What Actions are Proposed?

First: The creation of a tsunami inundation modeling unit within the National Weather Service. This unit would use the results of the inundation modeling studies funded under the Natural Hazards section of the Coastal Ocean Program to develop inundation maps for the populated areas in the United States most likely to be impacted by tsunamis.

Second: The establishment of a network of ocean bottom pressure sensors in the Gulf of Alaska and the west coast of the United States positioned to detect the passage and measure the magnitude of any tsunamis generated by an earthquake in seismically active areas of the United States.

Third: The formation of a tsunami research project to provide quality control on existing NOAA products and to facilitate the transfer of new technologies into warning operations.

What Will be the Impact on the Problem?

The availability of inundation maps for U.S. cities subject to tsunami will enable emergency management officials to establish effective evacuation plans and thus avoid the costs of overevacuation or the potential loss of life in the case of underevacuation. It will allow Federal agencies to comply with Executive Order 12699 by reducing the tsunami threat to Federal operations. The availability of quantitative data on tsunamis received from the ocean bottom sensors can reduce, by as much as 30 minutes, the time necessary to determine that an earthquake has generated a destructive tsunami. This time saved translates into a 30 percent increase in the time that emergency management officials have to evacuate people from the potential danger zone and prepare for the tsunami's arrival. Conversely, if it is determined that a destructive tsunami has not been generated, unnecessary evacuations with their economic disruptions can be avoided.

Resources Required

The FY-1995 request is for $2,600,000 and 5 FTE.

A Tsunami Hazard Reduction Program for the United States

What is the Challenge?

Coastal communities of the United States are threatened by tsunamis that are generated by both **local** earthquakes and **distant** earthquakes. For local tsunamis, residents have only a few minutes to seek safety. For distant tsunamis, residents have more time to evacuate threatened coastal areas but require timely and accurate assessment of the tsunami to avoid false alarms. Because of the extent of U.S. coastal areas in the Pacific—including Alaska, Hawaii, and the west coast, U.S. residents in Alaska can experience a local tsunami while residents of Hawaii and the west coast experience this disaster as a distant tsunami. **And**, west coast residents can experience a local tsunami that affects Alaska and Hawaii. The challenge is to design a tsunami hazard mitigation program to protect life and property from two very different types of tsunami events.

The present tsunami warning systems, whether operated by the United States, Japan, or the Former Soviet Union, can provide only three of five essential pieces of quantitative information. The systems can (1) advise that a potentially tsunamigenic earthquake has occurred and (2) issue the arrival times of the tsunami for U.S. coastal communities if a tsunami was generated. As time progresses, it can determine (3) whether or not a tsunami has been generated. But, the two quantitative and critical pieces of information the systems cannot now provide are (1) the size of the tsunami and (2) the tsunami's impact when it reaches shore. The challenge is to provide these two missing pieces of information.

What is Being Done Now?

NOAA scientists and coastal managers have developed two tools for dealing with tsunami hazards—inundation maps and warning systems. Inundation maps identify areas that are susceptible to flooding **before** a tsunami occurs and are used to develop evacuation and land-use plans. These maps are derived from numerical models that simulate the behavior of a tsunami to estimate the areas that could be flooded. In the past 2 years, scientists in the United States have made major improvements in this technology (Mader and Curtis, 1991; Liu and Yoon, 1991; Mader et al., 1993). NOAA's Coastal Ocean Program, in partnership with the Office of Oceanic and Atmospheric Research and the National Weather Service, have supported a research project to develop a standardized method for using numerical models to estimate tsunami inundation. The first product from this project was an inundation map for Hilo, Hawaii (see Figure 1).

The second tsunami hazard mitigation tool is a warning system to alert populations that threatened areas must be evacuated. The warnings are delivered through NOAA's Pacific and Alaska Tsunami Warning Centers. The Centers issue warnings for both local and distant tsunamis by locating and sizing earthquakes, computing the tsunami arrival times at various U.S. population centers, determining if a tsunami exists through a network of coastal tide gauges, and deciding on the need to issue a warning.

Instruments now exist that can be used to improve tsunami warnings by providing real-time, deep-ocean tsunami data. NOAA's Pacific Marine Environmental Laboratory (PMEL) recently developed a deep-water pressure sensor capable of detecting a tsunami in the open ocean (Gonzalez et al., 1991; Eble and Gonzalez, 1991). Five sensors are currently

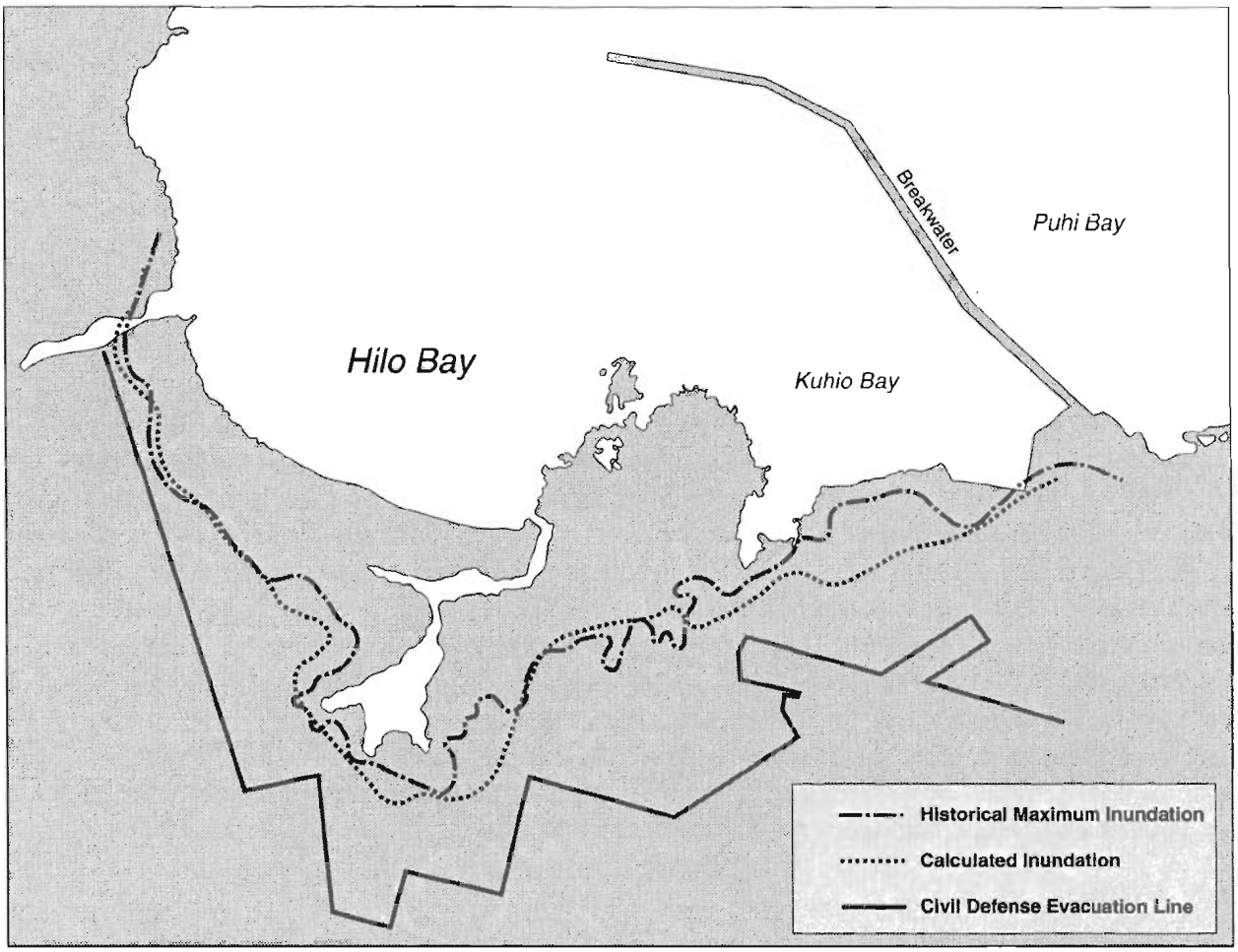

Figure 1. Tsunami inundation map derived from historical data and numerical model simulations. This version converts these data into a public-safety product.

in place in the Gulf of Alaska that record pressure changes at the ocean bottom and are later recovered so the record can be analyzed (Gonzalez, 1990). These data would provide earlier detection of the tsunami—thus increasing the warning lead time **and** providing quantitative information on the tsunami heights, which increases the accuracy of the tsunami impact. A real-time tsunami reporting system design is illustrated in Figure 2.

Why is Further Effort Needed?

Recent research indicates that tsunamis might be generated by large earthquakes in the Cascadia Subduction Zone (CSZ) off the U.S. west coast and at a number of locations along the Alaska and Aleutian Subduction Zone (AASZ). The AASZ has long been recognized as a region with very high seismic potential. Well-respected U.S. seismologists have predicted a major earthquake, greater than 8.0 on the Richter scale, to occur in the Shumagin Gap (Alaska) (Nishenko and Jacob, 1990). When the earthquake occurs, it is expected that

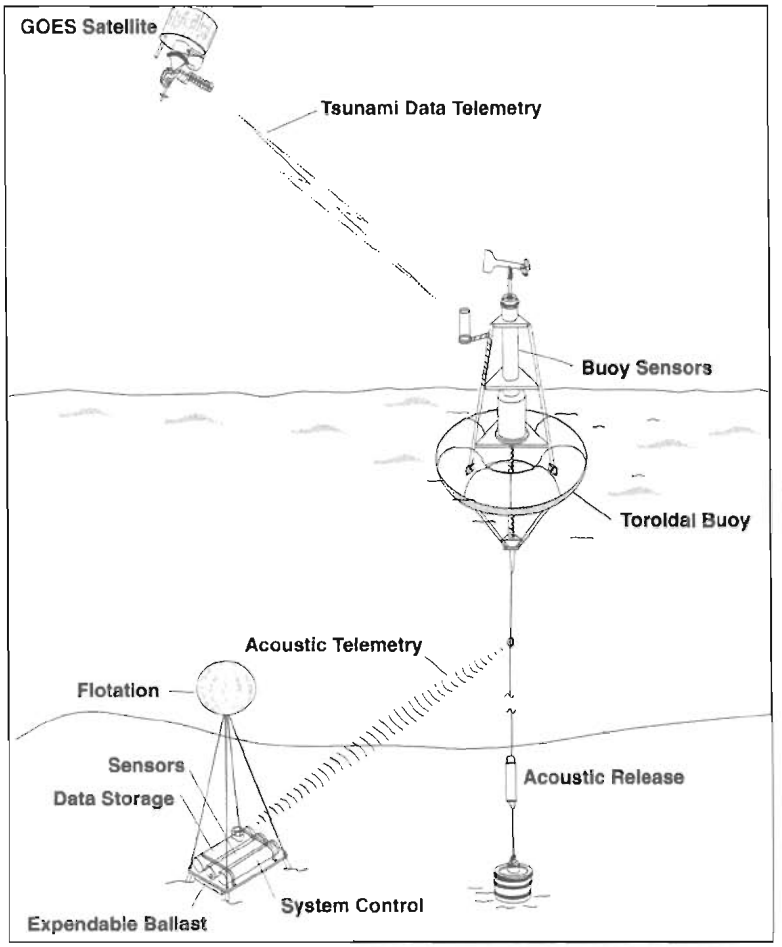

Figure 2. Design of a real-time tsunami buoy. Sensors on the seafloor detect minute changes in wave height and telemeter those measurements to a surface buoy. Equipment on the buoy retransmit these data to the warning centers in real time.

Alaska coastlines will be flooded within 15 minutes while Hawaii and the coasts of Washington, Oregon, and California will be hit by a major tsunami within 5 hours after the event. Under present conditions, the Alaskan and Pacific Tsunami Warning Centers (ATWC and PTWC) will issue warnings covering a limited area as soon as the earthquake is detected, located, and sized. It will then take about an hour for the Centers to receive confirmation from Alaskan coastal tide gauges that a major tsunami has been generated. With confirmation, the ATWC will expand its warning area to include the entire west coast of the United States, and the PTWC will issue a Pacific Basin-wide warning. Even at this time, the Centers will have only a rough idea of the potential size of the tsunami. They will receive no further information until the tsunami reaches Midway Island (about 3 hours after the earthquake) or the west coast of the United States (4 to 5 hours after the earthquake). At this point, it will be too late for Washington and Oregon emergency managers to change their plan of operation, and Hawaii emergency managers will have only about an hour and a half to adjust their plans.

In the CSZ, there is increasing geological and seismological evidence that great ($M > 8$) earthquakes have previously occurred in this region, that at least one segment of the subduction zone may be approaching the end of a seismic cycle culminating in such an

earthquake, that these earthquakes have generated tsunamis, and that coastal run-up values of such a tsunami may be several meters to several tens of meters (Heaton and Hartzell, 1987; Weaver and Shedlock, 1992).

Recently, a small tsunami was generated at the southern end of the CSZ by a large (7.1 M_s) earthquake near Cape Mendocino, California (Gonzalez and Bernard, 1992). This tsunami arrived at Eureka, California, only 15 minutes after the earthquake origin time. During a postearthquake scientific meeting on the Cape Mendocino earthquake/tsunami, sponsored by the Federal Emergency Management Agency (FEMA), one of the two most urgent actions suggested was tsunami inundation modeling for Northern California. This modeling project has been funded by FEMA and NOAA to produce inundation maps for Eureka and Crescent City, California, which illustrates the importance and urgency of tsunami preparedness.

While the prediction of just when these great earthquakes will occur is an inexact science, it is certain that they will happen, and, lacking any action by NOAA, the scenarios outlined above will be played out. The sooner NOAA takes the actions proposed in this initiative, the greater the probability will be that the emergency management officials will be in a position to take effective mitigating actions.

Executive Order 12699 directs all Federal agencies to ensure that federally constructed or assisted buildings satisfy cost-effective seismic building standards (Beatley and Berke, 1993). To comply with this Order, agencies are assessing the tsunami threat to facilities they operate. For example, when FEMA sets up relief operations following an earthquake or other disaster, it needs guidance on sites that are vulnerable to tsunami flooding. Other Federal agencies, which occupy lands close to the coast, also need guidance on tsunami potential effects to respond to this directive. At present, there is no standard way for this information to be obtained.

Why NOAA?

NOAA is the Nation's only agency responsible for tsunami warnings. The issuance of tsunami watches and warnings has been a part of the mission of NOAA and its predecessor agencies since the Seismic Sea Wave Warning Program was first established in 1946 at the U.S. Coast and Geodetic Survey's (USCGS) Honolulu Observatory. This service was extended by the establishment of the ATWC in Palmer, Alaska, after the great Alaskan earthquake of 1964. The relevance of the Tsunami Warning Program to NOAA's mission was confirmed in the 1970s. At that time, the tsunami warning program was the only part of the USCGS Seismology and Geomagnetism Program that was not transferred to the U.S. Geological Survey.

NOAA has the technical expertise and the leadership skills to make this initiative successful. The task is much too broad to be undertaken by a state or local government; they, other Federal agencies, and the private sector lack the technical expertise to complete the initiative. This activity is not a profit maker, a condition necessary to generate interest on the part of the private sector. It is, however, expected that a tsunami inundation modeling unit would function much like the Storm Surge Program currently functions. The unit would provide the capability and the expertise to model tsunami inundation, and state or local governments plus FEMA would provide the funds to create inundation charts for specific locations.

What Actions are Proposed?

The Tsunami Hazard Reduction Program consists of three elements: (1) inundation modeling, (2) early detection, and (3) research.

- Tsunami Inundation Modeling

To protect life and property from local and distant tsunamis, inundation maps are required to guide proper response to tsunami warnings. Inundation maps are derived from numerical models that simulate the behavior of tsunamis. The numerical models are first validated by comparison with existing historical tsunami data. These data are always too sparse to yield complete confidence in the model but do provide a level of confidence for emergency planning. Once the model is tested, it is used to simulate likely tsunami scenarios for a particular population center. For U.S. coastal areas, the scenarios would include two simulations—the local tsunami scenario and the distant tsunami scenario. As illustrated in Figure 3, U.S. coastal communities are threatened by both types of tsunami hazards. Local tsunami simulations require the input of knowledgeable geophysicists who can provide the type of earthquake motions expected from that particular location. The National Earthquake

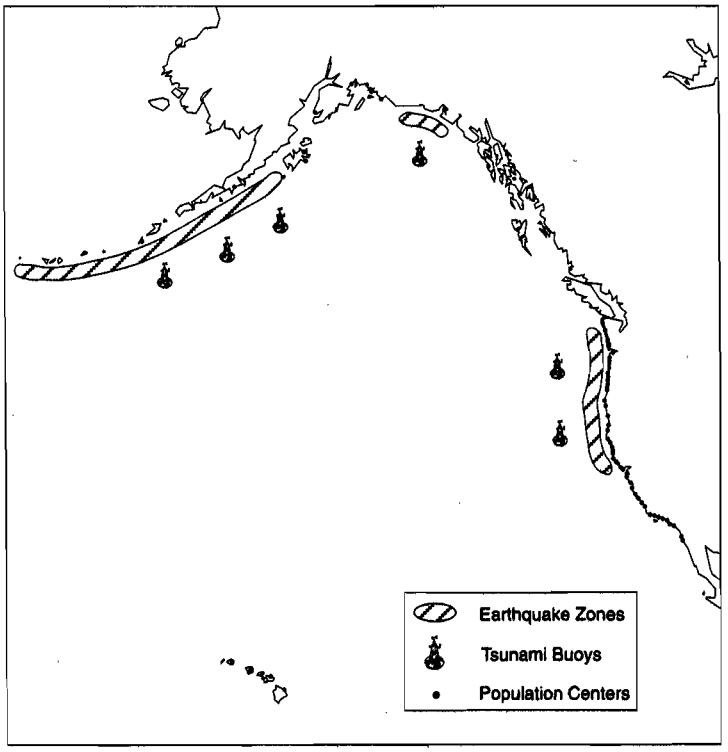

Figure 3. Tsunami hazard for the United States is defined by the earthquake zones capable of generating tsunamis in the Alaska-Aleutian Seismic Zone and the Cascadia Subduction Zone. The populations at risk from tsunami are identified as population centers. The buoys are positioned to provide early detection of tsunamis originating at these locations.

Hazards Reduction Program has developed earthquake scenarios for most seismically active areas of the United States. NOAA would use these estimates as the basis for the local tsunami scenario. For areas where scenario earthquakes have not been developed, NOAA would work with the U.S. Geological Survey to obtain reasonable estimates of earthquake motions.

Distant tsunami scenarios will use the same earthquake information estimated for local tsunamis as input for large-scale tsunami propagation models. The output from the propagation model would be used to simulate the arrival of the tsunami for the inundation model. This nested technique has been used successfully in other studies (Shuto, 1991). For non-U.S. tsunami sources, historical tsunami data would be used for estimating the impact of a distant tsunami. For example, data from the 1960 Chilean tsunami would be used in the distant tsunami scenario.

Based upon the results from the local and distant tsunami model studies, estimates of tsunami flooding would be provided to selected communities as a guide for developing evacuation zones. The evacuation zone for Hilo, Hawaii (Figure 1), is based on historical data and model studies.

The inundation estimates would be the product of a NOAA tsunami inundation modeling unit. This unit would initially use the models developed in 1990 to 1994 and would continue to seek improvements as more data become available. This unit would serve as the national standard for producing inundation estimates, provide the continuity and expertise for future changes in modeling technology, and serve as the tsunami information center for Executive Order 12699. The operation of this unit would be roughly analogous to the storm surge modeling project within the National Weather Service.

- Early Detection: Real-time Tsunami Observing Network

A major improvement in tsunami warning operations is the inclusion of a network of six deep-ocean tsunami gauges that report data in real time (Figure 3). This network would provide early detection and measurement of tsunamis to issue faster and more accurate warnings to U.S. populations. Placement of these gauges is determined by the most probable earthquake sources. Based on our present understanding, there are two zones to monitor: Cascadia Subduction Zone (Weaver and Shedlock, 1992) and Alaska and Aleutian Subduction Zone (Nishenko, 1991). This observational network has been in development and design for 6 years. The bottom pressure recorder, the most accurate tsunami gauge available, is an instrument that can withstand ocean bottom pressure (up to 5000 m) and still provide .5-cm resolution of a tsunami. During this 6-year development stage, six tsunamis have been measured that demonstrate the capability to detect tsunamis in the deep ocean (Gonzalez et al., 1991; Eble and Gonzalez, 1991). This instrument will be combined with new acoustic communications instrumentation to send the data to a surface buoy (Catipovic et al., 1990). As illustrated in Figure 2, these data would then be transmitted via satellite to the NOAA tsunami warning centers to improve the warning products. During FY 95, a prototype buoy will be built and tested, and in FY 96 and beyond, the network will be installed and maintained by PMEL. Communication technology for acoustically transmitting data from the seafloor to a surface buoy has been advanced (Catipovic, 1990) while communications from a surface buoy to the warning centers are possible today via the NOAA GOES satellite (Bernard et al., 1988). Costs and time estimates of these developments are accurate. Approximately 20 days of ship time per year will be required to servoce these buoys once a year. PMEL's 20-year history of deploying and maintaining buoys for extended periods of

time is well established and exemplified by the TOGA-TAO array project (Hayes et al., 1990).

- Research

An ongoing research activity is essential if both the operational modeling effort and the tsunami measurement program are to be brought to the level of accuracy and dependability of the existing NOAA hurricane and storm-surge forecasting capabilities. This program will consist of NOAA and academic scientists guided by a technical advisory committee of tsunami experts and overseen by the Coastal Ocean Program. The major upgrades proposed for modeling and observation activities will be matched by a significant increase in research to address fundamental issues affecting the quality of the operational products—tsunami inundation maps and tsunami warnings. Though intimately interlinked, this effort is best thought of in terms of three primary components: modeling, observational, and earthquake research.

Modeling research, both numerical and theoretical, will be an essential component of the research activity. Tsunami inundation maps that are presently produced (for only a few U.S. coastal communities) will benefit from the systematic effort by the Coastal Ocean Program to use numerical models that have been tested with the best field observations available (Gonzalez, et al., 1991; Mader and Curtis, 1991; Liu and Yoon, 1991). However, these models, although considered state of the art, still fall far short of the accuracy attainable by hurricane and storm-surge simulations, and much more research is needed to improve our understanding and our ability to numerically simulate the fundamental physical processes of tsunami generation, propagation, and inundation. The challenge is thus twofold: first, to upgrade our operational modeling capabilities to the present state of the art and, second, to improve the accuracy and dependability of this capability through a well-focused research program.

Observational research will be conducted to improve the quality and quantity of tsunami observations. High-quality tsunami observations are essential for the validation of numerical and theoretical models, but the existing data base is inadequate. Tsunami warning quality will immediately benefit from the availability of deep-ocean tsunami measurements by the proposed network. The mere ability to verify the presence or absence of a tsunami signal should reduce false alarms, and the accurate measurement of an amplitude will provide an improved basis for the assessment of the tsunami hazard. But, these data alone are inadequate for model validation. Tsunami currents must also be measured; observations are required immediately offshore and in the inundated zone; and remote sensing techniques must be brought to bear on the problem of collecting regional-scale data after a tsunami disaster. The technology to acquire such measurements must be developed through a systematic and dedicated engineering research effort.

Earthquake research must be focused on improving the technology to rapidly evaluate earthquake magnitude and the probability of tsunami generation. One method that holds promise requires the installation of broadband seismometers and the implementation of associated algorithms for a preliminary, but very rapid, assessment of tsunami hazard (Talandier and Okal, 1989). Another promising technology is the use of acoustic waves generated by the earthquakes that travel through the ocean. Those waves, known as T-phases, can be detected by underwater hydrophones and used to evaluate tsunami potential of underwater earthquakes (Walker et al., 1992). It is essential that such new approaches to the rapid evaluation of earthquake tsunami potential be researched. Three Pacific tsunamis were

generated in 1992 that killed over 2,000 people. Fortunately, the tsunami generated along the California coastline arrived at low tide and caused no fatalities.

What Resources are Needed?

Major Actions	FTE	FY 1995 Amount (in millions)
Inundation Modeling Unit	3	$0.6
Early Detection Network	1	1.0
Research	1	1.0
• Modeling ($.4 million)		
• Tsunami Observations ($.3 million)		
• Earthquake Studies ($.3 million)		
Total Request for FY 1995		$2.6

The inundation modeling unit requires two NOAA scientists, one technical support person, three non-Federal support programers, and one administrative support person. The unit requires access to a supercomputer (approximately 200 hours) and ownership of three high-performance workstations (to be replaced every 5 years) along with plotters and printers. A laboratory of approximately 90 square meters will house this unit. It is assumed that FEMA will partially support site-specific studies.

The early detection network requires one ocean engineer and two non-Federal support technicians. Twelve buoy systems will be built, six of which will be used at a time. Twenty-percent loss each year will require the replacement of one buoy system per year. Each buoy system costs $250,000. In FY 95, the prototype system will be built, and parts ordered for three systems. In FY 96, three buoys will be deployed as illustrated in Figure 3, and parts for three systems will be ordered. In FY 97 and FY 98, the network will be expanded by one buoy and three ordered buoys. In FY 99 and beyond, six buoys will be deployed, and parts for one buoy will be ordered.

Requirements for the three research elements follow:

Model studies will cost $400 thousand per year and will support one modeler at PMEL and university research. These studies require the purchase of computers and associated equipment along with supercomputer time.

Observational studies will cost $300 thousand per year to support scientists at PMEL and universities. These studies require the purchase of equipment and the conduct of small field experiments.

The earthquake studies will cost $300 thousand to support geophysicists at the National Weather Service warning centers and academia. These studies are very applied and will require the purchase of new seismological equipment and analysis packages.

What Are the Benefits?

These improvements should provide a coherent, stable tsunami mitigation program for the United States. The tsunami inundation modeling unit will systematically provide each Pacific coastal community and Federal agencies with estimates of tsunami flooding for use in emergency planning. The method for deriving these estimates will be well understood and reproducible. As improvements in methods evolve, each flooding estimate study will be

updated to reflect the "state-of-the-art" technology. As the population of the coastal zone increases by 50 percent over the next 15 years, the value of accurate estimates of flooding will grow as pressure for land use in these zones increases. For example, on September 1, 1992, a major earthquake centered off the coast of Nicaragua generated a tsunami with waves measuring from 8 to 15 m high. The waves struck more than 250 km of Nicaragua's Pacific coast, killing 116 persons (another 63 remain unaccounted for), directly or indirectly affecting more than 40,000 people, and causing total damage and losses estimated at $25 million (Jovel, 1992). Nicaragua is a developing country with no major cities on the coast. If a similar tsunami hit the California coastline, losses would be in the hundreds of millions of dollars. The United States presently spends about $100 million on the National Earthquake Hazard Reduction Program, but none of those resources are dedicated to tsunami preparedness. This initiative would represent a 2.6-percent increase in the national effort to mitigate the effects of tsunamis in the context of seismic hazard.

An additional benefit is the value of the inundation estimates in responding to Executive Order 12699, which directs Federal agencies to ensure that federally constructed or assisted buildings satisfy cost-effective seismic building standards. Presently, there is no process whereby an agency can secure information on the tsunami threat. Considering the potential damage to U.S. Navy facilities at Pearl Harbor and San Diego along with the U.S. Postal Service, the Army Corps of Engineers, and all other Federal agencies with facilities along the coast, an investment of $2.6 million per year is clearly justified.

The deep-ocean observational network will enable the warning centers to provide more accurate and timely warnings. Over the past 100 years, one destructive tsunami has occurred each year in the Pacific Basin (Lander and Lockridge, 1986). If we assume that at least one warning will be issued each year, the value of an accurate warning is worth much more than the $2.6 million requested. For example, the 1986 unnecessary tsunami evacuation of Honolulu cost the city over $1 million in lost business revenues. If you multiply this cost over the 80 population centers affected in the United States, it **pays** to avoid false alarms! But, more importantly, this program will save lives and reduce the impact to property when tsunamis occur.

References

Beatley, T., and P.R. Berke (1993), Time to shake up earthquake planning, *Issues in Science Tech.* **IX**, No. 2, Winter 1992-1993, pp. 82–89.

Bernard, E.N., R.R. Behn, G.T. Hebenstreit, G.I. Gonzalez, P. Krumpe, J.F. Lander, E. Lorca, P.M. McManamon, H.B. Milburn (1988), On mitigating rapid onset natural disasters: Project THRUST, *EOS Trans., Amer. Geophys. Union*, **69**, No. 24, pp. 649–661.

Catipovic, J. (1990), Performance limitations in underwater acoustic telemetry, IEEE J. Oceanic Engr., **15**, No. 3, pp. 205-216.

Catipovic, J., D. Frye, and D. Porta (1990), Compact digital signal processing enhances acoustic data telemetry, *Sea Tech.*, May, pp. 10–15.

Eble, M.C., and F.I. Gonzalez (1991), Deep-ocean bottom pressure measurements in the northeast Pacific, *J. Atmos. Oceanic Tech.*, **8**, No. 2, pp. 221–233.

Gonzalez, F.I. (1990), Deep ocean recordings of tsunamis, *Proc. 22nd Joint Meeting on Wind and Seismic Effects, UJNR Program, May 15–18, Gaithersburg, MD, NIST SP 796*, pp. 53–58.

Gonzalez, F.I., and E.N. Bernard (1992), The Cape Mendocino tsunami, *Earthquakes and Volcanoes*, **23**, pp. 135–138.

Gonzalez, F.I., C.L. Mader, M.C. Eble, and E.N. Bernard (1991), Deep-ocean data and model comparisons, *Natural Hazards*, **4**, pp. 119–139.

Hayes, S.P., L. Mangum, J. Picaut, A. Sumi, and K Takeuchi (1991), TOGA-TAO: A moored array for real-time measurements in the tropical Pacific Ocean, *Bull. Am. Meteor. Soc.*, **72**, No. 3, pp. 339–347.

Heaton, T.H., and S.H. Hartzell (1987), Earthquake hazards on the Cascadia Subduction Zone, *Science*, **236**, pp. 162–168.

Jovel, J.R. (1992), The tsunami of September 1992 in Nicaragua and its effects on development, United Nations Economic Commission for Latin America and the Caribbean (UNECLAC), 37 pp.

Lander, J.F., and P.A. Lockridge (1986), Uses of a tsunami data base for research and operations (abstract), *EOS, Trans. AGU*, **67**, p. 1003.

Liu, P.L.-F., and S.B. Yoon (1991), Estimation of tsunami wave heights along South Eastern Korea shoreline, *School of Civil and Environmental Engineering Report,* Cornell University, December 20, 88 p.

Mader, C.L., and G. Curtis (1991), Modeling Hilo, Hawaii, tsunami inundation, *Science of Tsunami Hazards*, **9**, pp. 85–94.

Mader, C.L., G. Curtis, and G. Nabeshima (1993), Modeling tsunami flooding of Hilo, Hawaii, *Recent Advances in Marine Science Tech.*, PACON International, pp. 79–86.

Nishenko, S.P. (1991), Circumpacific seismic potential: 1989–1999, *Pure Appl. Geophys.*, **135**, pp. 169–259.

Nishenko, S.P., and K.H. Jacob, (1990), Seismic potential of the Queen Charlotte-Alaska-Aleutian Seismic Zone, *J. Geophys. Res.*, **95**, pp. 2511–2532.

Shuto, N. (1991), Numerical simulation of tsunamis—its present and near future, *Natural Hazards,* **4**, pp. 171–1991.

Talandier, J., and E.A. Okal (1989), An algorithm for automated tsunami warning in French Polynesia based on mantle magnitudes, *Bull. Seismol. Soc. Am.*, **79**, pp. 1177–1193.

Walker, D.A., C.S. McCreery, and Y. Hiyoshi (1992), T-phase spectra, seismic moments, and tsunamigenesis, *Bull. Seismol. Soc. Am.*, **82**, pp. 1275–1305.

Weaver, C.S., and K.M. Shedlock (1992), Estimates of seismic source regions from consideration of the earthquake distribution and regional tectonics in the Pacific Northwest, *U.S. Geological Survey Open-File Report 91-441*, 51 p.

Performance Measures

Performance Measures	FY 1995	FY 1996	FY 1997	FY 1998	FY 1999	FY 2000	FY 2001
Percentage of Inundation Maps Provided to Coastal Communities	12%	24%	36%	48%	60%	72%	84%
Percentage of Tsunami Detection Network in Place	0%	50%	67%	84%	100%	100%	100%

Outyear Resource Levels

(dollars in thousands)

Major Components	FY 1995	FY 1996	FY 1997	FY 1998	FY 1999	FY 95–99
Inundation Modeling	600	624	650	675	700	730
Early Detection Network	1,000	1,040	1,080	1,120	1,170	1,220
Research	1,000	1,040	1,080	1,120	1,170	1,220
Total Request	2,600	2,704	2,810	2,915	3.040	3.170

Name	Affiliation	Phone	Fax
Eddie Bernard	NOAA PMEL	206-526-6800	206-526-6815
Michael Blackford	NOAA/NWS/PTWC	808-689-8207	808-689-4543
George Carrier	Harvard University	617-495-3788	617-495-9837
George Curtis	JIMAR/Uinv. of Hawaii	808-933-3383	808-933-3693
Augustine Furumoto	Tsunami Adviser, State of Hawaii	808-956-7864	808-956-3188
Frank González	NOAA/PMEL	206-526-6803	206-526-6815
Jim Good	Oregon State University SeaGrant	503-737-1339	503-737-2064
Stephen Hammond	NOAA/PMEL	503-867-0183	503-867-3907
Karla Heerman	FEMA–Pacific Area Office	808-541-2371	808-541-3959
Don Hull	Oregon Dept. of Geology	503-731-4100	503-731-4066
Zygmunt Kowalik	Univ. of Alaska, Fairbanks	907-474-7753	907-474-7204
Philip Liu	Cornell University	607-255-5090	607-255-9004
Bill Mass	NOAA/NWS/PTWC	808-689-8207	808-689-4543
Richard McCarthy	California Seismic Safety Comm	916-327-8879	916-322-9476
Chip McCreery	NOAA/NWS/PTWC	808-689-8207	808-689-4543
Dennis Moore	JIMAR/Univ. of Hawaii	808-956-4098	808-956-4104
Mel Nishihara	State of Hawaii Civil Defense	808-734-2161	808-737-4150
Dennis Sigrist	ITIC/NOAA-NWS	808-541-1657	808-541-1678
Vasily Titov	Univ. of S. California	213-740-0560	213-744-1426
Frank Tsai	FEMA	202-646-2753	202-646-3445
Brian Yanagi	Hawaii State Civil Defense	808-734-2161	808-737-4150

AGENDA

TSUNAMI INUNDATION WORKSHOP

University of Hawaii
November 16-18, 1993

Tuesday, November 16

0800 Background and purpose of workshop - E. Bernard
0830 Users of inundation maps, who will address issues such as:

1. Why do we need this information?
2. Which communities have the highest priority?
3. What is planned in terms of tsunami hazard mitigation?

Hawaii - Brian Yanagi
California - Dick McCarthy
Oregon - Jim Good

0915 A Perspective - G. Carrier
0930 JTRE engineering model description - G. Curtis
1000 Mader model description - D. Moore for C. Mader
1045 Shuto/Liu model description - P. Liu

1130-1230 Lunch

1230 Kowalik model description - Z. Kowalik
1315 Titov model description - V. Titov
1400 JTRE engineering model application - G. Curtis
1430 Mader model application - D. Moore for C. Mader
1515 Shuto/Liu model application - P. Liu
1600 Kowalik model application - Z. Kowalik
1645 Titov model application - V. Titov

Wednesday, November 17

0800-1200 Discussion of model issues/problems - led by F. Gonzalez
What are the merits/deficiencies of each model?
How does one inter compare models?
Are standard techniques possible?

1200-1300 Lunch

1300-1330 Bathymetric Data Sets - S. Hammond
1330-1415 Operational Issues concerning Mader model - D.Moore for C.Mader
1415-1500 Operational Issues concerning Shuto/Liu model - P. Liu
1500-1545 Operational Issues concerning Kowalik model - Z. Kowalik
1545-1630 Operational Issues concerning Titov model - V. Titov

Thursday, November 18

0800-1200 Discussion of operational issues, formulation of recommendations, and ranking priorities of recommendations - led by E. Bernard and D. Moore

Participants:

NOAA - Eddie Bernard, Frank Gonzalez, Steve Hammond, Mike Blackford, Dennis Sigrist
FEMA - Frank Tsai, Karla Heerman
State of Hawaii - Don Gransback, Brian Yanagi
University of Hawaii - Chuck Mader, George Curtis, Dennis Moore
State of Oregon - Don Hull, Jim Good
State of California - Dick McCarthy
University of Alaska - Zigmunt Kowalik
University of Southern California - Vasily Titov
Cornell University - Phil Liu
Harvard University - George Carrier

FINAL REPORT

HAWAII TSUNAMI INUNDATION/ EVACUATION MAP PROJECT

by

George D. Curtis
Tsunami Research Specialist

Submitted to:
Hawaii State Civil Defense Agency

April 19, 1991

JIMAR Contr. No. 91-237

FINAL REPORT:
Hawaii Tsunami Inundation/ Evacuation Map Project

George D. Curtis
Tsunami Research Specialist

SUMMARY

After the evacuation problems of the May 7, 1986 event, there was general agreement that better procedures and updated evacuation maps were needed. Eventually, funding was obtained from the legislature and a project initiated between JIMAR and State Civil Defense to a) refine the existing coverage of the inundation/evacuation maps with better data and methodology; b) extend this inundation coverage into areas developed since the prior maps were drawn up in 1961 and c) assist the county civil defense agencies as needed in converting the draft maps into evacuation maps and getting them published in the telephone directories.

All available data, maps, and sources were reviewed and a team organized for this effort. Additional data were used with a wave height data set compiled from UH data by the Corps of Engineers. A runup procedure developed by the Ocean Engineering Department was applied to these data and other historical information. A conservative statistical repeat time of 200 years, with allowance for high tide where needed was used in calculations to produce the maximum expectable inundation limit of waves. Runs were made every one-quarter to two miles along coasts, depending on topography. The best available topographic (contour) maps were used, with photos and visits, to incorporate the factors needed to determine the final line. All coastal areas analyzed were selected, on a priority basis, by County Civil Defense directors.

The mileages mapped on each island were as follows:

Island	Miles	% of Coast
Oahu	177	100
Kauai	95	84
Maui	58	35
Molokai	35	36
Lanai	3	6
Hawaii	54	17
	422	

This constitutes virtually all the developed/occupied shorelines of all islands except the Big Island. (Some areas of that island already had new, conservative evacuation maps.) The draft inundation maps were delivered to the counties and reviewed with them. Their staffs then drew evacuation lines mauka of the maximum expectable inundation lines, with inputs from police, fire, and others involved in the evacuation. Notes were added to aid in this. The maps were then reviewed, approved, and delivered to the graphic artist used by the telephone company to prepare for publication. This product was then re-reviewed by JIMAR and Civil Defense and any final changes incorporated. The last set of maps was approved on January 31, 1991. The Oahu directory with the new maps was distributed in February, with the other counties to follow in the next three months.

List of Tables

List of Figures

Appendixes

Introduction

After the major tsunami of 1946 attacked the islands a warning system was established, which has always functioned technically. But after the loss of sixty-one lives in the 1960 event in spite of a warning, it was recognized that better evacuation procedures were essential. A small team led by Doak Cox of HIG pioneered scientifically created inundation maps to be used for evacuation purposes. Cox postulated, after much review of data, a worst-case wave of fifty feet impacting the coast at the ten-foot depth line. He drew a surface sloping down at 1% until it intercepted the land; this set the hazard zone. (On most leeward areas, a thirty-foot wave was assumed.) His report (Cox, 1961) and marked USGS 1"=2000' maps were delivered to Civil Defense, and used as the basis for the maps published in the green pages of all telephone directories for public use. The maps covered most of the areas with significant coastal populations at that time.

In the years since, there have been few tsunamis, and the warning system has improved and gives fewer warnings of non-significant tsunamis. Thus, there was a lull in awareness by both the public and officials. This ended on May 7, 1986. It became obvious that better procedures were needed for evacuation, that zone limits were sometimes unclear, and did not exist for many areas populated since 1961. (The population of the state had increased more than 50%.)

In addition to the clear need, more data on tsunamis and better methods for applying it to determining inundation had evolved. The Corps of Engineers had drawn upon data collected by the Joint Tsunami Research Effort (JTRE) at the University and applied formulas developed in the Ocean Engineering Department to develop estimates of tsunami flooding for Federal insurance purposes. These provided a database and starting methodology for a project to refine and extend the inundation maps. It was suggested by Norman Lamb of the State Civil Defense that JIMAR propose a program for this purpose. A plan was developed, but no funds were available.

A bill was introduced in the State Legislature by Representative Bellinger to provide funds, but failed to pass. In the next session, with good support and testimony from State and County Civil Defense agencies, the bill passed and funds were allocated to Civil Defense for new maps. After four months' delay with contractual procedures, a grant was made to JIMAR and the program formally initiated. (We had actually begun two months earlier.)

The Project and Procedures

Since our proposal to State Civil Defense had provide a framework for the project, the initial step was to locate, gather, order, and organize, all known data and reports on tsunami effects in the Hawaiian islands. In addition, methodology used here and elsewhere had to be reviewed, compared, and updated. References herein listed are examples of what was to be used, in addition to numerous minor references.

Dr. Cox's accumulation of information as well as material from the files of William Adams and Gus Furumoto became available. Fred Camfield at the Corps

of Engineers Waterways Experiment Station provided information from their files. Maps, both historical and current, were obtained, borrowed, and ordered.

A team combining researchers experienced in tsunami work with people in other fields was formed. A very capable graduate student in Geography was hired and formed part of the team, which had their first meeting September 12, 1988 (ref 1). Thereafter, appropriate members met informally as required. Members included : Bill Adams, Doak Cox, George Curtis, Gus Furumoto, Norm Lamb, Hal Loomis, Joe Morgan, and Mark Smaalders from the University of Hawaii-Manoa, and Walt Dudley from UH-Hilo.

Of course, acquiring such materials was a continuing process, and map cases and files had to be obtained for the resultant collection. Of special interest are the maps that were obtained and were on hand. These include:

--USGS Quadrangle Charts--current and old; coastal Hawaii
--US Department of Agriculture large-scale topographic maps (5 feet contours), selected area
--Oahu Department of Land Utilization maps, 1"=1000' with 10' contours
--Corps of Engineers large-scale maps from various contractors, various coastal and flood-prone areas (5'-10' contours)
--Flood Insurance Rate Maps (FIRM) for most coastal areas; updated by subscription
--UH Press maps of each island; excellent for correct place names
--Bryan's sectional maps for Oahu streets; various road maps for limited areas of other islands
--marked-up historical tsunami maps

Obtaining adequate topographical maps was the largest single, ongoing task in the project, and a vital one.

The compilation of historical wave height data by the Corps of Engineers (with modification from JTRE) was available in ref 2, which included the synthesized wave envelope evolved by Houston. This data set was also found in a manual by M & E Pacific (for the Corps), ref 3, and subsequently borrowed from the Corps in digital form on a computer disk. The program was written at the Pacific Ocean Division and includes the formula from ref 6, as used by Houston. Topographical data was also obtained from the Corps in tabular form for the Big Island, but the digital version could not be found.

The other environmental information needed for an analysis is the near-shore ground characteristics--sand, rocky, vegetated, etc. For this purpose various shoreline atlases were obtained (ref 4 and 5) and subsequently supplemented by oblique photos.

Dr. Dudley at UH-Hilo coordinated work in the Kohala area with Hawaii County, and did field work at two complex hotel-resort developments in that area to provide actual elevations and shoreline configurations.

Methods

After review of methods of estimating inundation from known wave heights, it was decided to use the two-dimensional method (height and distance normal to the shore) developed by Bretschneider and Wybro of the Department of Ocean Engineering (ref 6). This had also been adopted by the Corps and a graphical version produced in a manual by a contractor.

The original formula was:

$$h_2 = h_1 - [\tan\theta = \frac{n^2 g\ F^2 h^{-v_3}}{(1.486)^2}]\ [\frac{F^2}{2} + 1]^{-1}\ \Delta x$$

and had been rearranged for routine use as:

$$\Delta x = \frac{\Delta h[\frac{F^2}{2} + 1]}{\tan\theta + \frac{n^2 g\ F^2\ h_A^{-1/3}}{(1.486)^2}}$$

where:

h = wave height	Δx and Δh = incremental distance and height
x = horizontal distance	n = Manning's friction coefficient
h_A = avg depth	g = gravity
F = Froude number	
$\tan\theta$ = ground slope	

A two-dimensional method does not consider interaction between adjacent segments, but has been found satisfactory and feasible for most shorelines. A three-dimensional method under development (ref 7) should be more accurate for complex embayments, but requires detailed 3-D data for input plus ample time. With the 2-D method, a more conservative limit is used in complex areas.

To ensure consistency in the work, a set of definitions, precepts, and a procedure were written up and distributed for review and use. The procedure is included as appendix A; the definitions and precepts are as follows:

TSUNAMI PROJECT
Definitions, 9/23/88 (Rev 4/90)

Inundation line (limit)--the inland limit of wetting, measured horizontally from the MSL line. Where MLLW was used, it should be converted to the MSL line. (Move inland to an elevation 0.7 ft higher.) The vegetation line is sometimes used as a reference. If it can be determined that it is more than ten ft from the MSL line, adjust; otherwise, ignore.

Runup (height, R)--the elevation of the ground above MSL that the water will reach. This is usually not equal to the wave height, or inundation depth, at the shoreline.

Wave height (h)--the height of the (highest) wave, at the MSL shoreline. In the absence of other information, considered to be measured 200 feet inland. Tide gauges show wave height in harbors,

which may be significantly different from actual wave heights or runups.

Precepts, 12/2/88

MEASUREMENTS--should be in feet and referenced to MSL. If other units are used, they must be referenced or noted.

SOURCE OF DATA--should be from the first reference, if available, should be noted with tsunami data, envelope, extrapolated, calculated, estimated, etc.

SYMBOLS--per the following list:

h	wave height at shoreline*
R	runup height*
IL	inundation limit*
IL_{100}, R_{100}, etc.	values calculated for a 100 year return time (note this time is only a general approximation)
IL_E	inundation limit of worst actual measured/calculated tsunami values

CHARTS, DIAGRAMS, TABLES--should be dated and initialed, and follow the above precepts.

The maximum expectable inundation (limit) is the primary product of the project. Appendix A should be consulted for details on the development of this limit; it is the actual written procedure used by those working on the project.

The definitions were later shown in a paper (ref 8) by the following illustration:

DEFINITION SKETCH

TSUNAMI TERMS

NOTE: R MAY BE GREATER OR LESS THAN h ; DO NOT CONFUSE.
PRESENT WATER LEVEL/LINE MAY BE USED IN LIEU OF MSL, IF STATED.

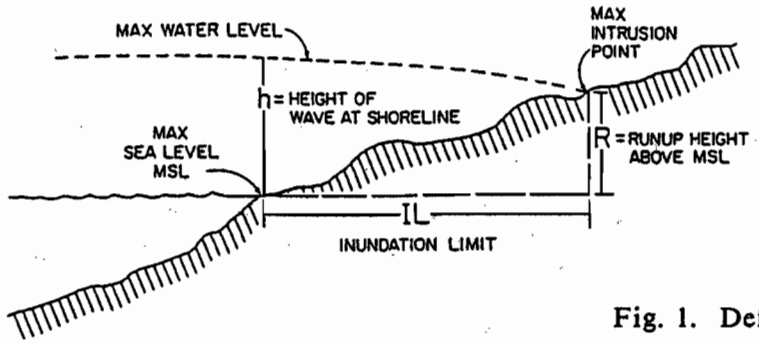

Fig. 1. Definition Sketch

Tests were made on a few areas, following the procedure and the following worksheet adopted for use:

TOPOGRAPHIC AND ROUGHNESS DATA											WAVE HEIGHTS						INUNDATION					
MILE #	1.	n	2.	n	3.	n.	4.	n	5	n	1946	1952	1957	1960	h_{100}	h_{200}	COX	FIRM	BRET h_{100}	BRET h_{200}	Hous h_{100}	Hous h_{200}
37.0	0, 0	$.0_35$	5, 100	$.0_35$	10, 700	.03	20, 1150	$.0_35$	40, 1400	$.0_35$	10'	6'	13'	8'	10'	13'	1100'	370'	500'	700	900	1050
37.25	0, 0	.04	5, 50	.04	10, 2100	.03	20, 2300	$.0_3$	—						11'	13'	2000'	400'	560'	825	1250	2000
37.5	0, 0	$.0_35$	5, 50	$.0_35$	10, 2250	.03	20, 2900	$.0_3$	—						10'	13'	—	400'	675	985	750	1725

Fig 2. Example

Progress of the Work

Meetings were held with State Civil Defense and with County Civil Defense officers to explain the project. Each county was asked to select their highest priority areas for us to begin work on. They were (in order):

Oahu	Kalanianole	
	Iroquois Point	
	Haleiwa	
Kauai	Kealia	
	Poipu	
	North Shore	
Maui	Molokai	S. Shore and Kepuhi
	Lanai	Manele
	Kaanapali	
Hawaii	S. Kohala	
	Kailua	

After gathering and reviewing data for each area, the wave heights were evaluated and applied to a series of transects, along each of these shorelines, following the procedure. The work was always done on the largest scale maps available, with the final inundation line transferred to a USGS Quad (1"=2000"). Copies of the large-scale maps were normally delivered to the county civil defense agency along with the USGS maps. In a few areas, census and traffic data were also provided to aid in determining evacuation lines.

In Waikiki and a few other areas, it is desirable to evacuate much of the population vertically in safe high rise buildings. This practice was discussed with the Structural Engineers Association of Hawaii and the American Society of Civil Engineers (Structural Technical Group) orally and in correspondence.

Their written recommendations were the basis for endorsing vertical evacuation and provided the wording used on the final maps; all were forwarded to Oahu Civil Defense for their concurrence and use. See Appendix D.

In Waikiki, the de-facto population is now 120,000 in one square mile, and vertical evacuation will be almost essential.

Where necessary, to evaluate the friction effects or to check maps, photos were requested for the area from the Civil Air Patrol. They were helpful in taking low altitude (500-1000') oblique photos of any selected area.

Historical photos, old news clippings, etc., were also checked where pertinent to verify the wave heights or inundation limits. Caution must be used to make such calculations and comparisons on the basis of calculations for the event in question rather than the maximum expectable situation.

In very few cases, as also noted by Cox, were useful inundation limit data available. Hilo is the prime example; here the limits of 1946, 1952, 1957, and 1960 were well recorded and mapped. The envelope of these events, with a safety factor, forms a satisfactory line. (This does not apply in the Keakaha area, where the data are spotty.) Fig. 3 is a compiled map of the inundation for those events.

A few cases of credible runup or wave heights and inundation limits in the same location were used for validation of the procedure. This showed that the method yielded reasonable agreement. In more cases, we were able to verify that the method produced conservative results in comparison with any report of runup or inundation. The one exception found was Kaiaka Bay, Oahu, where historical records showed some flooding outside of our line at the edge of Wailua. This is a shallow, but complex area, and will be used for further study by the 3-D method (ref 7). The line was, of course, adjusted. Appendix B shows the above comparisons.

The first inundation maps for the priority areas were delivered to the counties of Kauai, Oahu, and Maui on May 5 and 8, 1989. Several examples, with the old evacuation zones and proposed new evacuation zones color coded, were prepared, copied, and provided to civil defense and to interested legislators. These showed graphically the significant reduction in area to be evacuated. Fig. 4 is an example. The old zone is from ref 9.

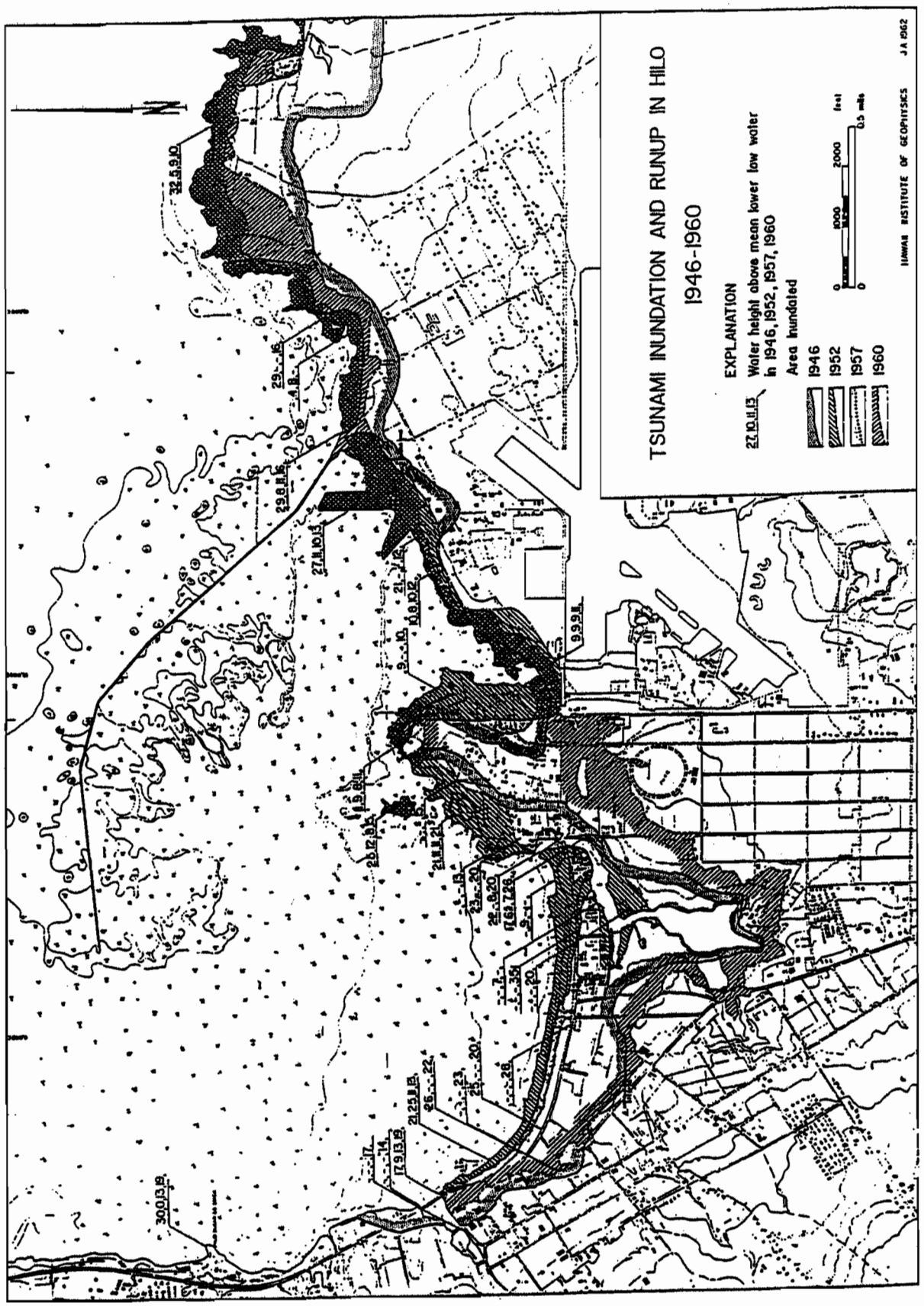

Fig. 3 Hilo Inundation Map

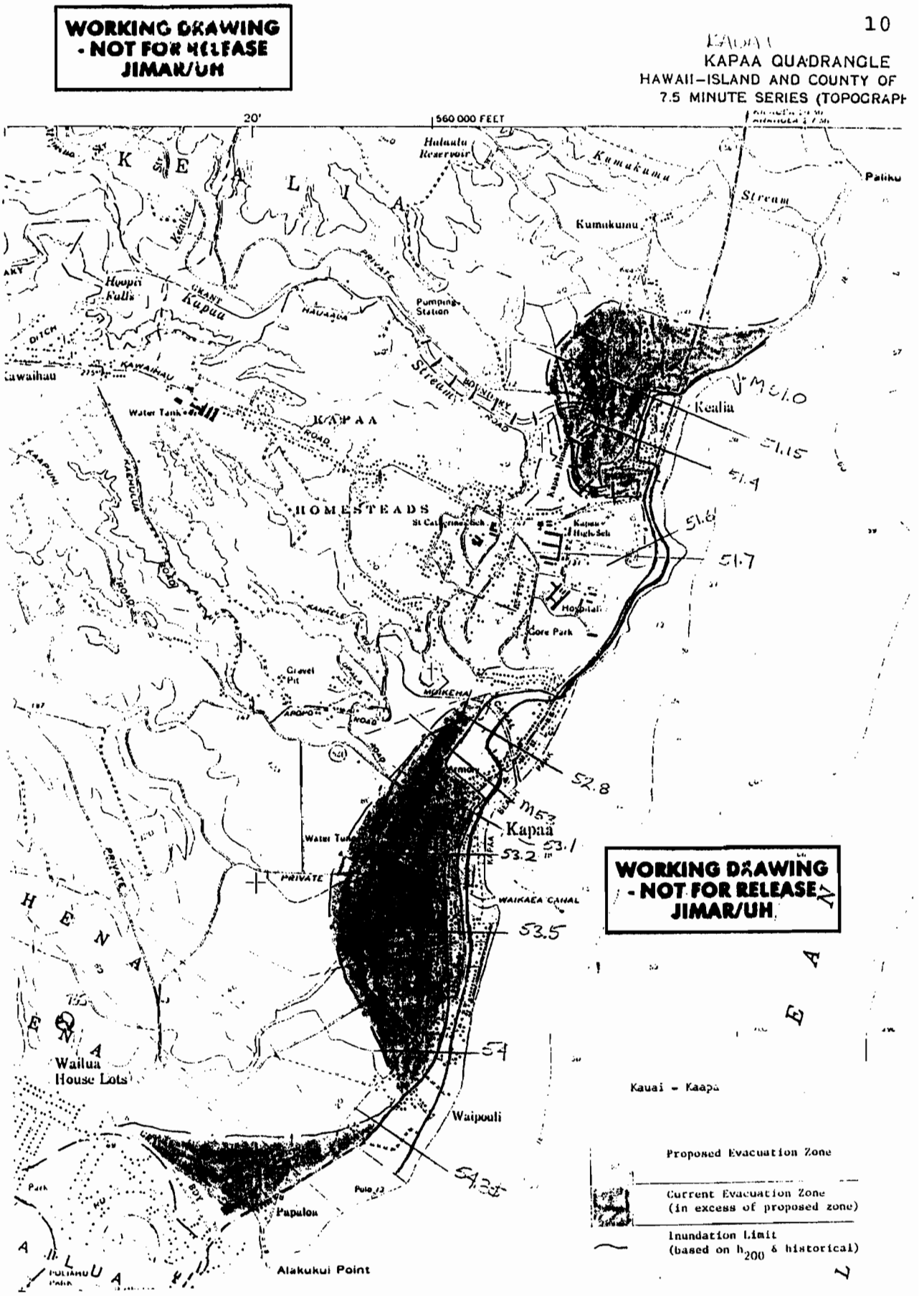

Fig. 4 Old and Proposed New Evacuation Zone Example, Kauai

As the work progressed, most calculations were made with the aid of the computer program. Standard input and output files and terminology were developed to facilitate both the original work, and any subsequent modifications. Printouts of these records are filed along with the worksheets, and were also placed on floppy disks, all of which are on file in the JIMAR office, as are the maps.

The priority areas listed earlier were complete and draft maps delivered to the county Civil Defense agencies for review and comment. Visits were made to each county to discuss the draft maps, status, next areas, and to seek better topographical maps of several areas. In addition, visits were made to Kauai and Maui Civil Defense offices for special group meetings and presentations to police, fire, public works, and other organizations involved in evacuation, who need the maps. These were arranged by the Civil Defense directors, and proved helpful to us all as well. For example, on Kauai, the police decided (from a draft map) it was best to evacuate a valley, thus no detail was needed there, but we gave special attention to the evacuation routes.

Presentations were also made to the State Civil Defense staff periodically. Draft maps were delivered for all requested areas per the schedule shown in Table 1; copies of the forwarding letters were sent to the State for coordination.

Evacuation Maps

The process of converting the draft inundation maps into evacuation maps was performed by the counties, with support from JIMAR where needed. This was accomplished in visits to Kauai and Maui and to some extent to Hawaii. Liaison was easily maintained with Oahu. After consultation with David Isaacs of Clarence Lee Design, the graphic artist for the telephone directory maps, a scheme was evolved to show the evacuation zones on maps he could easily trace, reduce, and xerox as needed for the final maps. Basically, this meant coloring the zones with blue highlighter, making a clear boundary, marking and naming streets and other reference features. Oahu used Bryan's sectional maps for this purpose; the others had to use USGS maps for most areas, although Hawaii prepared their own evacuation maps from various sources and had large, color versions available.

Oahu, Hawaii, Kauai, and Maui were done in turn by the graphic artist. He used three different scales for Oahu to combine detail in dense areas with coverage of the entire coast. (The scales were approximately 1"=1400' to 1"=4000'.) This resulted in nineteen map segments covering ten pages and 177 miles. We coordinated closely with the graphic artist in making out procedures for the Oahu maps, which were applied later to the other islands. Of course, many details were checked with or by Oahu Civil Defense. Finally, the maps were approved by us and Oahu Civil Defense and endorsed/ recommended to the State for publication.

A typical page is shown as Fig. 5.

In addition to the changes in the evacuation lines, the following features are found in the new maps:

--more use of street names to help residents locate their homes regarding the zones

Table 1

TSUNAMI INUNDATION/EVACUATION
DRAFT MAP SCHEDULE

ISLAND	AREA	DRAFT DATE	REMARKS
Kaua'i	Kealia-Papaloa	05/15/89	CD priority
	Hanamalu	05/22/89	Added
	Poipu	09/20/89	Topo map delay
	add'l.	05/02/90	
	Haena-Kilauea	07/05/89	
	Lihue area	01/10/90	
	West Kauai	05/01/90	
O'ahu	Southeast O'ahu	05/09/89	Critical area;
	thru Wailupe	06/20/89	Arrival direction noted
	South cast of Ewa	07/05/89	
	Kahala-Diamond Head	07/05/89	
	Waikiki	09/15/89	Vertical evac confirmed
	Haleiwa to Kualoa	09/30/89	New priority per OCD
	Leeward coast	03/20/90	
	Kailua-Lanikai	03/20/90	
	Haleiwa-Kaena	04/06/90	Add'l large map
Maui	South shore Molokai	05/02/89	No present zonation
	West shore Molokai	05/02/89	No present zonation
	Wailuku-Kahalui	05/02/89	High density area
	Lahaina-Kaanapali	09/25/89	Critical area; map problem, resolved
	Lana'i (Manele-Kaumulapau)	09/15/89	Development info obtained
	Kihei	10/20/89	
Hawai'i	Keahole-Kawaihae	04/21/89	Resort plans; minor
		10/01/89	rework (1/90)
	Hilo	09/15/89	Comparison only
	Kona	04/10/90	Comparison only

Note: Draft maps to be reviewed and final evacuation maps developed with counties; in progress.

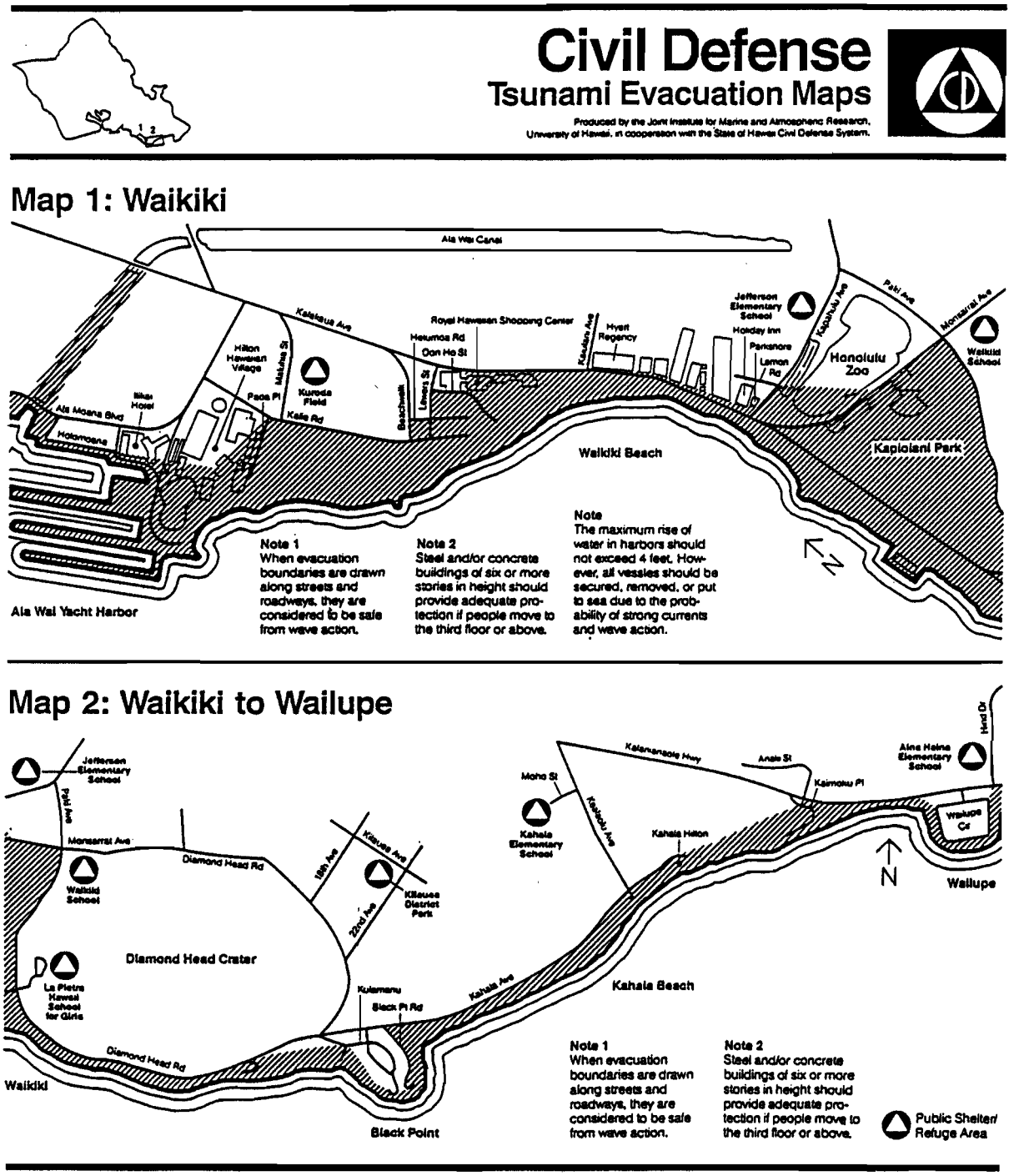

Fig. 5 Oahu Phone Book Map

--addition of evacuation shelter locations (Oahu only)
--better use of physical boundaries whenever feasible to minimize distance estimates
--refinement and addition of more vertical evacuation notes, and harbor notes
--addition of a note to show that roads used as boundaries are not in danger
--larger scale maps with much more detail
--and, at last, the correct title for the maps, evacuation, not inundation.

The new maps were included in the Oahu directory published in February 1991.

A similar process was used for the other islands, with necessary modifications due to distance, time, size of staff, etc. The inundation maps were reviewed in their entirety with Kauai and Maui Civil Defense directors. Examples from the Oahu work were used to show what the graphic artist would need, and any additional or more detailed information provided in a follow-up visit. The portions of the Big Island that we provided, that would be used this year, were reviewed with the staff there.

Mr. Isaacs used xerox reductions and manual drawings to prepare the draft maps for each island, but at some point converted them into computer graphics. This helped him finalize them, and will make it much easier to review them next time as they are all on disks.

Notes similar to those used on Oahu were added to the Kauai and Maui maps. Each of the maps were checked against our file maps, approved by both us and the Civil Defense directors, and endorsed to the State Civil Defense.

For Hawaii County, photos of the available color wall maps at Civil Defense headquarters were initially used for graphics; these clearly show the evacuation zones. However, the county subsequently provided small versions of the actual wall maps, also in color, which were easier to pick up detail from. At the request of the Hawaii Civil Defense administrator, the telephone directory maps show all the information on the large maps, including road blocks, fire stations, etc. No notes on road safety or harbor precautions were included. Several small segments for which we had developed inundation limits, but which they had not yet developed and field checked evacuation lines were deferred until next year. The existing (old) maps were used for those sections; these were reviewed and considered safe.

The Hawaii maps will be published in May, followed by Kauai and Maui in June, 1991.

Appendix C lists all the inundation maps delivered to the counties and the format used. Copies (or in some cases, originals) of these are on file at JIMAR.

Table 2 shows the miles and percent of shoreline mapped on each island. Figure 6 shows the coverage on a map of the islands. The lower percentage coverage on the other islands reflects the population density.

Table 2

TSUNAMI INUNDATION PROJECT:
SHORELINE MILES MAPPED--
ISLANDS OF HAWAII
1989-90

ISLAND	POPULATION (1987)	COAST MILES	MILES MAPPED*	% OF COAST MAPPED	POPULATION DENSITY**
O'ahu	877,000	177	177	100	2610
HAWAII	120,000	316	54	17	61
Maui	79,000	168	58	35	189
Kaua'i	60,000	113	95	84	282
Moloka'i	6,000	98	35	36	35
Lana'i	2,000	50	3	6	17
Totals/Avg.		922	422	46	

*Indicates development of maximum expectable inundation limits; plotted on appropriate maps

**Per square mile of inhabitable area

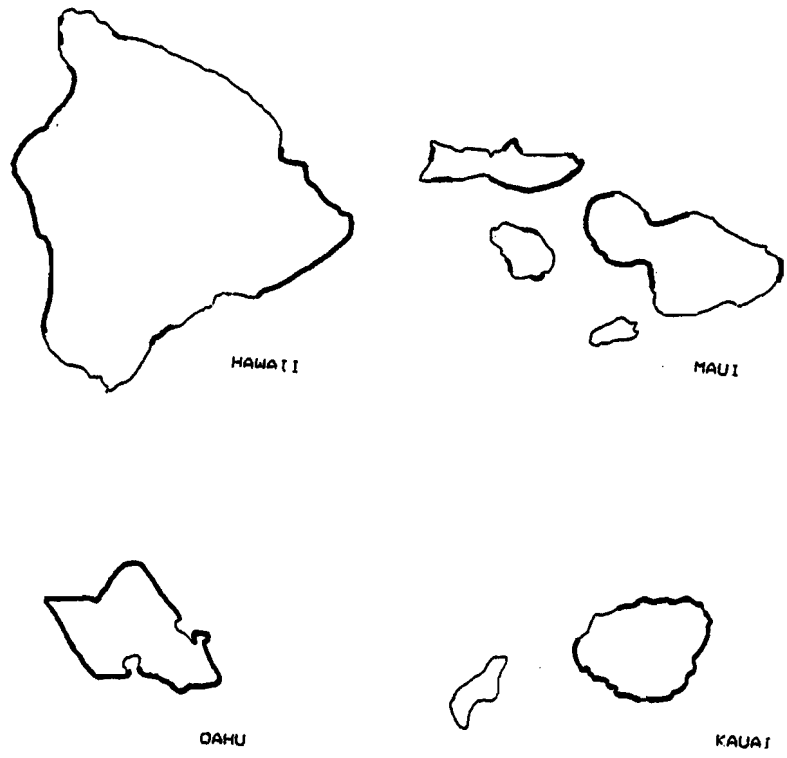

Fig. 6 Coastal Areas Covered

Additional Comments

The support of the State Civil Defense Office, the County Civil Agencies, and many other agencies, advisors, and sources is gratefully acknowledged. Some are listed in appendix E.

Appendix F lists papers published and presentations made to scientific organizations in connection with the project.

The FIRM maps have undergone revision in several areas in the past six years. Care should be taken to use the most current version in any comparisons of inundation or evacuation zones. The most recent revision includes hurricane flooding on the lee shores of Oahu and Kauai. The state has not agreed to include hurricane effects in the tsunami mapping; thus if they are again used for a hurricane evacuation a judicious safety factor should be included.

It should also be noted that the evacuation lines in airport areas were based by the counties only on safety and evacuation of people and do not consider airport/aircraft operations.

REFERENCES CITED

1. Minutes, "Tsunami Project Initial Meeting," JIMAR, Sept 12, 1988.

2. Houston, J. R., et al, "Tsunami-Wave Elevation Frequency of Occurrence for the Hawaiian Islands," Tech. Rpt. H-77-16, U.S. Army Corps of Engineers Waterways Experiment Station, Aug 1977.

3. "Manual for Determining Tsunami Runup Profiles on Coastal Areas of Hawaii," M & E Pacific for the Pacific Ocean Division, Corps of Engineers, August 1978.

4. Hwang, D., "Beach Changes on Oahu as Revealed by Aerial Photographs," Hawaii Institute of Geophysics and Urban Planning Program, University of Hawaii, July 1981.

5. "Hawaii's Shoreline," State Department of Planning and Economic Development, ca. 1965. (Similar, but newer atlases for Oahu and West Hawaii were also used).

6. Bretschneider, C. L. and P. G. Wybro, "Tsunami Inundation Prediction," Proc. of the 15th Conference on Coastal Engineering, ASCE, Ch60, 1976.

7. Mader, Charles L., "Numerical Tsunami Flooding-I," Science of Tsunami Hazards, Vol. 8, No. 1, 1990.

8. Curtis, George, "A Methodology for Developing Tsunami Inundation and Evacuation Zones," Proc. of the 4th Pacific Congress on Marine Technology, Tokyo, 1990.

9. Cox, Doak C., "Potential Tsunami Inundation Areas in Hawaii," Tsunami Research Program, Feb 1961. HIG Report No. 14.

GENERAL REFERENCES CONSULTED

Camfield, Fred, "Tsunami Engineering," U.S. Army Corps of Engineers CERC Special Report No. 6, Feb 1980.

Cox, Doak C., "Japanese Tsunamis in Hawaii--A Preliminary Report," UH Environmental Center SR:0025, 1980.

Cox, Doak C., "Tsunami Hazard at Ke-ahole Point, North Kona," UH Environmental Center SR:0028, 198?

Eaton, J.P., D. Richter, and W. Ault, "The Tsunami of May 23, 1960 on the Island of Hawaii," *Bull. of the Seismological Society of America*, 51(2):135-157, 1961.

FEMA, "Flood Insurance Study Guidelines and Specifications for Study Contractors," Federal Insurance Administration (FEMA) 37, 1985.

Houston, James and H. Lee Butler, "Numerical Model for Tsunami Inundation," Technical Report , Feb 1979. Hydraulics Laboratory, U.S. Army Engineer Waterways Experiment Station, Vicksburg, Mississippi.

Iida, K., D. Cox, and G. Pararas-Carayannis, "Preliminary Catalog of Tsunamis Occurring in the Pacific Ocean," HIG-67-10, Hawaii Institute of Geophysics, UH, 1967.

Iida, K. and T. Iwasaki, ed., Tsunamis: Their Science and Engineering, Tokyo: Terra Science Publishing Co. (HIG Library, 460 TSU), 1983.

Loomis, H. G., "Tsunami Wave Runup Heights in Hawaii," HIG-76-5, Hawaii Institute of Geophysics, UH, 1976.

Sea Engineering, Inc., "Shoreline Berm Runup and Stability Analysis--Hyatt Regency Waikoloa, Island of Hawaii," Report prepared for Belt, Collins, and Associates.

Shepard, F. P., G. A. MacDonald, and D. C. Cox, "The Tsunami of April 1946," Bull. Scripps Inst. of Oceanography, University of California, 5(6):391-528, 1950.

Appendix A

University of Hawaii at Manoa

Joint Institute for Marine and Atmospheric Research (JIMAR)
1000 Pope Road • Honolulu, Hawaii 96822
Cable Address: UNIHAW

December 9, 1988
(Rev. May 15, 1990)

To: Tsunami Team

From: George D. Curtis
Tsunami Specialist

Re: Tsunami Inundation/Evacuation Line and Zone Selection Procedure

Source Data

All known "run up," wave height, and inundation data are being compiled, annotated, and filed. Sea level references are included and questionable data noted. Source is shown where possible (original compiler or author). The written definitions and standards attached, are followed.

A primary source of wave height data is Houston's 1977 (revised) report. The numbers produced therefrom are checked against other sources at each available location. Note that Houston's numbers are either (1) statistical heights calculated for a small area from historical observations as compiled by Loomis in HIG-76-5, 1976 or (11) heights derived by interpolation and application of a model to the data. The numbers from (1) are generally driven by the 1946-57-60 events and can be checked against them. Checking those in (11) is a matter of judgement and primarily involves some knowledge of the topography in the area.

All wave height and runup data are maintained as referenced to MSL. A subsequent correction will be made for high tide.

Data from local tsunamis shall not be included. This is because examination of historical data shows that no evacuation is possible for such events via the formal warning systems. (This does not say inundation will not occur--only that where it is significant there will be no time for a warning and formal evacuation, and where there is time for a warning, the runup will not be noticeable).

Deriving the Inundation Limit

If inundation data are available (as in Hilo), the envelope of the 1946, 1957, and 1960 (and any other with a reliable higher limit) events is drawn, with an adjustment of +2 ft to 1946 and of +1 ft to 1960 MSL data to convert to high tide levels (MHHW). Where a Houston height only is available, the 200 year "return

time" will be used. The 200 year point (and the 46/57/60 envelope when available) will be shown on the plot for reference. The adjustment must of course be converted to horizontal limits. (see below)

If MSL runup height data are available, these would be applied to the topography with the above corrections.

In the usual case, only wave height data will be available (measured or calculated). In these cases, inundation will be determined by the method of Bretschneider and Wybro, as delineated in the M & E Pacific manual (use of the Corps of Engineers model installed at Ft. Shafter is being evaluated; it should produce similar results). The hard-to-resolve question is where to assume the wave heights were measured. Based on the evaluation of numerous reports, mostly by Cox, the following procedure will be followed:

1. If the slope appears steep enough that the land elevation exceeds the wave height in less than 200 ft., the intercept line will be used for an inundation limit (with tide adjustment)

2. If there is any record of where the wave height was measured, or if there appears to be a very likely location, that point shall be used.

3. If there are no clues or rationale to suggest another location, use 200' inland of the shoreline depicted on the Geological Survey maps.

4. Large-scale topo maps, the Huang beach report (Oahu), oblique photo slides, and personal observation may be used to aid in these decisions.

The points or line produced by this procedure should be plotted on a 1" = 1000' topo chart (or 1" = 2000' quad chart) and the line completed by interpolation, along contour lines. It should be plotted as a working drawing and so stamped. The same drawing should include where practical the FIRM line and the Cox line.

Notes of FIRM: The maps were revised in the early eighties, and only maps dated 1984 or later should be used. Earlier maps were often grossly misleading. Little information is available yet on the source of these errors. Note that these maps:

--Are supposed to be based on Houston's 100 year wave height and Bretschneider's runup

--Do not differentiate between river and ocean flooding and storm surge

--Are generally based on 200 ft inland runup measurements

Drawing the Final Line(s)

The high tide inundation limit, based on 46/57/60 envelope or Houston's 200 year wave is what is desired. We will refer to it as the "maximum expectable tsunami" height or limit. The gray zone in our calculations should be: "might people get their feet wet"?

We consider that some wetting from the highest wave on the maximum expectable tsunami might occur near the inundation limit defined by these procedures but this should be acceptable as:

--there would be no actual wave action (locations of bore formation are treated differently)

--any water at these locations would be much shallower than was considered acceptable (3 ft) on the old Federal flood insurance rate maps

--there would be no hazard to life

--vehicles could still move

--heavy rains also produce this sort of wetting

--in cooperation with County Civil Defense staffs, a final line will always be drawn mauka of our limit, located at physically identifiable landmarks

Special Considerations

Priority areas (those with high population density, recent development, previous errors, or evacuation routes/problems) will be treated first, and with the greatest care. These are defined in concert with the Counties.

Where direction-of-arrival data indicate a significant difference may be obtained in inundation area and limits, it shall be so plotted and made available to CD in selected, priority areas. These lines will not be used in public maps.

Additional Notes:

1. Manning's "n" will be selected via the Bretschneider, et al, 1978 User's Manual via photos, observation, etc. If in doubt, a lower value shall be used.

2. Where there are reports of a bore, both bore and non-bore calculations will be made and the higher value used.

INUNDATION COMPARISONS

Appendix B

LOCATION	YEAR	HISTORIC HEIGHT (in ft)	HISTORIC INUNDATION LIMIT (IL)	CALCULATED IL	MAX. EXPTD. IL	COMMENTS
Kahuku (airfield) m 27	1946	24	1800	2100	2600	Runup 21'
Punaluu m 39.5	1946	12	800	675	900	calc. 16% short
	1952	7	280	350		
Queen's Beach m 86	1946	13-15	300-600	700	800	Runup 19'
Waimanalo m 81	1946	8	300	310	420	Runup 7'
Waimea m 17.4	1946	18	280	410	440	Steep terrain
Sprecklesville m 73.5	1946	23	800	1350	1400	Runup 28'
Lower Paia m 75.5	1946	18	800	830	1026	
Haena						
m 20.2	1946	45	500	850	800	Steep end
m 21	1946	26	1500	1600	1700	of terrain
m 21.45	1946	34	2000	2800	2600	
Pakala Pt.	1946	32	750	700	800	
Hanamalu	1946	22	500	620	500	Runup 40'

Note: 1. m = coast mile on Corps of Engineers and FIRM maps
2. IL calculated for historic wave height
3. Maximum expected IL is per statistical procedure for "200 year" wave or greater

Appendix C

MAPS SUBMITTED TO CIVIL DEFENSE

AREA	BASE MAP	DATE SUBMITTED
OAHU		
HONOLULU		
KALANIANOLE, HAWAII(KAHALA-KOKO HEAD)	DLU MAP	5/9/89
WINDWARD COAST		
KAILUA, HAWAII(MOKAPU PT.-LANIKAI)	DLU MAP	3/19/90
WAIMANALO, HAWAII(BELLOWS AFB-HANAUMA BAY)	DLU MAP	3/19/90
KAAAWA, HAWAII(KAHANA BAY-KUALAO PT.)	DLU MAP	7/9/90
HAUULA, HAWAII(HALEIWA-PUNALUU)	DLU MAP	9/89
LEEWARD COAST		
MAKAHA, HAWAII(KAENA PT.-KEAAU)	USGS	3/19/90
MALI, HAWAII(KEAAU-NANAKULI)	USGS	3/19/90
NANAKULI, HAWAII(NANAKULI)	USGS	3/19/90
BARBERS PT., HAWAII(NANAKULI-BARBERS PT)	USGS	3/19/90
KAENA PT., HAWAII(HALEIWA-MAKAHA)	DLU MAP	4/6/90
WAIANAE, HAWAII(MAKAHA-NANAKULI)	DLU MAP	4/6/90
BARBERS PT., HAWAII(NANAKULI-BARBERS PT)	DLU MAP	4/6/90
EWA, HAWAII(BARBERS PT.-IROQUOIS PT.)	USGS	3/19/90
KAUAI		
LIHUE AREA		
LIHUE, HAWAII(AHUKINI CAMP-KAAMALA PT)	USGS	5/1/90
KAPAA, HAWAII(WAILUA RIVER-AHUKINI)	USGS	5/1/90
NAWILIWILI-LIHUE(HANAMAULU-COAST)	ORTH-PHOTO	5/1/90
NAWILIWILI-LIHUE(COAST OFF AIRPORT)	ORTH-PHOTO	5/1/90
NAWILIWILI-LIHUE(NININI PT.-KALAPAKI)	ORTH-PHOTO	5/1/90
NAWILIWILI-LIHUE(KALAPAKI-NIUMALU)	ORTH-PHOTO	5/1/90
KEKAHA TO KOLOA COAST		
KEKAHA, HAWAII(MANA PT-LAAUOKALA PT.)	USGS	5/21/90
HANAPEPE, HAWAII(POO PT-KOHEO PT.)	USGS	4/30/90
KOLOA, HAWAII(MAKAOKAHAI-MAKAHUENA PT.)	USGS	5/1/90
HAENA TO KILAUEA		
HAENA, HAWAII(KAILIU PT.-WAINIHA BAY)	USGS	9/5/89
HANALEI, HAWAII(WAINIHA BAY-KAUAPEA)	USGS	9/5/89
ANAHOL, HAWAII(KAUAPEA BEACH-KEPUHI)	USGS	7/6/90
MAUI		
WEST MAUI		
NAPILI, HAWAII(NAKALELE PT.-MAHINAHINA PT.)	USGS	11/7/89
LAHAINA, HAWAII(HONOKOWAI CAMP-LAUNIUPOKO PT.)	USGS	11/7/89
OLOWALU, HAWAII(AWALUA-MOPUA)	USGS	11/7/89
WAILUKU-PAIA		
WAILUKU, HAWAII(WAIHEE PT.-HOBRON PT.)	USGS	5/1/89
PAIA, HAWAII(KAHULUI AIRPORT-KUAU)	USGS	5/22/89
MAALAEA-WAILEA		
MAALAEA, HAWAII(PAPALAUA-WAIMAHAIHAI)	USGS	11/14/89
PUU O KALI, HAWAII(KALUAHAKOKO-LILIOHOLO)	USGS	11/14/89

AREA	BASE MAP	DATE SUBMITTED
LANAI / MOLOKAI		
LANAI		
LANAI, HAWAII(PAOPAO PT.-KAHEA)	USGS	9/25/89
LANAI, HAWAII(KAANAPAPA PT.-SHIPWRECK BEACH)	USGS	9/25/89
LANAI, HAWAII(KAUMALAPAU HARBOR-MAKOLE)	USGS	9/25/89
LANAI, HAWAII(HULOPOE BAY-HALEPALACE LANDING)	USGS	9/25/89
HULOPOE BEACH TO MANELE BAY	SPECIAL DWG	9/13/89
KAUMALAPAU HARBOR	SPECIAL DWG	9/25/89
MOLOKAI		
ILIO POINT, HAWAII(POHAKUMAULIULI-PUU KOAI & KAPUKUWAHINE-HALENA	USGS	5/22/89
KAUNAKAKAI, HAWAII(KALANIANAOLE COLONY -NALULUA & PUWAHI-KAUPIKIAWA)	USGS	5/22/89
KAMALO, HAWAII(KAPUKAULUA-KALUAAHA)	USGS	5/22/89
HALAWA, HAWAII(KALUAAHA-KAALAEA & LAMALOA HEAD-MOKUPAPAPA)	USGS	5/22/89
HAWAII		
HILO AREA		
HILO, HAWAII(ALEALEA PT.-LEWLEIWI PT.)	USGS	6/26/89
SOUTH KOHALA - NORTH KONA		
KAWAIHAE, HAWAII(KAAIHAE LIGHT-KAUNAOA BEACH)	USGS	4/89
PUU HINAI, HAWAII(KAUNAOA PT.-NANUKU INLET)	USGS	4/89
ANAEHOOMALU, HAWAII(MAKAIWA BAY-OHIKI BAY)	USGS	4/89
KIHOLO BAY, HAWAII(HOU PT.-KAHUWAI BAY)	USGS	4/89
MAKALAWENA, HAWAII(KUKIO BAY-ALOHA PT.)	USGS	4/89
MAHUKONA, HAWAII(MAKAOHULE PT-KAOMA PT)	USGS	10/29/90
UPOLU, HAWAII(KOKOKI-HONOIPU LANDING)	USGS	10/29/90
KAILUA KONA - MILOLII		
KAILUA, HAWAII(KAILUA BAY-KAHULUI)	USGS	3/26/90
KEALAKEKUA, HAWII(PUAPUAA PT.-NUENUE)	USGS	3/26/90
HONAUNAU, HAWAII(KEAWEKAHEKA PT.-PALIANIHI PT.)	USGS	3/26/90
MILOII, HAWAII(KIPAHOEHOE BAY-NIUOU)	USGS	3/26/90
HAMAKUA COAST		
LAUPAHOEHOE, HAWAII(LAUPAHOEHOE PT.-KILAU STREAM)	USGS	10/29/90
WAIPIO, HAWAII(WAIPIO BAY)	USGS	10/29/90
HAKALAU, HAWAII(HAKALAU BAY)	USGS	10/29/90
KAU		
HONUAPO, HAWAII(HANAKAULUA-HONUAPO BAY)	USGS	10/29/90
PUNALUU, HAWAII(KANEELEELE HEIAU-KOHAAHU)	USGS	10/29/90

Appendix D

University of Hawaii at Manoa

Joint Institute for Marine and Atmospheric Research (JIMAR)
1000 Pope Road • Honolulu, Hawaii 96822
Cable Address: UNIHAW

March 5, 1990

Mr. George Kekuna
Oahu Civil Defense Agency
650 S. King Street
Honolulu, HI 96813

Dear Mr. Kekuna:

As previously discussed, we have reviewed the existing recommendation in the telephone directory on vertical evacuation, particularly for Waikiki. I have also located a City Council Resolution, No. 86-340, requesting an update on the prior recommendation for vertical evacuation. We are now able to provide a positive and coordinated response.

As you know, in addition to consulting others here at U.H., I requested opinions from the Structural Engineers of Hawaii (SEOH) and the American Society of Civil Engineers (ASCE) Structural Technical Group. After review and meetings, both organizations responded favorably and their letters are enclosed.

Thus, we suggest wording on the map along these lines: "People in the Waikiki area should avoid moving through the streets. Steel and concrete buidings of six or more stories should provide adequate protection if people move to the third floor or above."

According to census data and state statistics, the de facto population of Waikiki is now approximately 120,000. Clearly, "vertical evacuation" is needed to the maximum extent, and I am glad we are able to affirm its feasibility as a safe measure.

Sincerely,

George D. Curtis
Tsunami Research Specialist

encl

cc: Norman Lamb

Appendix E

Key People Involved

State Civil Defense
Roy Price
Norman Lamb
Don Gransback

County Civil Defense Agencies

Cayetano Gerardo	Kauai
George Kekuna	Oahu
Frank Apel	Oahu
Sal Menor	Maui
Harry Kim	Hawaii
Bruce Butts	Hawaii

Corps of Engineers
Isa Minashima, Shafter Flats Map Office, ph. 438-9596
Willie Chang, Fort Shafter, Flood Control, ph. 438-2883
Steve Philbin, Emergency Response, ph. 438-1673
Fred Camfield, Waterways Experiment Station, Vicksburg

FEMA
John Burian, Baker, Inc. (contractor), ph. (703) 838-0400
Frank Tsai, ph. (202)646-2753

County Agencies
Oahu DLU, Alvah Kondo, ph. 523-4100
Maui DLU, Alan Shinamoto, ph. 243-7735
Maui Public Works-Ralph Nagamine, ph. 243-7845

Contractors, etc.
R. M. Towill, Doug Mukai, ph. 842-1133
M & E Pacific
Clarence Design; David Isaacs, ph. 941-5021

Military
Marvin Tung-Loong, PMRF-BS, ph. 471-6623
Milo Hoensheid-Navy Emergency Management, ph. 471-3084

University of Hawaii-Manoa
Bill Adams
Doak Cox
George Curtis
Gus Furumoto
Norm Lamb
Hal Loomis
Charles Mader
Joe Morgan
Mark Smaalders

University of Hawaii-Hilo
Walter Dudley

--and many others who helped

Appendix F

Papers Published

"Developing Tsunami Evacuation Zones for Hawaii" (with Mark Smaalders), Proc. Tenth Meeting, Big Island Science Conference, University of Hawaii, Hilo, April 1989.

"A Methodology for Developing Tsunami Inundation and Evacuation Zones," Pacific Congress on Marine Technology, Tokyo, July 1990; in Conference Proceedings.

"Maximum Expectable Inundation from Tsunami Waves," International Workshop on Long Wave Runup (NSF Sponsor), U.S.C. Marine Science Center, August 1990. Proceedings date: May 1991.

"Inundation and Tsunami Waves," Second U.S.-Japan Natural Resources Workshop on Tsunamis, Hilo and Honolulu, November 1990. Proceedings date: April 1991.

MODELING HILO, HAWAII TSUNAMI INUNDATION

Charles L. Mader
George Curtis
JTRE - JIMAR Tsunami Research Effort
University of Hawaii, Honolulu, HI., U.S.A.

ABSTRACT

The flooding of Hilo, Hawaii by the tsunamis of April 1, 1946, May 23, 1960 and March 28 1964 have been numerically modeled using the non-linear shallow water code *SWAN* including the Coriolis and friction effects. The modeling of each tsunami generation and propagation across the Pacific Ocean to the Hawaiian Island chain was modeled using a 20 minute grid of ocean depths. This furnished a realistic input direction and profile for the modeling of the tsunami interaction with the Hawaiian Islands on a 5 minute grid. The resulting wave profile and direction arriving outside Hilo Bay was used to model the tsunami wave interaction with the bay, harbor and town on a 100 meter grid. Each element of the grid was described by its height above or below sea level and by a DeChezy friction coefficient determined from the nature of the topography.

The 1946 and 1964 tsunamis were generated by earthquakes in Alaska. The 7.5 magnitude 1946 tsunami flooding of Hilo was much greater than the 8.4 magnitude 1964 tsunami. This was reproduced by the numerical model. The directionality of the tsunami from its source was the primary cause for the smaller earthquake resulting in greater flooding of Hilo. The 1960 tsunami was generated by an earthquake in Chile. The observed largest wave was the third bore-like wave. The numerical model reproduced this behavior. The observed levels of flooding for each event was reproduced by the numerical model with the largest differences occuring in the Reeds Bay area where the local topography is poorly described by a 100 meter grid. The observed levels of flooding at individual locations was not well described by the model. Since the front and back of a building at a particular location has been observed to have flooding levels varying by a factor of two, a higher resolution grid including the buildings will be required to describe the flooding at individual locations.

INTRODUCTION

The flooding of Hilo, Hawaii by the tsunamis of 1946, 1960 and 1964 was modeled using the *SWAN* non-linear shallow water code which includes Coriolis and frictional effects. The *SWAN* code is described in Reference 1. Most of the calculations were performed on an IBM PS/2 model 80 with 8 megabytes of memory. The 20 and 5 minute topography was obtained from the NOAA ETOPO 5 minute grid of the earth. The 100 meter grid topography and friction coefficients were obtained using available USGS and other topographic maps, photographs and reports.

The extent of flooding for each event is well documented; however the flooding at individual locations was strongly observer dependent. Often the reported flooding at individual locations varied by a factor of two between the different observers and whether the front or the back of a building was used to evaluate the flooding at a location. The available data sources were collected, and a range of flooding observed for each location determined.

A Hilo tsunami date was selected and the following calculations performed:

First - A 20 minute grid calculation of the North Pacific (and when required for the entire Pacific) was performed to model the tsunami generation and propagation to the region of the Hawaiian Island chain. The 20 minute North Pacific grid was from 120 E to 110 W and 10 N to 65 N and 390 by 165 cells. The wave profile arriving in the region of the chain was used to select a realistic input direction and profile for the second step.

Second - A 5 minute grid calculation of the tsunami wave from the first step interacting with the Hawaiian Island chain was performed. For the 1946 and 1964 tsunami the 5 minute Hawaiian Island grid was from 163 W to 154 W and 18 N to 24 N and 108 by 72 cells. The wave direction and profile arriving in the region of Hilo Bay was used to select a realistic input direction and profile for the third step.

Third - A 100 meter grid calculation of the tsunami wave from the second step interacting with Hilo Bay and Hilo harbor, and the resulting flooding was performed using the input wave direction and profile from the second step. The 100 meter Hilo Bay was 100 by 168 cells and the lower left grid corner was located at 155 degrees, 5 minutes, 40 seconds and 19 degrees, 42 minutes, 45 seconds.

The results of the calculations were compared with the available Hilo flooding levels for each event studied.

TSUNAMI of APRIL 1, 1946

The tsunami of April 1, 1946 was caused by an earthquake of 7.5 magnitude off the Aleutian islands at 53.5 N, 163 W, 12:29 GMT. with a second quake at 12:57 GMT. The source was located about 60 miles SW of Scotch Cap, Unimak Island where the tsunami destroyed the lighthouse and radio towers located more than 30 meters above sea level.

The tsunami arrived at Hilo at about 7:00 a.m. HST with a small crest followed by a large recession. The third wave was the largest. Using the first measurable half-wave period, the period was determined from the Honolulu tide gage to be 15 minutes as described by Green (Ref. 2.) No instrumental record of the tsunami at Hilo was made. The tide at the time of the tsunami was at 20 cm above MLLW and falling.

The earthquake source was estimated by Furamoto (Ref. 3) from the travel times to be 100 km wide and 350 km along the trench. Imaginary wavefronts from observation stations were projected back toward the tsunami source. The presumed source was within the region circumscribed by

the interacting wavefronts. A source with these dimensions was chosen which would result in a large negative initial wave at Hawaii and a run-up of 30 meters near Scotch Cap lighthouse. The source had a sharp dip of 20 meters along the trench on the deep ocean side and decreased linearly to 0 meters along the shallow ocean side of the source. For a 20 minute grid, a cross section consisted of cells of -20.0, -15.0, -10.0 -5.0 meters initial displacement.

The wave arriving north of the Hawaiian Islands was a 1.0 meter high, 1000 second period wave with an initial negative pulse. It arrived from the North with the highest energy directed at the islands. This wave was used as the source for the Hawaiian Island calculation.

The tsunami wave interacted with the Hawaiian Islands and refracted around the island of Hawaii such that the tsunami arrived from the North-East on the Hilo side of the island.

The wave arriving outside Hilo Bay had an initial negative amplitude of 2.0 meters and a 1000 second period, followed by four 1000 second period waves with amplitudes of 3 to 4 meters. This wave was used as the source of the Hilo Bay calculation.

The Hilo Bay calculation was performed for the entire bay for the wave starting from the North and from the North-East. The wave from the North refracted into a North-East wave as it interacted with the bay topography. Both calculations gave similar wave interaction and flooding in Hilo harbor.

The flooding was performed using a constant DeChezy friction coefficient of 30, and using the topography determined DeChezy coefficient array shown in Figure 1. The roughness coefficients for Hilo harbor and town were determined in the Look Lab Hilo Bay model study (Ref. 4). The coefficient of 60 is for open smooth areas, 40 for lava like surfaces, 30 for coral and rougher surfaces, 20 for scattered trees and buildings, 10 for buildings and closely spaced trees.

The calculated and observed inundation limits for Hilo are shown in Figure 2. The calculated and observed inundation limits agree to within the 100 meter grid resolution of the numerical model throughout most of the flooded region.

The calculated and observed flooding levels at various locations in the harbor are listed in Table 1 and shown graphically in Figure 3. The flooding levels are strongly dependent upon the friction. A constant friction model is inadequate to describe either the limits of inundation or the flood levels at individual locations. The numerical model does not exhibit the observed large variability in flooding at different locations. The 100 meter grid is inadequate to resolve local effects of topography or friction that are important at individual locations. The hydraulic model reproduces the observed local flooding levels better than the numerical model. The model values were obtained using the hydraulic model of Hilo at Look Laboratories reported in references 5 and 6.

TSUNAMI of MARCH 28, 1964

The tsunami of March 28, 1964 was caused by an earthquake of 8.4 magnitude in Alaska near Prince William sound at 61 N, 147.5 W, 13:36 GMT.

The tsunami arrived at Hilo at about 17:30 HST with a crest followed by other crests. The second wave was the largest. Using the first measurable half-wave period, the period was determined from the Hilo tide gage to be 50 minutes. A record of the tsunami off Wake island in 800 feet of water was made by Van Dorn (Ref. 7). The wave observed at Wake Island was 15 cm high with a 50 minute period. The tide at the time of the tsunami was at 30 cm above MLLW and rising.

The earthquake source was studied in detail by Plafker (Ref. 8.). The formation of the tsunami

and its interaction (not flooding) with Hilo Bay was modeled by Hwang and Divoky (Ref. 9 and 10). The tsunami was also modeled by Houston, Whalin, Garcia, and Butler (Ref. 11).

The source was 300 km wide and 800 km long aligned along a SW-NE direction. The source was 7 cells wide. The initial amplitudes from ocean to land had heights of +5.0, +9.0, +10.0, +9.0, +5.0, +1.0, -2.0 meters. This source resulted in a wave at Wake Island similar to that observed by Van Dorn (Ref. 7).

The wave arriving north of the Hawaiian Islands was much weaker than for the 1946 tsunami. The wave had a profile of a 0.50 meter high, half-wave with a period of 4000 sec, followed by a 0.1 meter high half-wave with a period of 2000 sec, then by a 0.25 meter high full wave with a period of 1750 sec.

The tsunami wave interacted with the Hawaiian Islands and refracted around the island of Hawaii such that the tsunami arrived from the North-East on the Hilo side of the island. The wave arriving outside Hilo Bay had an initial positive amplitude of 1.0 meters, 4000 second period half-wave, followed by a 1.0 meter 2000 second period half wave, then by a 1.0 meter, 1750 period full wave. This wave was used as the source for the Hilo Bay calculation.

The Hilo Bay calculation was performed for the entire bay for the wave starting from the North and from the North-East. The wave from the North refracted into a North-East wave as it interacted with the bay topography. Both calculations gave similar wave interaction and flooding in Hilo harbor.

The flooding was performed using a constant DeChezy friction coefficient of 30, and using the topography determined DeChezy coefficient array shown in Figure 1.

The calculated and observed inundation limits for Hilo are shown in Figure 4. The calculated and observed inundation limits are much smaller than for the April 1, 1946 tsunami. Throughout most of the flooded region the calculated model gave more inundation than was observed.

The calculated and observed flooding levels at various locations in the harbor are listed in Table 2 and shown graphically in Figure 5. The flooding levels are strongly dependent upon the friction. A constant friction model is inadequate to describe either the limits of inundation or the flood levels at individual locations. The numerical model does not exhibit the observed large variability in flooding at different locations. The 100 meter grid is inadequate to resolve local effects of topography or friction that are important at individual locations. The hydraulic model reproduces the observed local flooding levels better than the numerical model.

The 1946 and 1964 tsunamis were generated by earthquakes in Alaska. The 7.5 magnitude 1946 tsunami flooding of Hilo was much greater than the 8.4 magnitude 1964 tsunami. This was reproduced by the numerical model. The directionality of the tsunami from its source was the primary cause for the smaller earthquake resulting in greater flooding of Hilo. The 1946 tsunami wave peak energy was directed toward Hawaii while the 1964 tsunami wave peak energy was directed east of Hawaii toward the Pacific coast of North America. The large waves observed at Crescent City for the 1964 tsunami and not for the 1946 tsunami are consistent with this directionality difference.

TSUNAMI of MAY 23, 1960

This study required development of a full North and South Pacific grid to determine the nature of the wave arriving at Hilo from South America. A one degree grid from 110 E to 65 W and 65 S to 65 N of 185 by 130 cells and a 20 minute grid of 555 by 390 cells was developed. The one degree grid could only resolve the source with a two cell wide source and gave waves with

periods two times larger than observed. So the 20 minute grid tsunami wave profiles were used to describe the 1964 tsunami.

The tsunami of May 23, 1960 was caused primarily by an earthquake at 19:11 GMT on May 22, 1960 of 8.5 magnitude occurring near Peru, Chile and centered at 38 N and 73.5 W. The major earthquake was preceeded by two 7.5 magnitude quakes at 10:03 and another at 19:10 GMT.

The main tsunami wave crested at Hilo at 12:13 a.m. HST on May 23. The first wave peak was followed by a second peak at 12:46 a.m. then by a third peak (a bore at the harbor entrance) about 20 minutes later which was more than twice as high as the previous waves. This wave was the highest and most destructive tsunami wave in Hilo's history.

The tide at 12:07 a.m. HST was at 60 cm above MLLW and increasing. By the time the largest third and fourth waves arrived the tide was cresting at 70 cm above MLLW.

The earthquake was studied by Plafker and Savage (Ref. 12). The formation of the tsunami and its propagation across the Pacific Ocean toward Hawaii was numerically modeled by Hwang and Divoky (Ref. 9). They concluded that peak wave heights occur along a path roughly normal to the major axis of the elongated source region. They suggested that the preferential directivity may account for the severity of the Chilean tsunami in Japan.

The source was 6 cells or 150 km wide and 21 cells or 800 km long aligned along a N-S direction. The source was six cells wide and an initial upward displacement of 1,2,4,6,4,-2 meters along the width. The waves arrived at the Hawaiian Island chain from the South-East. The wave had a profile of a 0.225 meter high, 3000 second half wave followed by a 0.525 meter high 1500 second wave and then followed by a 0.49 meter high 1500 second wave. The wave that arrived at Johnson Island was similar to the wave reported by Van Dorn (Ref 7).

The 5 minute Hawaiian Island grid was from 170 W to 140 W and 15 N to 25 N and 360 by 120 cells. The tsunami wave interacted with the Hawaiian Islands and refracted such that the wave arrived from the East on the Hilo side of the island. The wave arriving outside Hilo Bay had an initial amplitude of 0.4 meter and a period of 3000 second for 1500 sec, followed by a 1.5 meter 1500 second wave, and then by a 2.0 meter 1500 second wave.

The flooding was performed using a topography determined DeChezy coefficient. The roughness coefficients for Hilo harbor and town were determined by the Look Lab Hilo Bay model study and is shown in Figure 1.

The calculated and observed inundation limits for Hilo are shown in Figure 6. The calculated and observed inundation limits agree to within the 100 meter grid resolution of the numerical model throughout most of the flooded region with the calculated model giving more inundation than observed between Reeds Bay and Pier 2.

The calculated and observed flooding levels at various locations in the harbor are listed in Table 3 and shown graphically in Figure 7. The numerical model does not exhibit the observed large variability in flooding at different locations. The 100 meter grid is inadequate to resolve local effects of topography or friction that are important at individual locations. The hydraulic model reproduces the observed local flooding levels better than the numerical model.

The calculated third wave was largest and steepest in agreement with the observations although the difference in amplitude between the second and third wave is not as large as observed.

The numerical modeling results support the suggestion of Hwang and Divoky that the preferential directivity accounts for the severity of the Chilean tsunami in Hawaii and Japan. The interaction of the tsunami wave with Hilo Bay resulted in modifying the amplitude of the waves from the second being the largest to the third being the largest, steepest and most bore-

like. The wave arriving at Wake Island exhibited none of these characteristics. The interaction of tsunami waves with Hilo Bay is strongly dependent upon their period and their interaction with bay topography and with each other. The relative amplitude and steepness of the waves outside of Hilo Bay may be quite different from the waves flooding the town of Hilo.

CONCLUSIONS

The flooding of Hilo, Hawaii by the tsunamis of April 1, 1946, May 23, 1960 and March 28 1964 have been numerically modeled using the non-linear shallow water code SWAN including the Coriolis and friction effects. The modeling of each tsunami generation and propagation across the Pacific Ocean to the Hawaiian Island chain followed by modeling of the tsunami interaction with the Hawaiian islands on a finer grid and then modeling the tsunami wave interaction with the bay, harbor and town using a high resolution grid results in inundation limits that reproduce the essential features of the actual inundation limits.

The 1946 and 1964 tsunamis were generated by earthquakes in Alaska. The 7.5 magnitude 1946 tsunami flooding of Hilo was much greater than the 8.4 magnitude 1964 tsunami. This was reproduced by the numerical model. The directionality of the tsunami from its source was the primary cause for the smaller earthquake resulting in greater flooding of Hilo. The 1960 tsunami was generated by an earthquake in Chile. The observed largest wave was the third bore-like wave. The numerical model reproduced this behavior. The observed levels of flooding for each event was reproduced by the numerical model with the largest differences occuring in the Reeds Bay area where the local topography is poorly described by a 100 meter grid. The observed levels of flooding at individual locations was not well described by the model. Since the front and back of a building at a particular location has been observed to have flooding levels varying by a factor of two, a higher resolution grid including the buildings will be required to describe the flooding at individual locations.

Acknowledgments

The authors gratefully acknowledge the contributions of Dr. Gus Furamoto, Dr. Harold Loomis, Dr. Lester Spielvogel, Dr. Doak Cox, Dr. Dennis Moore, Dr. Eddie Bernard, Dr. Walter Dudley, Dr. George Carrier, and Dr. Frank Gonzalez. George Nabashima generated the 100 meter grids. The encouragement and support by the members of the Pacific Tsunami Warning Center is also gratefully acknowledged.

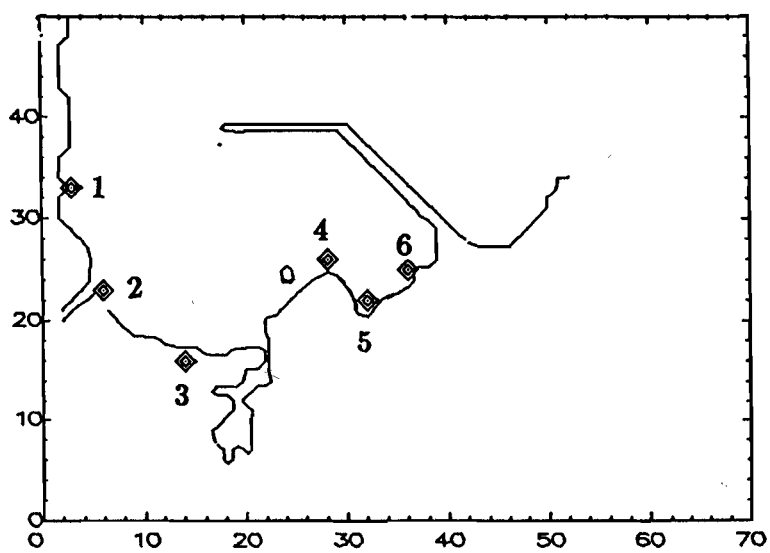

1 Hilo Sugar Mill
2 Wailuku Bridge
3 Theater
4 Waiakea
5 Reeds Bay
6 Pier

TABLE 1

April 1, 1946 Tsunami

Number	Location	Observed	Constant Friction	Topographic Friction	Look Lab Model
1	Hilo Sugar Mill	7.6	9.5	6.2	
2	Wailuku Bridge	7.3-8.5	8.7	5.8	6.1
3	Theater	6.1-8.5	9.0	6.6	
4	Waiakea	6.7-7.9	6.8	4.8	4.2
5	Reeds Bay	2.4-3.0	8.0	5.7	2.4
6	Pier 2	5.8	7.0	6.0	3.4

TABLE 2

March 28, 1964 Tsunami

Number	Location	Observed	Constant Friction	Topographic Friction	Look Lab Model
1	Hilo Sugar Mill		2.8	1.9, 2.0	
2	Wailuku Bridge	1.8	3.0	2.0, 2.1	2.7
3	Theater	0.0	2.9	2.0, 2.0	0.0
4	Waiakea	1.5	3.0	2.5, 3.0	1.8
5	Reeds Bay	2.1	3.0	2.6, 3.5	2.3
6	Pier 2	2.4	3.0	2.5, 3.5	2.1

TABLE 3

May 23, 1960 Tsunami

Number	Location	Observed	Topographic Friction	Look Lab Model
1	Hilo Sugar Mill	4.6-6.1	3.7	6.7
2	Wailuku Bridge	4.3-5.8	4.5	3.8
3	Theater	6.7-8.5	4.5	7.6
4	Waiakea	4.6-6.1	4.2	3.5
5	Reeds Bay	2.7-3.7	4.9	4.1
6	Pier 2	3.6-4.3	5.0	4.4

REFERENCES

1. Charles L. Mader *Numerical Modeling of Water Waves,* University of California Press, Berkeley, California (1988).
2. C. K. Green, "Seismic Sea Wave of April 1, 1946 as Recorded on Tide Gauges," Transactions of 1946 of American Geophysical Union, Vol 27, no 4, 490-502 (1946).
3. A. S. Furamato, private communication (1991).
4. Hilo Harbor Model Conference on 23-24 November 1964 at Look Laboratory of Oceanographic Engineering, Honolulu, HI, Corps of Engineers, U. S. Army Engineer District, Honolulu.
5. "Advanced Information for Participants Hilo Harbor Model Conference on 23-24 November 1964 at Look Laboratory of Oceanography, Honolulu, HI" by U. S. Army Engineering District, Honolulu, HI.
6. "Physically Feasible Means for Protecting Hilo from Tsunamis," Third Report of the Hilo Technical Tsunami Advisory Council to the Board of Supervisors, Hawaii County through its Tsunami Advisory Committee,' December 31, 1965. The committee was Doak C. Cox, Masashi Hom-ma, Masatsugu Suzuki, Ryutaro Takahasi and Robert L. Wiegel.
7. William G. Van Dorn,"Tsunami Response at Wake Island," Journal of Marine Research, Vol 28, no 3, 336-344 (1970).
8. G. Plafker, "Tectonics of the March 27, 1964 Alaska Earthquake" U. S. Geological Survey Professional Paper 543-I, I1-I74 (1969).
9. Li-San Hwang and D. Divoky. "Numerical Investigations of Tsunami Behavior," Tetra Tech, Inc. report (1975).
10. "A Numerical Model of the Major Tsunami," THE GREAT ALASKA EARTHQUAKE OF 1964, National Academy of Sciences (1972).
11. James. R. Houston, Robert W. Whalin, Andrew W. Garcia, H. Lee Butler, "Effect of Source Orientation and Location in the Aleutian Trench on Tsunami Amplitude along the Pacific Coast of the Continental United States" Research Report H-75-4 of U. S. Army Engineering Waterways Experiment Station, Vicksburg, Miss.
12. G. Plafker, and J. C. Savage, "Mechanism of the Chilean Earthquakes of May 21 and 22, 1960", Geological Society of America Bulletin, Vol 81, p 1001-1030 (1970).

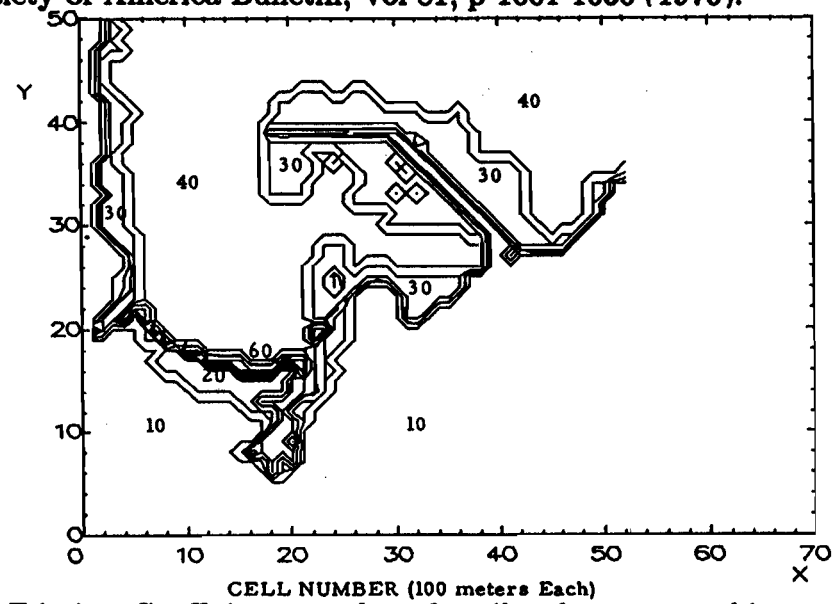

Fig 1. The DeChezy Friction Coefficients used to describe the topographic roughness in Hilo Bay, harbor and town.

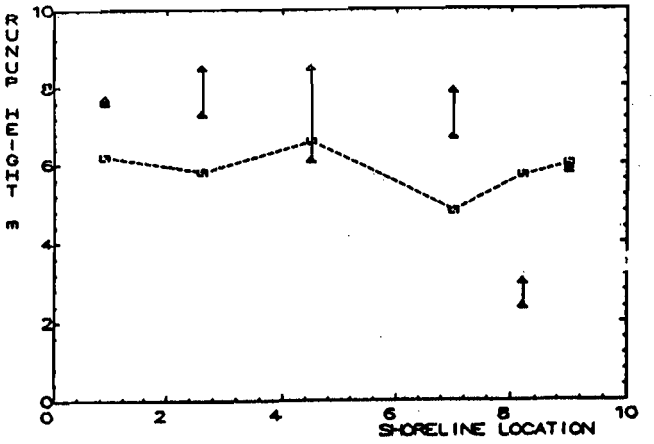

Figure 3. The calculated and observed flooding levels for the April 1, 1946 tsunami at various locations along the shoreline.

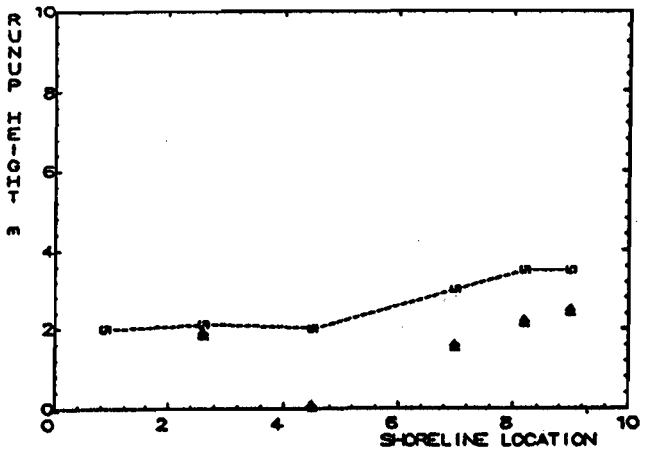

Figure 5. The calculated and observed flooding levels for the March 28, 1964 tsunami at various locations along the shoreline.

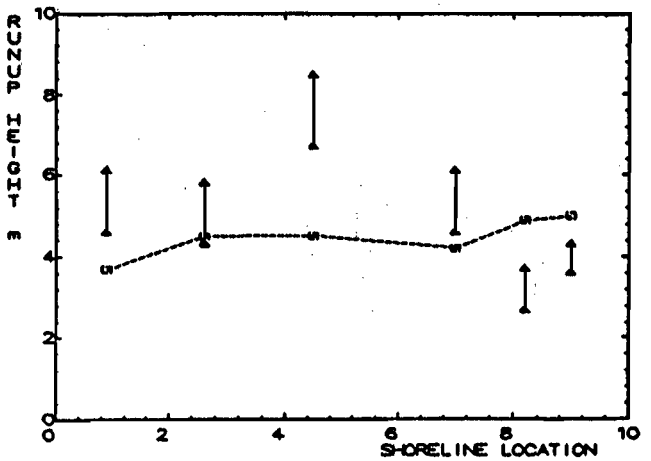

Figure 7. The calculated and observed flooding levels for the May 23, 1960 tsunami at various locations along the shoreline. The locations from left to right are Hilo Sugar Mill, Wailuku Bridge, Theater, Waiakea, Reeds Bay, and Pier 2.

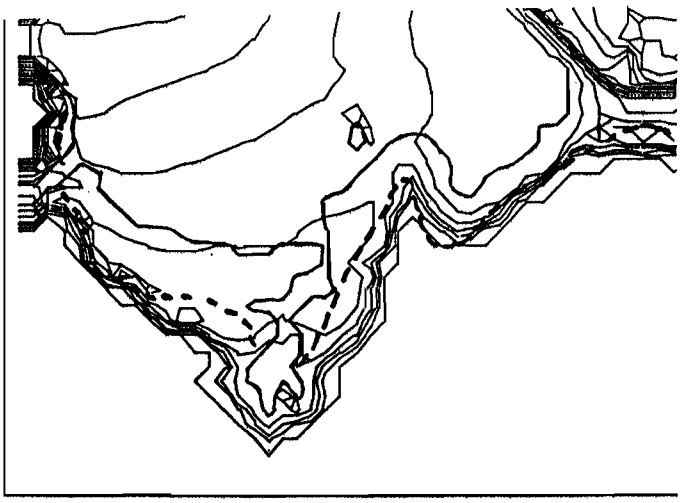

Fig 2. The calculated and observed Hilo inundation limits for the tsunami of April 1, 1946. The observed limit is the heavy dashed line.

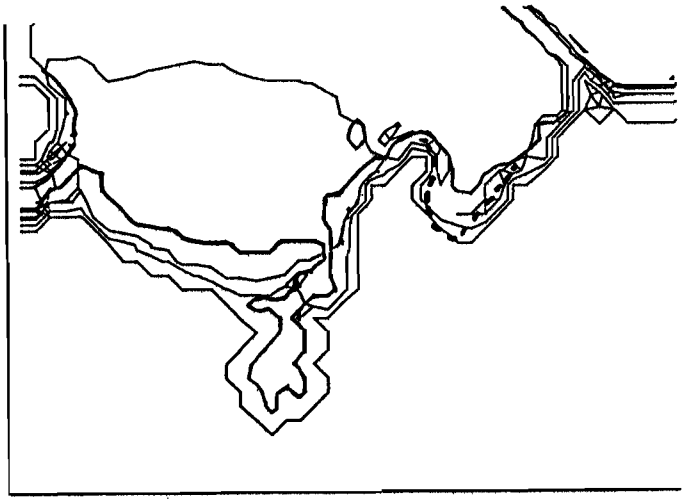

Fig 4. The calculated and observed Hilo inundation limits for the tsunami of March 28, 1964. The observed limit is the heavy dashed line.

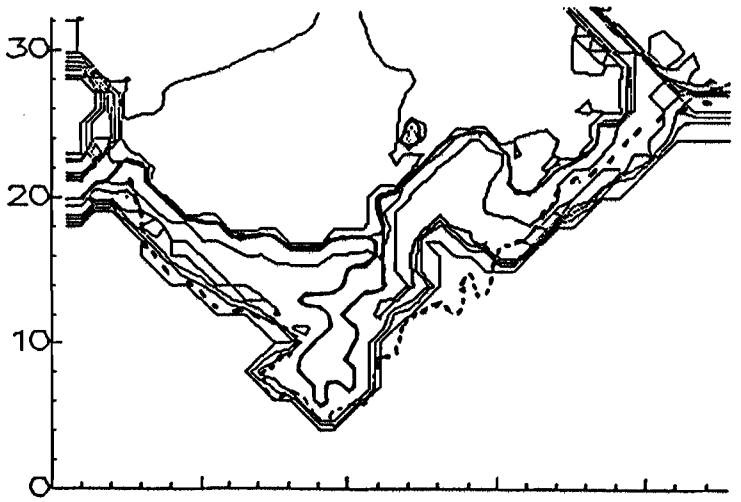

Fig 6. The calculated and observed Hilo inundation limits for the tsunami of May 23, 1960. The observed limit is the heavy dashed line.

MODELING TSUNAMI FLOODING OF HILO, HAWAII

Charles L. Mader, George D. Curtis, and George Nabeshima
University of Hawaii
Honolulu, Hawaii, U.S.A.

ABSTRACT

The interaction of tsunami waves with Hilo Bay and harbor is being numerically modeled for specific historical events. The modeling is performed using the *SWAN* code which solves the nonlinear long wave equations.

The 1946, 1960 and 1964 tsunamis are being studied. The tsunami generation and propagation to the Hawaiian Islands were modeled using a 20 minute grid for the North Pacific or for the entire Pacific Ocean. The wave arriving in the region of the Hawaiian Islands was then modeled using a 5 minute grid to follow the wave to the mouth of Hilo Bay. The wave arriving at the mouth of Hilo Bay was then modeled using a 100 meter grid of Hilo Bay, harbor and town. Each grid had a friction coefficient to describe the local roughness (trees, grass, buildings, coral, etc.). The models gave approximately the observed maximum areas of flooding.

The observed levels of flooding at individual locations was not well described by the 100 meter grid, so a 10 meter grid of Hilo was developed to resolve the flooding at individual locations and around large buildings.

The high resolution 10 meter grid of Hilo was used to model the flooding around Hilo Theater by the 1960 tsunami wave. The Hilo Theater was located near the shore, in flat and unobstructed terrain 2.7 meters above sea level. The tsunami flooded level reached 8.5 meters at the seaward side and 6.7 meters at the rear of the Hilo Theater. The third bore-like wave arriving at the harbor entrance in the 100 meter grid model was used as the tsunami source for the high resolution study of flooding around Hilo Theater. The maximum level of flooding observed at Hilo Theater was reproduced by the high resolution numerical model.

THE NUMERICAL MODEL

The tsunami waves and their interaction with the study site topography were numerically modeled using the *SWAN* code which solves the shallow water long wave equations. It is described in detail in the monograph *Numerical Modeling of Water Waves* by Mader (1988).

The long wave equations solved by the *SWAN* code are

$$\frac{\partial U_x}{\partial t}+U_x\frac{\partial U_x}{\partial x}+U_y\frac{\partial U_x}{\partial y}+g\frac{\partial H}{\partial x}=FU_y+F^{(x)}-g\frac{U_x(U_x^2+U_y^2)^{1/2}}{C^2(D+H-R)},$$

$$\frac{\partial U_y}{\partial t}+U_x\frac{\partial U_y}{\partial x}+U_y\frac{\partial U_y}{\partial y}+g\frac{\partial H}{\partial y}=FU_x+F^{(y)}-g\frac{U_y(U_x^2+U_y^2)^{1/2}}{C^2(D+H-R)},$$

and

$$\frac{\partial H}{\partial t} + \frac{\partial (D+H-R)U_x}{\partial x} + \frac{\partial (D+H-R)U_y}{\partial y} - \frac{\partial R}{\partial t} = 0 ,$$

where

U_x	=	velocity in x direction (i index)
U_y	=	velocity in y direction (j index)
g	=	gravitational acceleration
t	=	time
H	=	wave height above mean water level
R	=	bottom motion
F	=	Coriolis parameter
C	=	coefficient of DeChezy for bottom stress
$F(x), F(y)$	=	forcing functions of wind stress and barometric pressure in x and y direction
D	=	depth.

As described in the monograph, the *SWAN* code has been used to study the interaction of tsunami waves with continental slopes, shelves, bays and harbors such as Hilo harbor.

The *SWAN* code has been used to study the interaction of tsunami waves with continental slopes and shelves, as described in Mader (1974). Comparison with two-dimensional Navier-Stokes calculations of the same problems showed similar results, except for short wavelength tsunamis.

The SWAN code was used to model the effects of tides on the Musi-Upang estuaries, South Sumatra, Indonesia, by Hadi (1985). The computed tide and water discharge were in good agreement with experimental data.

The *SWAN* code was used to model the large waves that were observed to occur inside Waianae harbor under high surf conditions in Mader and Lukas, (1985). These waves have broken moorings of boats and moved boats up the boat-loading ramps into the parking lot. The numerical model was able to reproduce actual wave measurements. The *SWAN* code was used to evaluate various proposals for decreasing the amplitude of the waves inside the harbor. From the calculated results, it was determined that a significant decrease of the waves inside the harbor could be achieved by decreasing the harbor entrance depth. Engineering companies used these results to support their recommendations for improving the design of the harbor.

The effect of the shape of a harbor cut through a reef on mitigating waves from the deep ocean was studied using the *SWAN* code in Mader, et al. (1986). A significant amount of the wave energy was dissipated over the reef regardless of the design of the harbor. The reef decreased the wave height by a factor of 3. The wave height at the shore can be further decreased by another factor of 2 by a 'V'-shaped or parabolic bottom shape.

Other examples of applications of the *SWAN* code are presented in Mader and Lukas (1984). They include the wave motion resulting from tsunami waves interacting with a circular and triangular island surrounded by a 1/15 continental slope and from surface deformations near the island. The effects of a surface deformation in the Sea of Japan similar to that of the May 1983 tsunami was modeled. The interaction of a tsunami wave with Hilo Bay was described.

The *SWAN* code was used to model the effect of wind and tsunami waves on Maunalua Bay, Oahu as described in the State Department of Transportation draft (1988). The calculated wave behavior at any location in the bay was a function of complicated and time varying wave reflections and interactions.

The *SWAN* code was used to model the interaction of waves with a site near the Mauna Lani Resort on the South Kohala Coast on the Island of Hawaii in Mader (1990a). The calculated results agreed with the results obtained using the procedures developed and applied for flood insurance purposes by the U. S. Army Corps of Engineers and the recent JIMAR study at the University of Hawaii of tsunami evacuation zones for the site.

The 1987-88 Alaskan Bight tsunamis were modeled in Gonzalez, et al. (1990) using the *SWAN* code. The deep sea pressure gauge measurements for those tsunamis could be described using realistic source models for the tsunamis.

A numerical study of effect of the shallow water approximation on tsunami flooding was performed in Mader (1990b). Calculations using the full Navier-Stokes model were compared to *SWAN* code calculations.

The 1946 and 1964 tsunamis were caused by Alaskan earthquakes and the 1960 tsunami by an earthquake in Chile. The 1946 and 1960 tsunamis resulted in extensive flooding of Hilo while the 1964 tsunami caused limited flooding.

The tsunami generation and propagation to the Hawaiian Islands were modeled using a 20 minute grid for the North Pacific or for the entire Pacific Ocean (Mader and Curtis, 1991). The wave arriving in the region of the Hawaiian Islands was then modeled using a 5 minute grid to follow the wave to the mouth of Hilo Bay. The wave arriving at the mouth of Hilo Bay was then modeled using a 100 meter grid of Hilo Bay, harbor and town. Each grid had a friction coefficient to describe the local roughness (trees, grass, buildings, coral, etc.). The use of computational grids of different grid sizes over different geographical domains to model tsunamis is similar to that reported by Kowalik and Whitmore (1991).

The models gave approximately the observed maximum areas of flooding. The large amount of flooding from the 7.6 magnitude 1946 Alaskan earthquake and small amount of flooding from the 8.5 magnitude 1964 Alaskan earthquake were reproduced by the numerical models. This demonstrated the large effect of wave directionality and the necessity of modeling the entire process of tsunami generation, propagation and flooding for each event.

The observed levels of flooding at individual locations was not well described by the 100 meter grid, so a 10 meter grid of Hilo was developed to resolve the flooding at individual locations and around large buildings.

APPLICATION OF THE NUMERICAL MODEL TO INUNDATION OF HILO THEATER

The high resolution 10 meter grid of Hilo was used to model the flooding around Hilo Theater by the 1960 tsunami wave. The Hilo Theater was located near the shore, in flat and unobstructed terrain 2.7 meters above sea level. The tsunami flooded level reached 8.5 meters at the seaward side and 6.7 meters at the rear of the Hilo Theater. A photograph of the Hilo Theater after the May 1960 tsunami is shown in Figure 1.

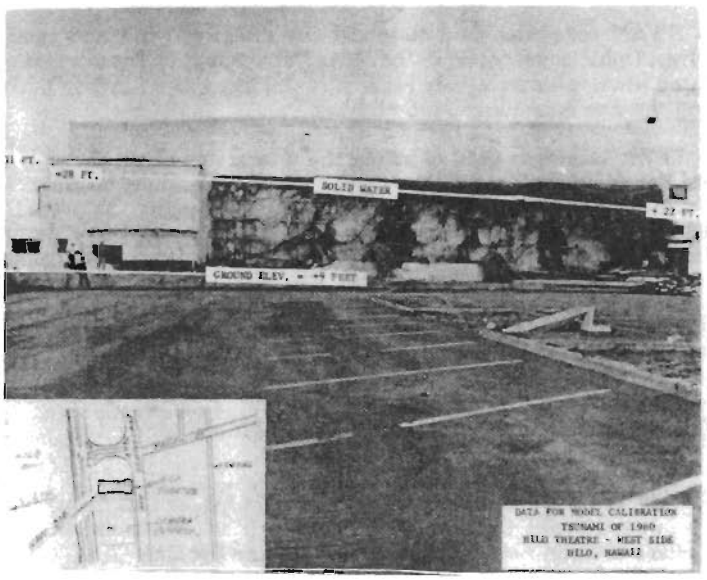

Figure 1. The Hilo Theater after the 1960 tsunami. The solid water water line is 28 to 22 feet above sea level. The building is located 9 feet above sea level. The inset shows the location of the theater relative to the shore line. The photograph is taken from the parking lot on the west side of the building. Note the four men standing on the right side of the photograph.

The grid was 240 by 240 cells of 10 meters on a side. The time step was 0.2 second. The theater building was described by 3 by 6 cells with a height of 11.9 meters. The third wave was a bore-like wave inside the harbor entrance 3 meter high from the North-West. The initial water level was 1 meter lower than the normal sea level to approximate the second wave recession that occurred before the third wave arrived. The wave had a period of 1500 seconds with the first rise occuring in 60 seconds to approximate the bore-like wave.

The surface level of the water, land and theater building is shown at various times in Figure 2. The contour interval is one meter. The building is 11.9 meters high.

The height of the water at locations near the harbor entrance and near the building as a function of time are shown in Figure 3. The front of the theater building (Location 5) was flooded to the 8.5 meter level and the rear of the building (Location 6) to the 8.0 meter level. The rear of the building was calculated to flood to a higher level than observed.

The inundation of the town of Hilo is shown in Figure 4. The inundation continues after the maximum flooding of the theater occurs. The maximum level of inundation calculated is similar to that observed from the 1960 tsunami.

The maximum levels of flooding observed at Hilo Theater was reproduced by the high resolution numerical model using a realistic description for the 1960 tsunami wave.

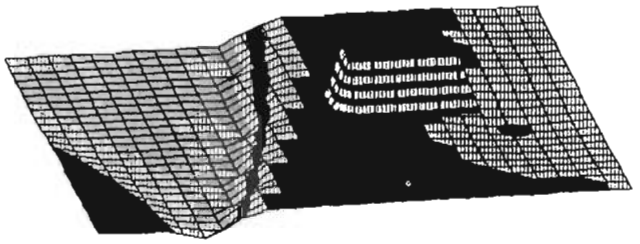

HEIGHT .25E+02sec, INC= .10E+01

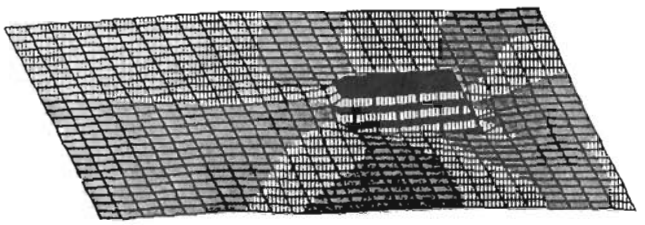

HEIGHT .12E+03sec, INC= .10E+01

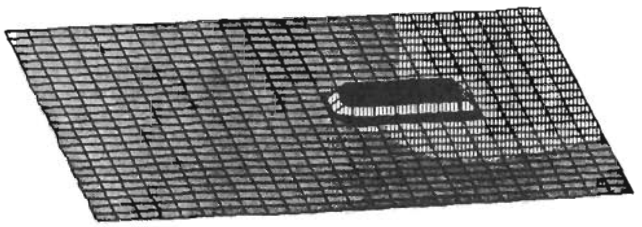

HEIGHT .30E+03sec, INC= .10E+01

Figure 2. The surface level of the water, land and theater building is shown at various times. The contour interval is one meter. The building is 11.9 meters high. The initial water surface is 1 meter below normal sea level to approximate the second wave withdrawal.

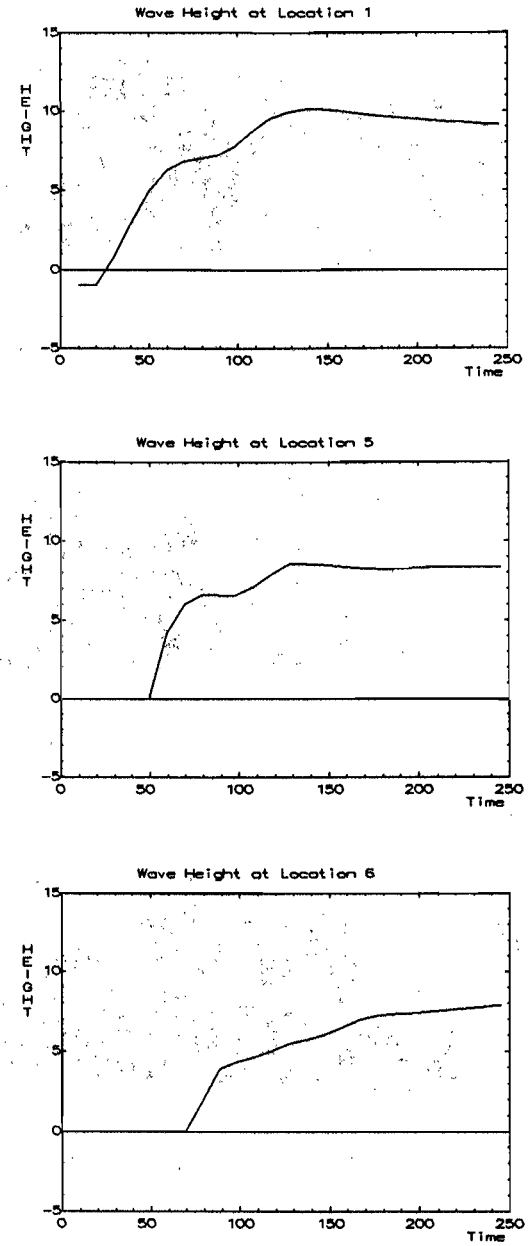

Figure 3. The height of the water at locations near the harbor entrance and near the building as a function of time are shown. Location 1 is in the ocean near the harbor entrance, Locations 5 and 6 are on the front and back of the side of the theater as shown in Figure 1.

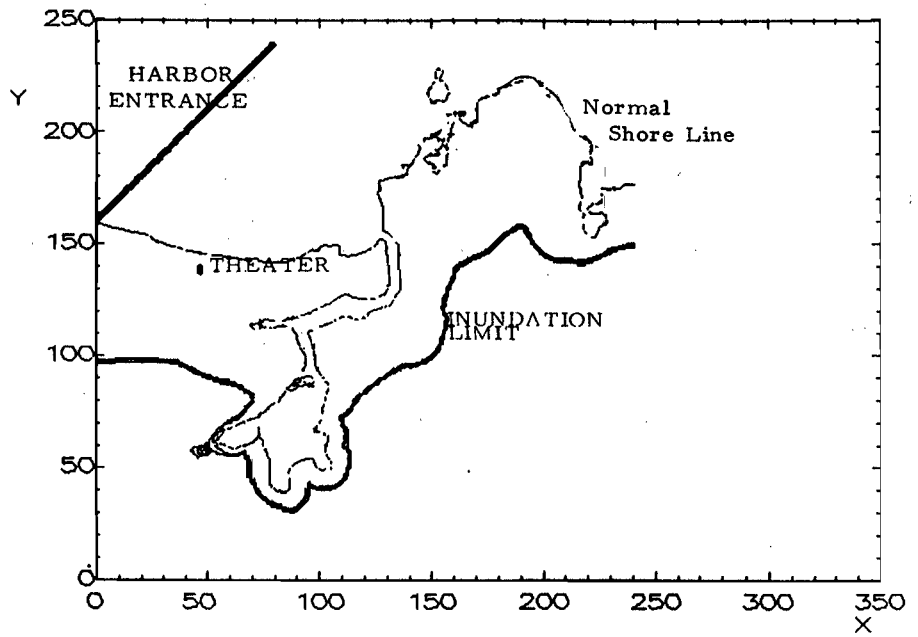

Figure 4. The inundation of the town of Hilo is shown. The inundation continues after the maximum flooding of the theater occurs. The location of the normal shore line and the theater building is also shown.

REFERENCES

Gonzalez, F.I., C.L. Mader, M.C. Eble, and E.N. Bernard. 1990. The 1987-88 Alaskan Bight tsunamis: deep ocean data and model comparisons. *Intl. J. Natural Hazards.* 4:119-140.

Hadi, S. 1985. A numerical tidal model of Musi-Upang estuaries. Ph.D. diss., University of Hawaii, Honolulu.

Kowalik, Z.K., and P.M. Whitmore. 1991. An investigation of two tsunamis recorded at Adak, Alaska. *Science of Tsunami Hazards.* 9:67-84.

Mader, C.L. 1988. Numerical Modeling of Water Waves. Berkeley: Univ. of California Press.

Mader, C.L. 1974. Numerical simulation of tsunamis. *J. Phys. Oceanography.* 4:74-82.

Mader, C.L. 1990a. Modeling tsunami flooding. In: Proc. Pacific Congress on Marine Science and Technology, PACON90. Honolulu: PACON Intl.

Mader, C.L. 1990b. Numerical tsunami flooding study - I. *Science of Tsunami Hazards.* 8:67-77.

Mader, C.L., and G. Curtis. 1991. Modeling Hilo, Hawaii tsunami inundation. *Science of Tsunami Hazards.* 9:85-94.

Mader, C.L. and S. Lukas. 1984. SWAN - a shallow water, long wave code: applications to tsunami models. Univ. Hawaii, Joint Institute for Marine and Atmospheric Research, Report JIMAR 84-077.

Mader, C.L., and S. Lukas. 1985. Numerical modeling of Waianae Harbor. In: Aha Hulikoa Hawaiian Winter Workshop Proc.

Mader, C.L., M. Vitousek, and S. Lukas. 1986. Numerical modeling of atoll reef harbors. In: Proc. of the Intl. Symp. on Natural and Man-Made Hazards, Rimouski .

State Department of Transportation, Harbors Division. 1988. Oahu Intraisland Ferry System - draft environmental impact statement.

A Leap-Frog Scheme for Linearized Boussinesq Equations

Yong-Sik Cho[1], Seung Nam Seo[2] and Philip L.-F. Liu[3]

Abstract

An explicit leap-frog finite differences scheme is proposed to obtain solutions for the linearized Boussinesq equations. The grid size, Δx, and the time step size, Δt, must satisfy the following relationship,

$$h^2 = \frac{(\Delta x)^2}{4}\left[1 - gh\frac{(\Delta t)^2}{(\Delta x)^2}\right]$$

where h is the depth and g is the gravitational accerlation. The scheme is stable when the Courant number, $C_r = \sqrt{gh}\Delta t/\Delta x$, is less than 0.866. Numerical results are compared with theoretical solutions. Excellent agreements are observed.

[1]Graduate Student, School of Civil and Environmental Engineering, Cornell University

[2]Principal Researcher, Korea Ocean Research and Development Institute, Korea

[3]Professor, School of Civil and Environmental Engineering, Cornell University

1. Introduction

Most of large-scale tsunamis are caused by undersea earthquakes. The extent of the fault of these earthquakes is usually very large, while the maximum vertical displacement of the seafloor is relatively small. The linear, nondispersive wave theory is, therefore, appropriate to describe the propagation of leading tsunami wave in the vicinity of generation area (Mei, 1989). However, when a tsunami propagates over a long distance the frequency dispersion becomes important (Kajiura and Shuto, 1990). Linear Boussinesq equations should be used to model the transoceanic propagation of a tsunami.

The linearized Boussinesq equations can be written as (e.g. Mei, 1989)

$$\eta_t + (hu)_x + (hv)_y = 0 \tag{1}$$

$$u_t + g\eta_x = \frac{h}{2}[(hu_t)_x + (hv_t)_y]_x - \frac{h^2}{6}(u_{tx} + v_{ty})_x \tag{2}$$

$$v_t + g\eta_y = \frac{h}{2}[(hu_t)_x + (hv_y)]_y - \frac{h^2}{6}(u_{tx} + v_{ty})_y \tag{3}$$

where $\eta(x,y,t)$ is the free surface displacement, g the gravitational acceleration, h water depth, u and v the depth-averaged velocities in the x- and y-direction, respectively and the subscripts represent the partial derivatives with respect to the variables. Eliminating u and v from equations (1) - (3), we obtain the following equation in terms of η.

$$\eta_{tt} - g(h\eta_x)_x - g(h\eta_y)_y - \left\{\frac{h^2}{2}[(h\eta_x)_x + (h\eta_y)_y]_x\right\}_x + \left[\frac{h^3}{6}(\eta_{xx} + \eta_{yy})_x\right]_x$$
$$- \left\{\frac{h^2}{2}[(h\eta_x)_x + (h\eta_y)_y]_y\right\}_y + \left[\frac{h^3}{6}(\eta_{xx} + \eta_{yy})_y\right]_y = 0 \tag{4}$$

For the constant depth case equation (4) can be simplified to

$$\eta_{tt} - gh(\eta_{xx} + \eta_{yy}) - \frac{gh^3}{3}(\eta_{xxxx} + 2\eta_{xxyy} + \eta_{yyyy}) = 0 \tag{5}$$

We remark here that the fourth derivatives in equation (5) are the frequency dispersion terms. If they are ignored, the Boussinesq equation is reduced to the wave equation, which can be derived directly from the linear shallow water equations.

To solve the linearized Boussinesq equations, equations (1) - (3), numerically, one can integrate them by using either a finite differences or a finite element method. Because the frequency dispersion terms in the Boussinesq equations have the highest order of differentiation, the accuracy of any numerical solutions depends on the technique used to approximate these terms and, in general, more computing time is needed for more accurate solutions. Therefore, solving the Boussinesq equations directly may not be the most economical approach for simulating a large-scale tsunami propagation.

An alternative method is to solve a set of lower order partial differential equations for η, u and v; e.g., linear shallow water equations. The numerical dispersion generated by the numerical scheme is then manipulated to represent the frequency dispersion terms, i.e., the higher derivative terms, in the linearized Boussinesq equations. For example, Imamura and Goto (1988) used an explicit leap-frog finite differences scheme for shallow water equations and determined a relationship between water depth, spatial and temporal mesh sizes so that the numerical dispersion terms mimic partially the frequency dispersion in the Boussinesq equations. In Imamura and Goto's (1988) formulation, the cross-differentiation term, η_{xxyy}, can not be recovered correctly. Liu and Yoon (1991) developed a finite element leap-frog scheme for shallow water equations and showed that the modified equation was indeed identical to the linear Boussinesq equations. However, the finite element scheme has a severe restriction on the time step size due to the stability condition. In this paper, we present a modified explicit finite differences scheme which gives the same dispersion relationship as that from the linear Boussinesq

equations. The stability condition of the proposed scheme is also investigated.

In Section 2, the explicit scheme used by Imamura and Goto (1988) is summarized first. A modified explicit leap-frog scheme is then proposed. The numerical characteristics of these two schemes are discussed. Numerical solutions of both explicit schemes for different initial conditions and boundary conditions are compared with the analytical solutions given by Carrier (1991) in Section 3. Finally, concluding remarks are given in Section 4.

2. Numerical Schemes

In this section, we first summarize the explicit finite differences leap-frog method employed by Imamura and Goto (1988). A modified explicit scheme is then proposed. The modified equations (Warming and Hyett, 1974) associated with each scheme are derived. The stability of the proposed scheme is also examined. In the following analysis, only the constant depth case is discussed.

2.1 Imamura and Goto's explicit leap-frog scheme

Denoting $P = uh$ and $Q = vh$ as the discharge in the x- and y-direction, we can rewrite the linear shallow water equations from equations (1) - (3) as

$$\eta_t + P_x + Q_y = 0 \tag{6}$$

$$P_t + gh\eta_x = 0 \tag{7}$$

$$Q_t + gh\eta_y = 0 \tag{8}$$

in which h is a constant depth. Imamura and Goto (1988) used the following staggered explicit leap-frog finite differences scheme.

$$\frac{\eta_{i,j}^{n+1/2} - \eta_{i,j}^{n-1/2}}{\Delta t} + \frac{P_{i+1/2,j}^{n} - P_{i-1/2,j}^{n}}{\Delta x} + \frac{Q_{i,j+1/2}^{n} - Q_{i,j-1/2}^{n}}{\Delta y} = 0 \tag{9}$$

$$\frac{P_{i+1/2,j}^{n+1} - P_{i+1/2,j}^{n}}{\Delta t} + gh\frac{\eta_{i+1,j}^{n+1/2} - \eta_{i,j}^{n+1/2}}{\Delta x} = 0 \tag{10}$$

$$\frac{Q_{i,j+1/2}^{n+1} - Q_{i,j+1/2}^{n}}{\Delta t} + gh\frac{\eta_{i,j+1}^{n+1/2} - \eta_{i,j}^{n+1/2}}{\Delta y} = 0 \tag{11}$$

As shown in figure 1, indices (i, j) and n denote spatial nodes and the time level, respectively. Δx and Δy represent the spatial step sizes in the x- and the y-direction, respectively and Δt stands for the temporal step size. The truncation errors in equations (9) - (11) are in the order of magnitude of $O((\Delta t)^2, (\Delta x)^2, (\Delta y)^2)$.

2.2 A modified explicit leap-frog scheme

We propose a modified staggered leap-frog finite differences scheme as follows:

$$\frac{\eta_{i,j}^{n+1/2} - \eta_{i,j}^{n-1/2}}{\Delta t} + \frac{P_{i+1/2,j}^{n} - P_{i-1/2,j}^{n}}{\Delta x} + \frac{Q_{i,j+1/2}^{n} - Q_{i,j-1/2}^{n}}{\Delta y} = 0 \tag{12}$$

$$\begin{aligned}&\frac{P_{i+1/2,j}^{n+1} - P_{i+1/2,j}^{n}}{\Delta t} + gh\frac{\eta_{i+1,j}^{n+1/2} - \eta_{i,j}^{n+1/2}}{\Delta x} \\ &+ \frac{\gamma gh}{12\Delta x}\left[(\eta_{i+1,j+1}^{n+1/2} - 2\eta_{i+1,j}^{n+1/2} + \eta_{i+1,j-1}^{n+1/2}) - (\eta_{i,j+1}^{n+1/2} - 2\eta_{i,j}^{n+1/2} + \eta_{i,j-1}^{n+1/2})\right] = 0\end{aligned} \tag{13}$$

$$\begin{aligned}&\frac{Q_{i,j+1/2}^{n+1} - Q_{i,j+1/2}^{n}}{\Delta t} + gh\frac{\eta_{i,j+1}^{n+1/2} - \eta_{i,j}^{n+1/2}}{\Delta y} \\ &+ \frac{\gamma gh}{12\Delta y}\left[(\eta_{i+1,j+1}^{n+1/2} - 2\eta_{i,j+1}^{n+1/2} + \eta_{i-1,j+1}^{n+1/2}) - (\eta_{i+1,j}^{n+1/2} - 2\eta_{i,j}^{n+1/2} + \eta_{i-1,j}^{n+1/2})\right] = 0\end{aligned} \tag{14}$$

where γ takes a value of one for the proposed algorithm. However, if γ is zero, equations (13) and (14) become the same as equations (10) and (11), respectively. The finite differences representation of the continuity equation remains the same in both schemes.

2.3 Numerical dispersion and modified equations

In this section, we investigate the numerical dispersion generated by the proposed scheme and by Imamura and Goto's scheme. Following the approach suggested by Warming and Hyett (1974), we apply Taylor series expansions of variables, η, P and Q at a node (n,i,j) to equations (12) - (14):

$$0 = \eta_t + P_x + Q_y + \frac{(\Delta t)^2}{24}\eta_{ttt} + \frac{(\Delta x)^2}{24}P_{xxx} + \frac{(\Delta y)^2}{24}Q_{yyy} + O\left((\Delta t)^4, (\Delta x)^4, (\Delta y)^4\right) \tag{15}$$

$$0 = P_t + \frac{\Delta x}{2}P_{xt} + \frac{\Delta t}{2}P_{tt} + \frac{(\Delta x)^2}{8}P_{xxt} + \frac{\Delta x \Delta t}{4}P_{xtt} + \frac{(\Delta t)^2}{6}P_{ttt} + gh\left[\eta_x + \frac{\Delta x}{2}\eta_{xx} + \frac{\Delta t}{2}\eta_{xt} + \frac{(\Delta x)^2}{6}\eta_{xxx} + \frac{\Delta x \Delta t}{4}\eta_{xxt} + \frac{(\Delta t)^2}{8}\eta_{xtt} + \frac{\gamma(\Delta x)^2}{12}\eta_{xxy}\right] + O\left((\Delta x)^3, (\Delta x)^2\Delta t, \Delta x(\Delta t)^2, (\Delta t)^3\right) \tag{16}$$

$$0 = Q_t + \frac{\Delta y}{2}Q_{yt} + \frac{\Delta t}{2}Q_{tt} + \frac{(\Delta y)^2}{8}Q_{yyt} + \frac{\Delta y \Delta t}{4}Q_{ytt} + \frac{(\Delta t)^2}{6}Q_{ttt} + gh\left[\eta_y + \frac{\Delta y}{2}\eta_{yy} + \frac{\Delta t}{2}\eta_{yt} + \frac{(\Delta y)^2}{6}\eta_{yyy} + \frac{\Delta y \Delta t}{4}\eta_{yyt} + \frac{(\Delta t)^2}{8}\eta_{ytt} + \frac{\gamma(\Delta y)^2}{12}\eta_{yyx}\right] + O\left((\Delta y)^3, (\Delta y)^2\Delta t, \Delta y(\Delta t)^2, (\Delta t)^3\right) \tag{17}$$

To derive modified equations from equations (15) - (17), all the higher time derivatives are replaced by the corresponding spatial derivatives. Because the truncation errors in equations (15) - (17) are of third order or higher, it is sufficient to keep only the leading order terms in the substitutions. Hence, we have

$$\begin{aligned} \eta_t &= -P_x - Q_y + O\left((\Delta x)^2, (\Delta y)^2, (\Delta t)^2\right) \\ P_t &= -gh\eta_x + O\left((\Delta x)^2, \Delta x \Delta t, (\Delta t)^2\right) \\ Q_t &= -gh\eta_y + O\left((\Delta y)^2, \Delta y \Delta t, (\Delta t)^2\right) \end{aligned} \tag{18}$$

$$\eta_{tt} = gh(\eta_{xx} + \eta_{yy}) + O\left((\Delta x)^2, \Delta x \Delta t, \Delta y \Delta t, (\Delta y)^2, (\Delta t)^2\right)$$

$$P_{tt} = gh(P_{xx} + Q_{xy}) + O\left((\Delta x)^2, \Delta x \Delta t, \Delta y \Delta t, (\Delta y)^2, (\Delta t)^2\right)$$
$$Q_{tt} = gh(P_{xy} + Q_{yy}) + O\left((\Delta x)^2, \Delta x \Delta t, \Delta y \Delta t, (\Delta y)^2, (\Delta t)^2\right) \quad (19)$$

$$\eta_{ttt} = -gh(P_{xxx} + Q_{xxy} + P_{xyy} + Q_{yyy}) + O\left((\Delta x)^2, \Delta x \Delta t, \Delta y \Delta t, (\Delta y)^2, (\Delta t)^2\right)$$
$$P_{ttt} = -(gh)^2(\eta_{xxx} + \eta_{xyy}) + O\left((\Delta x)^2, \Delta x \Delta t, \Delta y \Delta t, (\Delta y)^2, (\Delta t)^2\right)$$
$$Q_{ttt} = -(gh)^2(\eta_{xxy} + \eta_{yyy}) + O\left((\Delta x)^2, \Delta x \Delta t, \Delta y \Delta t, (\Delta y)^2, (\Delta t)^2\right) \quad (20)$$

Substituting equations (18) - (20) into equations (12) - (14) yields the following modified equations:

$$0 = \eta_t + P_x + Q_y$$
$$-C_o^2 \frac{(\Delta t)^2}{24}(P_{xxx} + Q_{xxy} + P_{xyy} + Q_{yyy}) + \frac{(\Delta x)^2}{24} P_{xxx} + \frac{(\Delta y)^2}{24} Q_{yyy}$$
$$+O\left((\Delta x)^4, (\Delta x)^2(\Delta t)^2, \Delta x(\Delta t)^3, \Delta y(\Delta t)^3, (\Delta y)^2(\Delta t)^2, (\Delta y)^4, (\Delta t)^4\right) \quad (21)$$

$$0 = P_t + C_o^2 \eta_x + C_o^2 \frac{(\Delta x)^2}{24} \eta_{xxx} + \gamma C_o^2 \frac{(\Delta y)^2}{12} \eta_{xyy} - C_o^4 \frac{(\Delta t)^2}{24}(\eta_{xxx} + \eta_{xyy})$$
$$+O\left((\Delta x)^3, (\Delta x)^2 \Delta t, (\Delta y)^2 \Delta t, \Delta x(\Delta t)^2, \Delta y(\Delta t)^2, (\Delta y)^3, (\Delta t)^3\right) \quad (22)$$

$$0 = Q_t + C_o^2 \eta_y + C_o^2 \frac{(\Delta y)^2}{24} \eta_{yyy} + \gamma C_o^2 \frac{(\Delta x)^2}{12} \eta_{xxy} - C_o^4 \frac{(\Delta t)^2}{24}(\eta_{xxy} + \eta_{yyy})$$
$$+O\left((\Delta x)^3, (\Delta x)^2 \Delta t, (\Delta y)^2 \Delta t, \Delta x(\Delta t)^2, \Delta y(\Delta t)^2, (\Delta y)^3, (\Delta t)^3\right) \quad (23)$$

where $C_o = \sqrt{gh}$ is the phase velocity of a linear shallow water wave.

Eliminating P and Q from equations (21) - (23) and using equations (18) - (20), we get a combined modified equation for η.

$$0 = \eta_{tt} - C_o^2(\eta_{xx} + \eta_{yy}) - C_o^2 \left(\frac{(\Delta x)^2}{12} \eta_{xxxx} + \frac{(\Delta y)^2}{12} \eta_{yyyy}\right)$$
$$-\gamma C_o^2 \left(\frac{(\Delta x)^2}{12} \eta_{xxyy} + \frac{(\Delta y)^2}{12} \eta_{xxyy}\right) + C_o^4 \frac{(\Delta t)^2}{12}(\eta_{xxxx} + 2\eta_{xxyy} + \eta_{yyyy})$$
$$+O\left((\Delta x)^3, (\Delta x)^2 \Delta t, (\Delta y)^2 \Delta t, \Delta x(\Delta t)^2, \Delta y(\Delta t)^2, (\Delta y)^3, (\Delta t)^3\right) \quad (24)$$

If a uniform grid, $\Delta x = \Delta y$, is used, the above equation can be simplified to be:

$$0 = \eta_{tt} - C_o^2(\eta_{xx} + \eta_{yy}) - C_o^2\frac{(\Delta x)^2}{12}(1 - {C_r}^2)(\eta_{xxxx} + 2\eta_{xxyy} + \eta_{yyyy})$$
$$+(1-\gamma)C_o^2\frac{(\Delta x)^2}{6}\eta_{xxyy} + O\left((\Delta x)^3, (\Delta x)^2\Delta t, \Delta x(\Delta t)^2, (\Delta t)^3\right) \qquad (25)$$

where $C_r(= C_o\Delta t/\Delta x)$ is the Courant number. For the modified explicit scheme, $\gamma = 1$ and the last term in equation (25) vanishes. On the other hand, when $\gamma = 0$, equation (25) is the same as that derived by Imamura and Goto (1988).

The leading order terms in equation (25) are the same as those in the wave equation. The terms of $O((\Delta x)^2)$ and of higher order are the results of numerical descretization. Comparing equation (25) with the linear Boussinesq equation (5), one realizes that these equations are identical as long as the following relation is satisfied

$$h^2 = \frac{(\Delta x)^2}{4}\left[1 - gh\frac{(\Delta t)^2}{(\Delta x)^2}\right] \qquad (26)$$

with $\gamma = 1$. In other words, if Δt and Δx are chosen according to the above relationship, the numerical dispersion from the modified explicit leap-frog scheme mimics the frequency dispersion in the linearized Boussinesq equations. That is, we actually get numerical solutions which satisfy the Boussinesq equations by solving equations (12) - (14). Furthermore, the accuracy of the numerical scheme has been raised from second-order to third-order.

When Imamura and Goto's (1988) scheme is used ($\gamma = 0$), we can not get the perfect match between the modified equation, equation (25), and the Boussinesq equation (5), because of the appearance of the additional cross differentiation term, η_{xxyy}, in equation (25). To examine the effect of these terms on the phase velocity, we consider a progressive wave:

$$\eta = Ae^{i(k_x x + k_y y - \omega t)} \quad , \quad k^2 = {k_x}^2 + {k_y}^2 \qquad (27)$$

where $\hat{i} = \sqrt{-1}$ is the imaginary number and k_x and k_y are x- and y-component of wave number vector k, respectively. Substituting equation (27) into equation (25) and using equation (26), we have

$$C = \frac{\omega}{k} = \sqrt{gh}\sqrt{1 - \frac{(kh)^2}{3} + (1-\gamma)\frac{(\Delta x)^2}{6}\left(\frac{k_x k_y}{k}\right)^2} \tag{28}$$

Once again when $\gamma = 1$ (i.e., the modified explicit leap-frog method is used) the dispersion relationship (28) becomes the same as that derived from the linear Boussinesq equation. For one-dimensional problems with waves traveling in either x- or y-direction, i.e., either k_y or k_x equals to zero, both explicit schemes yield the same phase velocity as that suggested by the Boussinesq equation. For obliquely traveling waves, however, the phase velocity is faster than that of the Boussinesq wave when $\gamma = 0$ (i.e., Imamura and Goto's scheme) and the largest discrepancy occurs when waves propagate in the direction of $(2n+1)\frac{\pi}{4}$, n = 0, 1, 2, ..., with respect to x-axis.

2.4 Stability analysis

In this section, we determine the stability conditions for the numerical algorithms given in equations (12) - (14). Assuming that solutions for these equations can be written in the following Fourier forms (Lapidus and Pinder, 1982):

$$\eta = \eta_o \rho^t e^{\hat{i}k_x x} e^{\hat{i}k_y y} \tag{28a}$$

$$P = P_o \rho^t e^{\hat{i}k_x x} e^{\hat{i}k_y y} \tag{28b}$$

$$Q = Q_o \rho^t e^{\hat{i}k_x x} e^{\hat{i}k_y y} \tag{28c}$$

in which η_o, P_o and Q_o are initial values. We look for the stable condition which requires the absolute value of amplification factor, $|\rho^{\Delta t}|$, be less than or equal to unity. Substituting equation (28) into equations (12) - (14) and using the following

notations: $t = N\Delta t$ ($N = 0, 1, 2, ..., n, ...$), $x = I\Delta x$ ($I = 0, 1, 2, ..., i, ...$), and $y = J\Delta y$ ($J = 0, 1, 2, ..., j, ...$), we obtain

$$(\rho^{\Delta t/2} - \rho^{-\Delta t/2})\eta_o + 2\hat{i}r_x \sin\theta_x P_o + 2\hat{i}r_y \sin\theta_y Q_o = 0 \tag{29}$$

$$\frac{2\hat{i}}{3}C_o^2 r_x \sin\theta_x (3 - \gamma \sin^2\theta_y)\rho^{\Delta t/2}\eta_o + (\rho^{\Delta t} - 1)P_o = 0 \tag{30}$$

$$\frac{2\hat{i}}{3}C_o^2 r_y \sin\theta_y (3 - \gamma \sin^2\theta_x)\rho^{\Delta t/2}\eta_o + (\rho^{\Delta t} - 1)Q_o = 0 \tag{31}$$

where

$$r_x = \frac{\Delta t}{\Delta x}, \quad r_y = \frac{\Delta t}{\Delta y}, \quad \theta_x = \frac{k_x \Delta x}{2}, \quad \theta_y = \frac{k_y \Delta y}{2} \tag{32}$$

The system of linear equations given in equations (29) - (31) is homogeneous. For nontrivial solutions the determinant of the coefficient matrix must vanish. Consequently, we find two equations for the amplification factor $\rho^{\Delta t}$.

$$\rho^{\Delta t/2} - \rho^{-\Delta t/2} = 0 \tag{33}$$

$$(\rho^{\Delta t} - 1)^2 + \frac{4}{3}C_o^2 \left[r_x^2 \sin^2\theta_x (3 - \gamma \sin^2\theta_y) + r_y^2 \sin^2\theta_j (3 - \gamma \sin^2\theta_x)\right]\rho^{\Delta t} = 0 \tag{34}$$

Obviously, $\rho^{\Delta t} = 1$ is the solution for equation (33). From equation (34) the amplification factor can be determined as

$$\rho^{\Delta t} = \frac{2 - B \pm \sqrt{B^2 - 4B}}{2} \tag{35}$$

where

$$B = \frac{4}{3}C_o^2 \left[r_x^2 \sin^2\theta_x (3 - \gamma \sin^2\theta_y) + r_y^2 \sin^2\theta_y (3 - \gamma \sin^2\theta_x)\right] \tag{36}$$

The stability condition

$$|\rho^{\Delta t}| \leq 1 \tag{37}$$

is satisfied if $B^2 - 4B$ is less than or equal to zero, i.e.,

$$0 \leq B \leq 4 \tag{38}$$

Substituting equation (36) into equation (38) and assuming that $\Delta x = \Delta y$ for simplicity, we obtain

$$C_r \leq \frac{\sqrt{3}}{\sqrt{\sin^2\theta_x(3 - \gamma\sin^2\theta_y) + \sin^2\theta_y(3 - \gamma\sin^2\theta_x)}} \tag{39}$$

where C_r is the Courant number. If Imamura and Goto's explicit scheme is used ($\gamma = 0$), the stability condition can be simplified to be

$$C_r \leq \frac{1}{\sqrt{\sin^2\theta_x + \sin^2\theta_y}} \tag{40}$$

The largest allowable Courant number is $\frac{1}{\sqrt{2}}$ when $\sin\theta_x = \sin\theta_y = 1$. On the other hand, if the modified explicit scheme is used ($\gamma = 1$), the largest Courant number is 0.866. Therefore, for the same Δx and C_o values, the modified explicit scheme allows slightly larger time step sizes than those required by Imamura and Goto's scheme.

3. Numerical Results

In this section numerical schemes are verified with analytical solutions. Three examples are chosen here to test the accuracy of both explicit schemes: a Gaussian source, a finite strip without a wall boundary and a finite strip with a wall boundary.

In the first example the initial surface displacement of the Gaussian source is given by

$$\eta(r,0) = 2e^{-(r/a)^2}, \quad \eta_t(r,0) = 0 \tag{41}$$

where a means the radius of the Gaussian hump and $r = \sqrt{x^2 + y^2}$ is the distance from the origin. The analytical solution to the linear Boussinesq equation can be written as (Carrier, 1991)

$$\eta(r,t) = \int_0^\infty a^2 e^{-(ak)^2/4} k \cos\left(\frac{\sqrt{gh}kt}{\sqrt{1+\frac{(kh)^2}{3}}}\right) J_o(kr)dk \tag{42}$$

where J_o is Bessel function of the first kind of order zero. Introducing the following dimensionless variables,

$$h' = \frac{h}{a}, \quad x' = \frac{x}{a}, \quad y' = \frac{y}{a}, \quad k' = ak, \quad t' = \frac{\sqrt{gh}}{a}t \tag{43}$$

equation (42) can be rewritten as

$$\eta(r,t) = \int_0^\infty k' e^{-(k')^2/4} \cos\left\{\frac{k't'}{\sqrt{1+\frac{(k'h')^2}{3}}}\right\} J_o(k'r')dk' \tag{44}$$

where the primes stand for dimensionless quantities. For convenience, the primes will be dropped from here on. Figure 2 shows the behavior of the solutions for different water depths. The dispersive effects become more important for deeper water depth and for longer traveling distance.

Numerical solutions of both explicit schemes were obtained for depth $h = 0.2$ with a square grid, $\Delta x = \Delta y = 0.5$. The dimensionless time step Δt is set to be 0.3, which is calculated from the dimensionless version of equation (26). An open boundary condition based on the linear shallow water equation is imposed along boundaries of the computational domain which consists of 301 by 301 grid points. The open boundary condition is, in terms of physical variables,

$$\eta\sqrt{gh} = \sqrt{P^2 + Q^2} \tag{45}$$

which can be derived from the Sommerfeld radiation boundary condition. Strictly speaking, the condition can only be applied to long waves. However, we can still

use this condition for the case where most of the energy is concentrated near the low frequency end of the initial wave spectrum. In figure 3, the comparison of analytical solutions with numerical solutions are presented at dimensionless time $t = 40$, 50 and 60. In this figure, the symbol denotes the numerical solutions along $0°, 45°$ and $90°$ directions with respect to x-axis. As mentioned in Section 2, Imamura and Goto's explicit scheme does not show correct phase velocity and surface displacement along the diagonal direction. On the other hand, the solution of the modified explicit scheme is not sensitive to the propagation direction and is in very good agreement with the analytical solutions, especially for leading waves.

In the second example, we present numerical solutions for a finite strip source without a wall boundary. The initial free surface displacement is given by, in dimensionless variables,

$$\begin{aligned} \eta(x,y,0) &= \frac{1}{\sqrt{\pi}} \int_0^L 2e^{-[(x-\xi)^2+y^2]} d\xi \\ &= [\mathrm{erf}(L-x) + \mathrm{erf}(x)]e^{-y^2} \\ \eta_t(x,y,0) &= 0 \end{aligned} \tag{46}$$

where L is the dimensionless length of the strip and erf is the error function. The solution of the linear Boussinesq equation with the initial condition can be written as

$$\eta(x,y,t) = \frac{1}{\sqrt{\pi}} \int_0^L d\xi \int_0^\infty k \mathrm{J}_0(k\sqrt{(x-\xi)^2+y^2}) \cos\left(\frac{kt}{\sqrt{1+\frac{(kh)^2}{3}}}\right) e^{-k^2/4} dk \tag{47}$$

A schematic sketch of the configuration for the strip source problem is given in figure 4, where α measures the angle from the normal to the major axis of the strip and r is distance from the origin. θ is used for measure of orientation with respect to x-axis. Figure 5 is the time history of the surface displacements at $r = 120$, $\alpha = 0°$ radiated from a finite strip length $L = 40$ and the effect of dispersion

Table 1: Parameters used for a finite strip source

h	Δx=Δy	Δt	no. of grid points
0.2	0.50	0.30	521 x 521
0.1	0.25	0.15	1041 x 1041

on phase velocity and wave height is clearly shown. Numerical results are obtained for the cases of depth $h = 0.2$ and 0.1. The parameters used in the calculations is shown in table 1.

In both cases, the dimensionless computational domain is 260 by 260 and the origin is located at the center of the domain. In figure 6, we compare analytical solutions with numerical solutions for $h = 0.2$ with two different orientation 0° and 45°. The modified explicit scheme gives consistent results in spite of different orientations of the source, while the solution of Imamura and Goto's explicit scheme is acceptable only for 0° orientation. We can also find similar trend for the case $h = 0.1$ as shown in figure 7.

Final example is chosen for a finite strip source with a wall boundary. The initial free surface displacement is the same as equation (46) but at $y = b$ a reflecting wall exists. Using the method of images the analytical solution can be obtained.

$$\eta(x,y,t) = \frac{1}{\sqrt{\pi}} \int_0^{L\cos\theta} \frac{d\xi}{\cos\theta} \int_0^{\infty} k \cos\left(\frac{kt}{\sqrt{1+\frac{(kh)^2}{3}}} \right) e^{-k^2/4} \left[J_0(kr_1) + J_0(kr_2) \right] dk \quad (48)$$

in which r_1 and r_2 are given by

$$r_1 = \sqrt{(x-\xi)^2 + (y - \xi\tan\theta)^2}, \quad r_2 = \sqrt{(x-\xi)^2 + (y - 2k + \xi\tan\theta)^2}$$

Numerical results are obtained for $h = 0.1$ and same parameters shown in table 1 are used. Figure 8 shows comparison of analytical solution with numerical solution for the modified explicit scheme. Excellent agreement is observed.

4. Concluding Remarks

To model the transoceanic propagation of tsunami waves, a modified explicit finite differences method is proposed. It is shown through the modified equation approach that the present modified explicit scheme corrects the explicit scheme derived by Imamura and Goto (1988) to give the same phase velocity as that of the linear Boussinesq equation.

Several numerical results of both explicit methods are presented and compared to the analytical solutions for transient wave propagation over a constant depth. Numerical solutions of Imamura and Goto's explicit scheme are sensitive to the wave propagation direction, On the other hand, solutions of the modified explicit scheme are in very good agreement with the analytical solutions, especially for leading waves. Two types of boundary conditions, reflecting wall and open boundary, are tested. The modified explicit scheme performs very well.

The modified explicit scheme has already been applied to practical problems. Liu *et al.* (1993) simulated the transoceanic propagation of 1960 Chilean tsunami. A nested multiple grid system with different time step sizes and grid cells was used to model the bathymetry variations in the Pacific Ocean.

Acknowledgement

The research is supported, in part, by the NOAA Office of Sea Grant, U.S. Department of Commerce, under Grant # NA90AA-D-SG078 to the New York Sea Grant Institute, and by the NSF through research grants (BCS 9024965, BCS 9109988, BCS 9115552) to Cornell University.

References

Carrier, G. F. (1991). "Tsunami propagation from a finite source," *Proc. of 2nd UJNR Tsunami Workshop*, NGDC, Honolulu, HI, 101-115.

Imamura, F. and Goto, C. 1988, "Truncation error in numerical tsunami simulation by the finite difference method", *Coastal Eng. in Japan*, JSCE **31**, 245-263.

Kajiura, K. and Shuto, N. (1990). Tsunami in *The SEA*, Vol. 9, Part B, 395-420.

Lapidus, L. and Pinder, G. F. (1982). *Numerical Solution of Partial Differential Equations in Science and Engineering*, John Wiley & Sons, U.S.A.

Liu, P. L.-F. and Yoon, S. B. (1991). *Estimation of Tsunami Wave Heights along South-Eastern Korean Shoreline.* A technical report, School of Civil and Environmental Engineering, Cornell University, (unpublished).

Liu, P. L.-F., Yoon, S. B., S. N. Seo and Y.-S. Cho (1993). "Numerical simulations of tsunami inundation at Hilo, Hawaii, *Proc. of the IUGG/IOC Inter. Tsunami Sym.*, Wakayama, Japan, 257-269.

Mei, C. C. (1989). *The Applied Dynamics of Ocean Surface Waves*, World Scientific Publishing Co., U.S.A.

Warming, R. F. and Hyett, B. J. (1974). "The modified equation approach to the stability and accuracy analysis of finite-difference methods," *J. Comp. Phys.*, 14, 159-179.

Figure Caption

Figure 1. A sketch of the staggered finite differences grid system.

Figure 2. Analytical solutions for a Gaussian hump.

Figure 3 (a),(b),(c). Comparisons of numerical results of Imamura and Goto's scheme with analytical solutions (——) for a Gaussian hump.

Figure 3 (d),(e),(f). Comparisons of numerical results of the modified scheme with analytical solutions (——) for a Gaussian hump.

Figure 4. A sketch of a finite strip.

Figure 5. Analytical solutions for the finite strip: $L = 40$, $r = 120$, $\alpha = 0°$, $\theta = 0°$.

Figure 6 (a), (b). Comparisons of numerical results with analytical solutions for the finite strip: $h = 0.2$, $\theta = 0°$, $\alpha = 0°$.

Figure 6 (c), (d). Comparisons of numerical results with analytical solutions for the finite strip: $h = 0.2$, $\theta = 45°$, $\alpha = 0°$.

Figure 7 (a), (b). Comparisons of numerical results with analytical solutions for the finite strip: $h = 0.1$, $\theta = 0°$, $\alpha = 0°$.

Figure 7 (c), (d). Comparison of numerical results with analytical solutions for the finite strip: $h = 0.1$, $\theta = 45°$, $\alpha = 0°$.

Figure 8. Comparison of numerical result with analytical solution for the finite strip with a wall boundary ($y = b$): $h = 0.1$, $\theta = 0°$, $\alpha = 0°$.

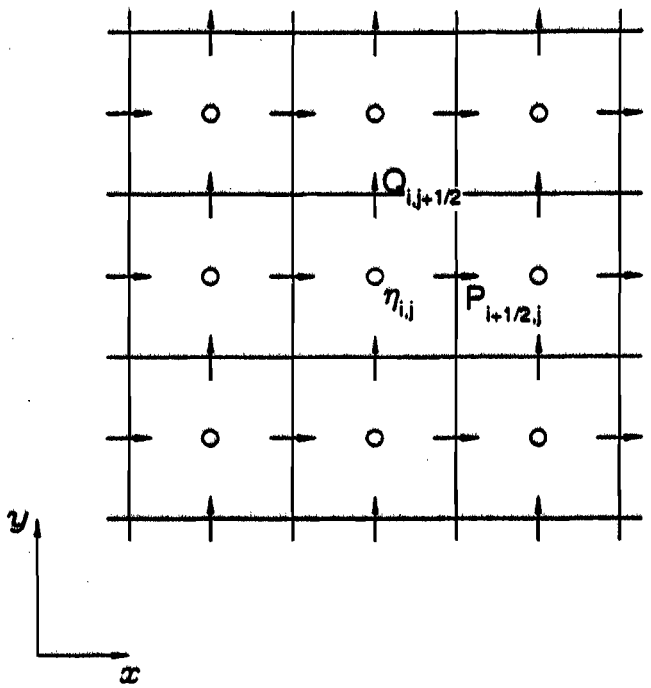

Figure 1.

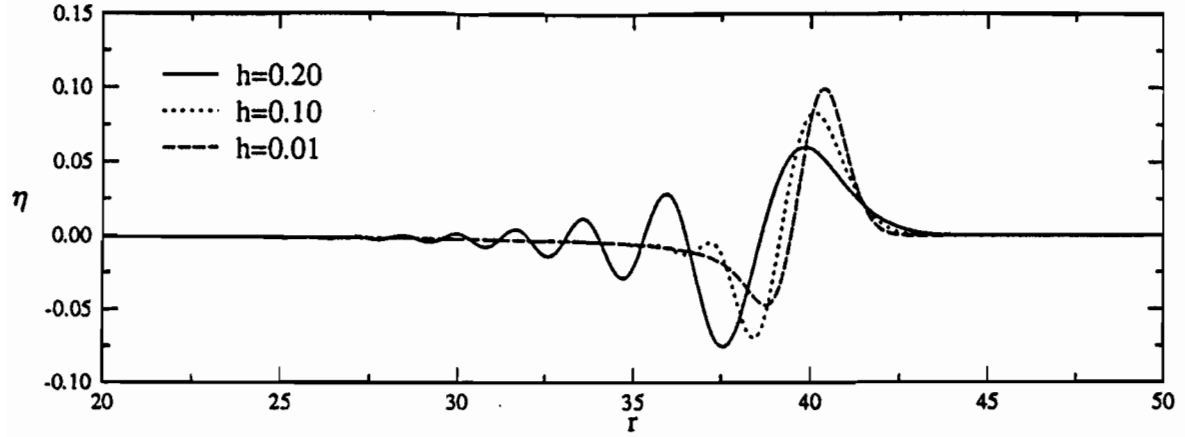

(a) t = 40

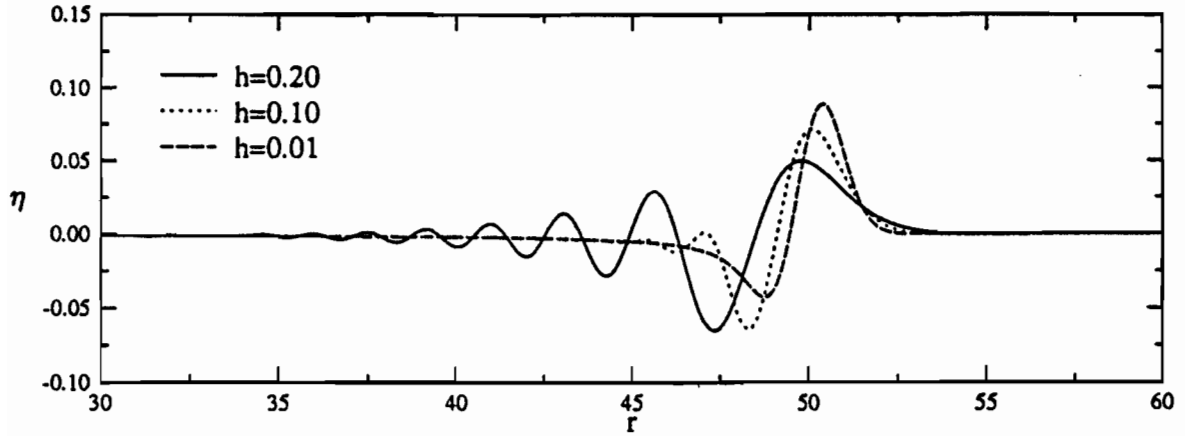

(b) t = 50

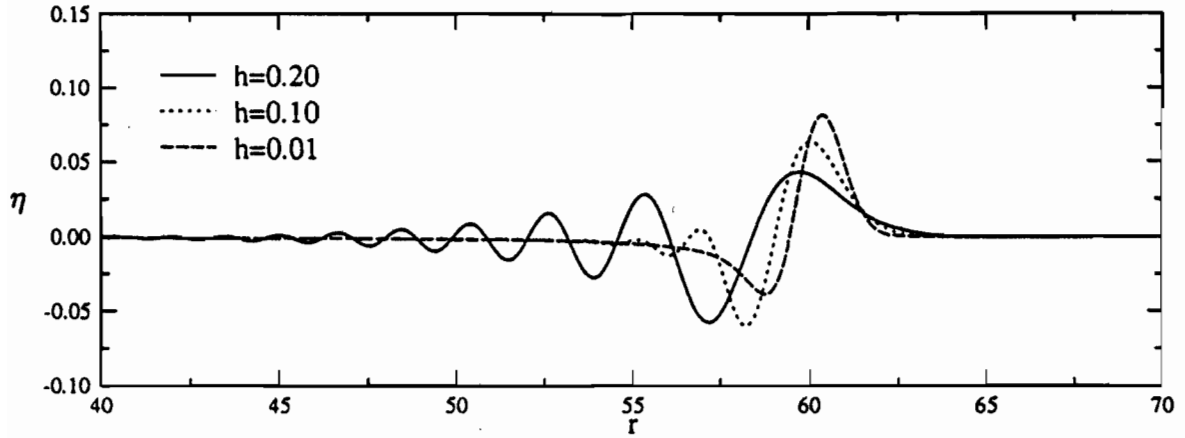

(c) t = 60

Figure 2.

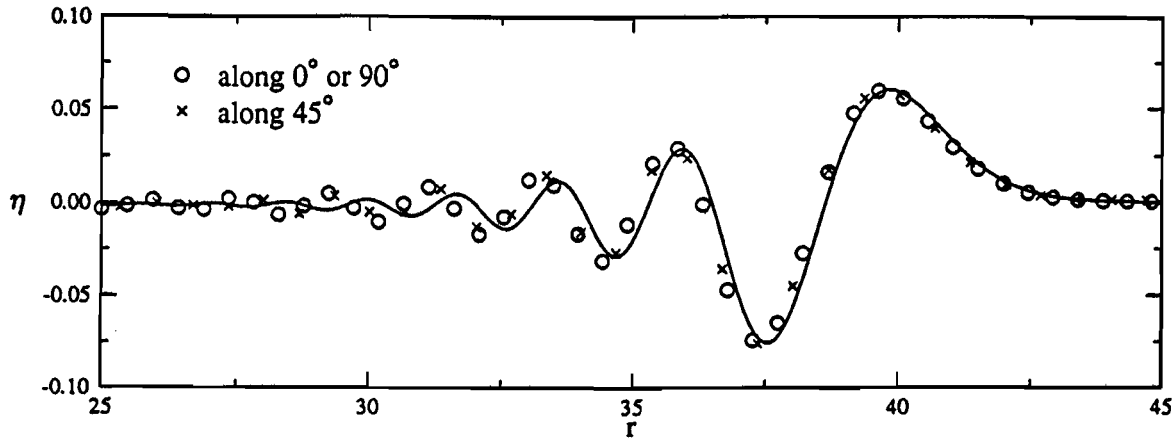

(d) t = 40

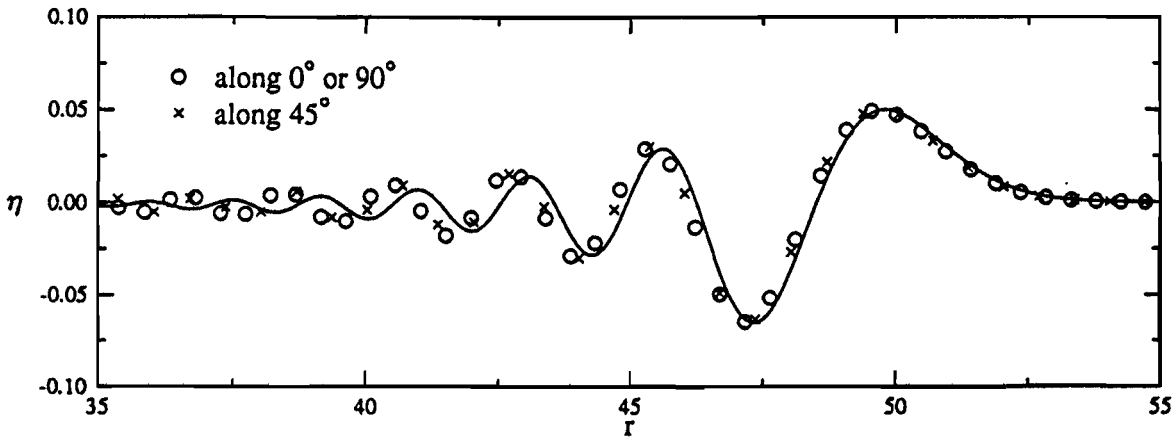

(e) t = 50

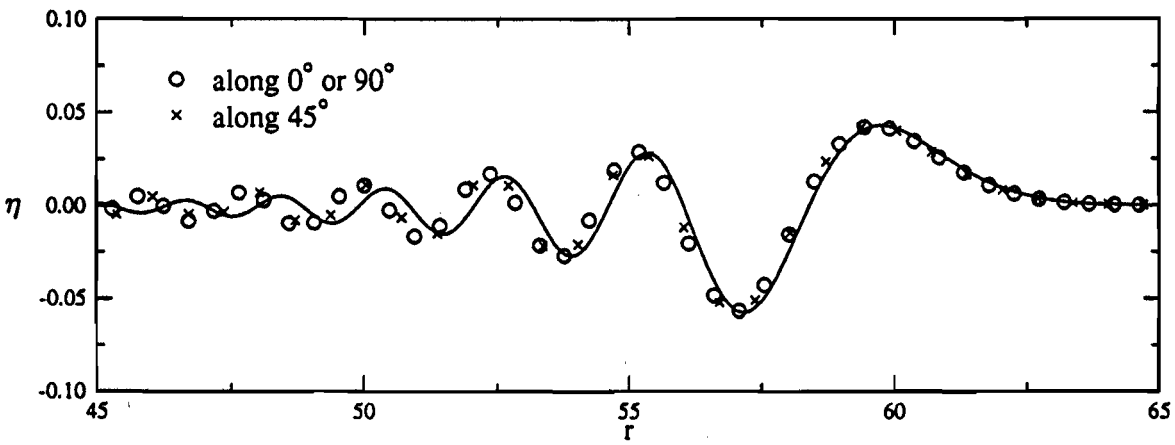

(f) t = 60

Figure 3 (d),(e),(f).

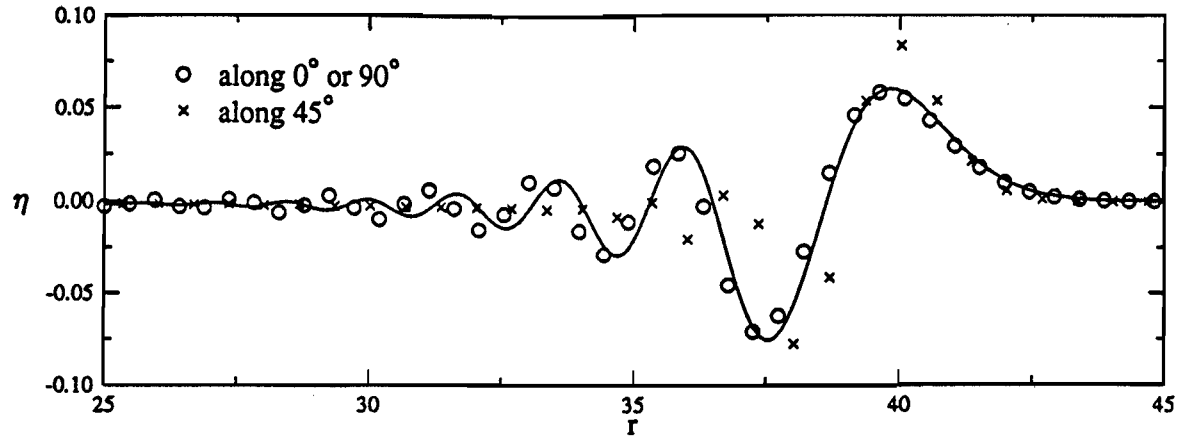

(a) t = 40

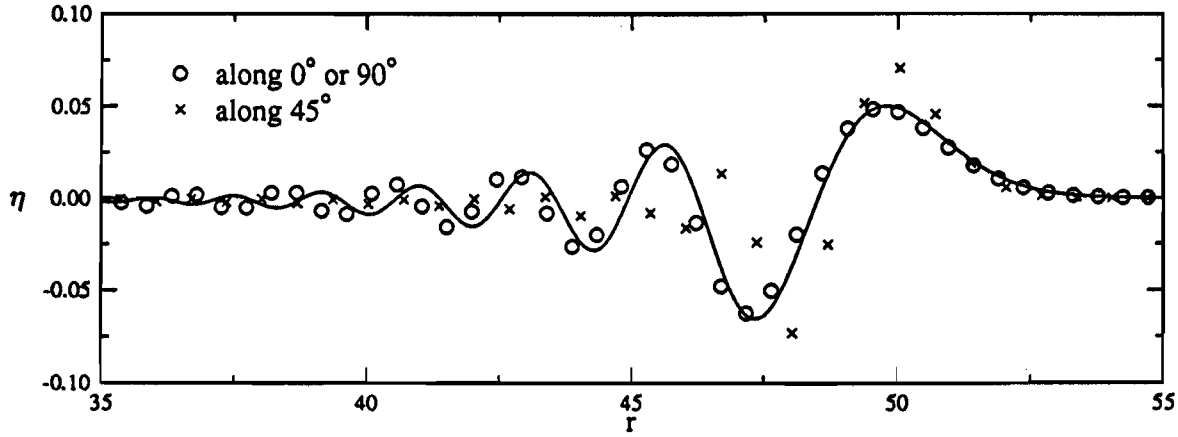

(b) t = 50

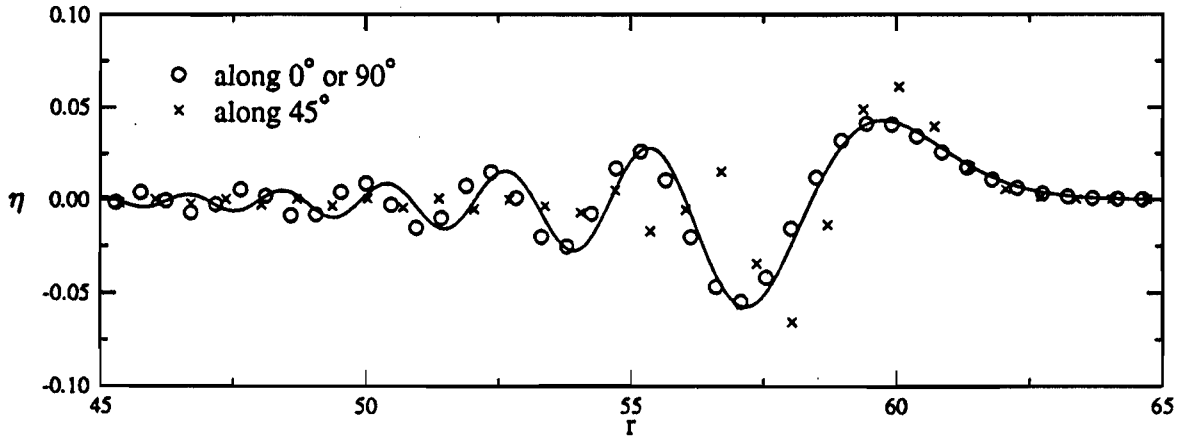

(c) t = 60

Figure 3 (a),(b),(c).

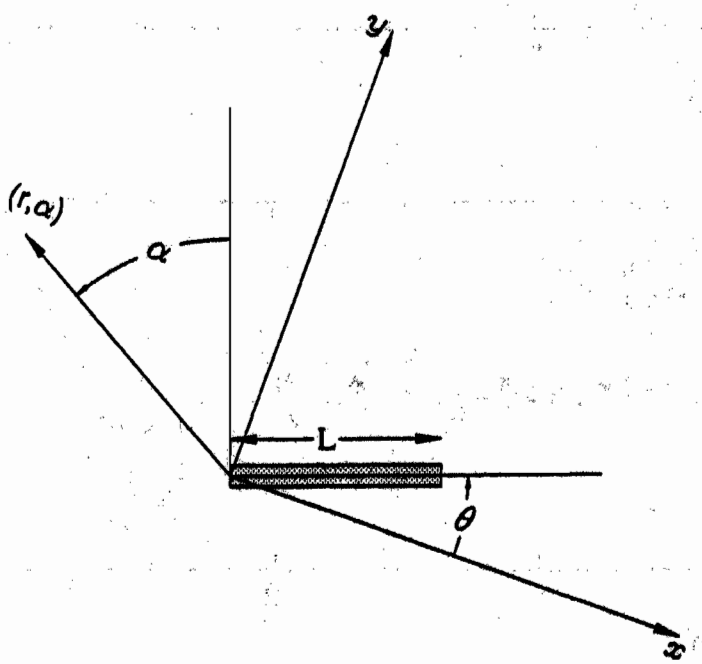

Figure 4.

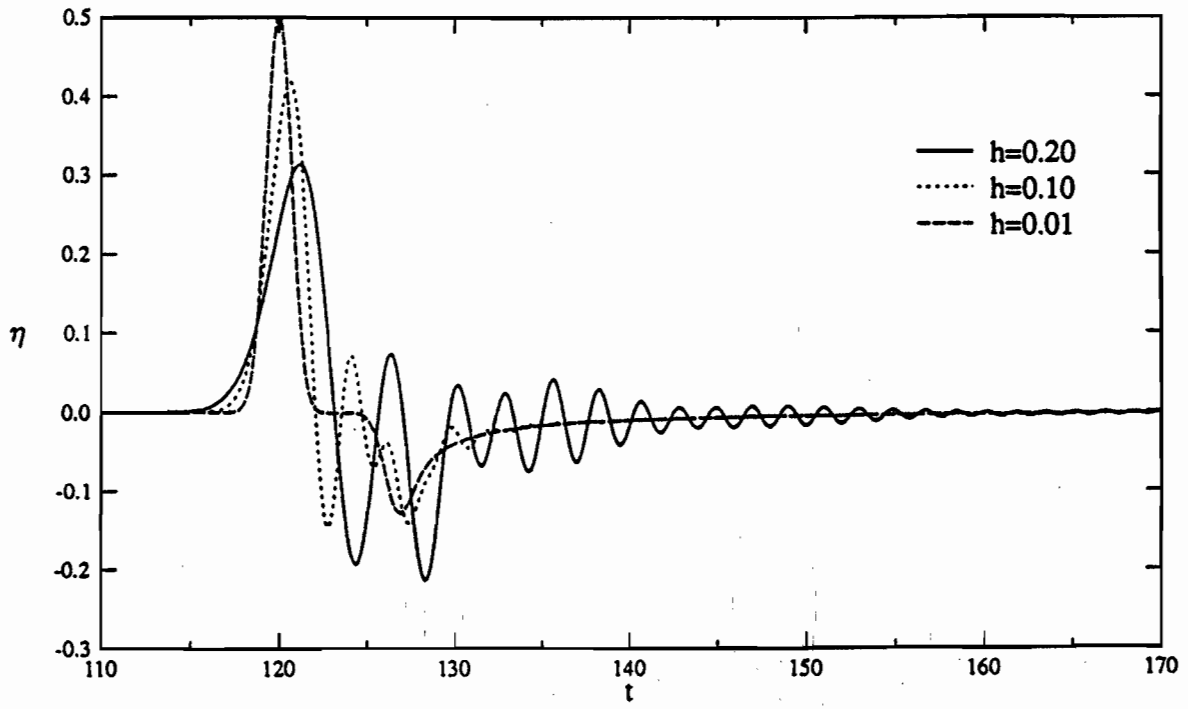
0.5
0.4
0.3
0.2
0.1
0.0
-0.1
-0.2
-0.3
η
110
120
130
140
150
160
170
t
h=0.20
h=0.10
h=0.01

Figure 5.

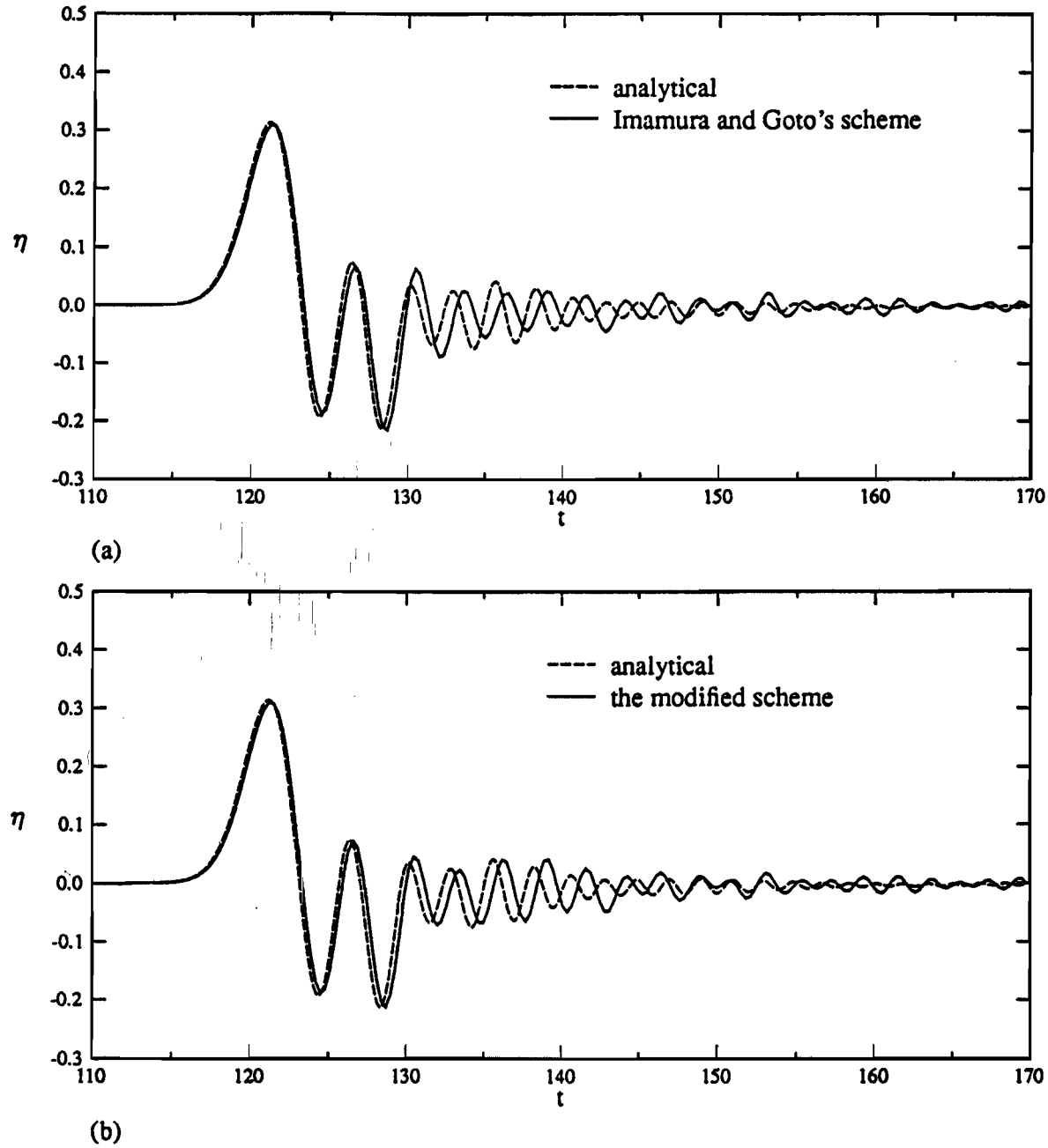
0.5
0.4
0.3
0.2
0.1
0.0
-0.1
-0.2
-0.3
η
110
120
130
140
150
160
170
t
analytical
Imamura and Goto's scheme
(a)
analytical
the modified scheme
(b)

Figure 6 (a), (b).

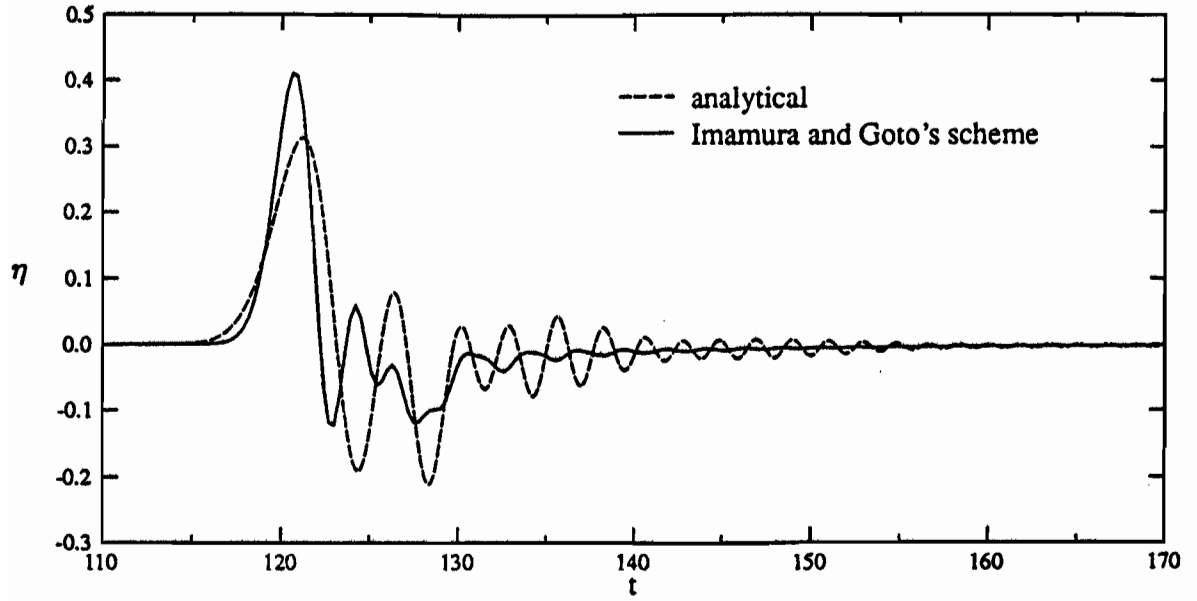

(c)

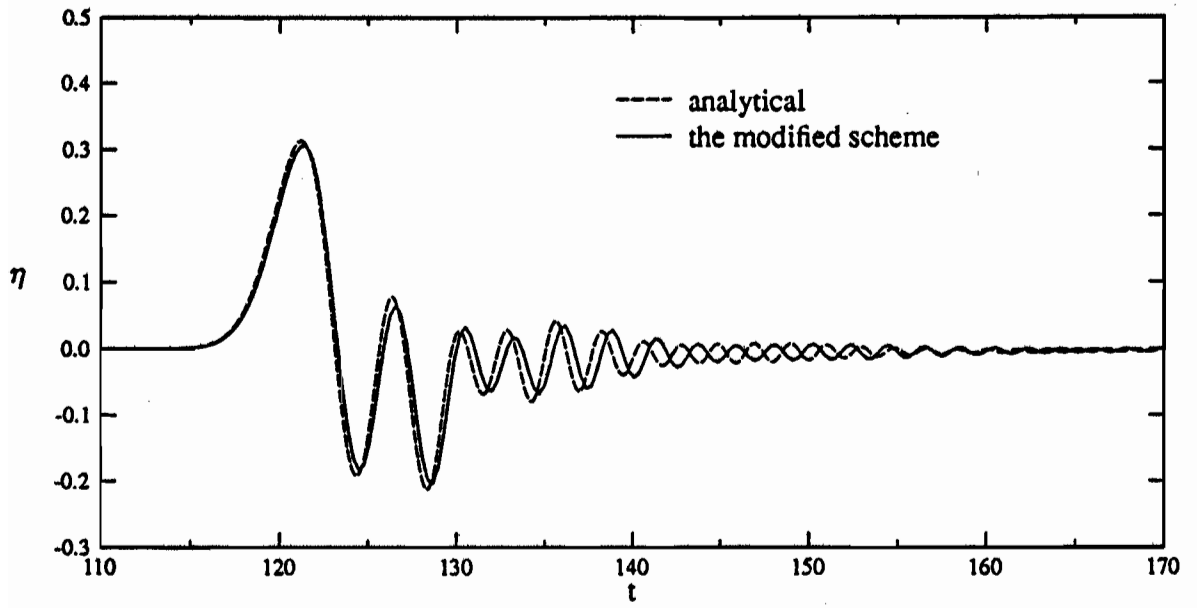

(d)

Figure 6 (c), (d).

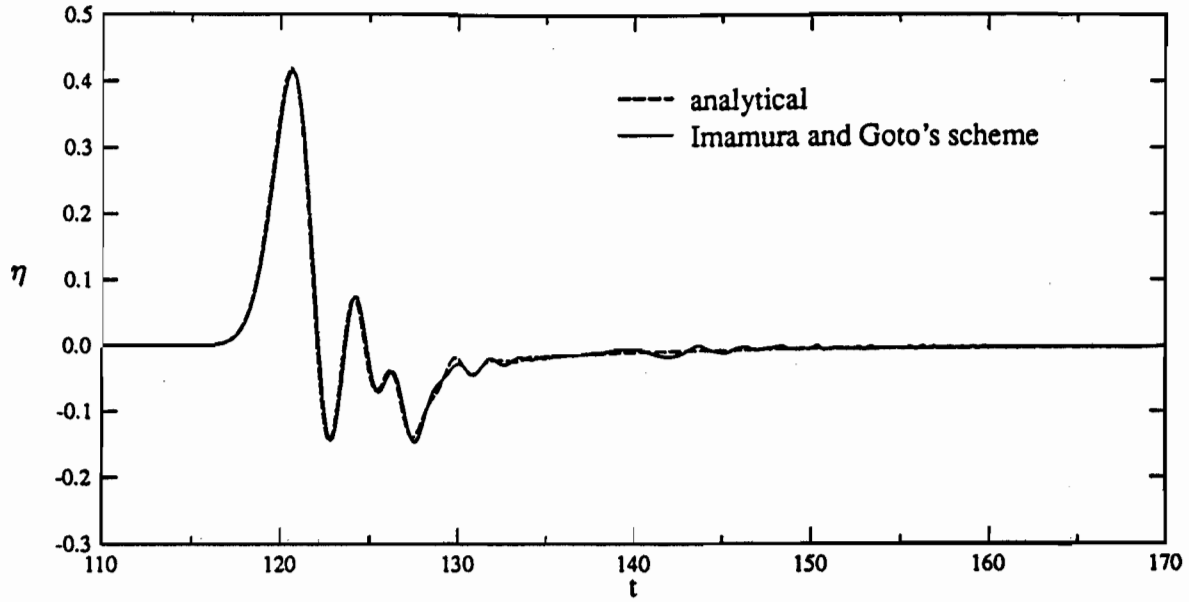

(a)

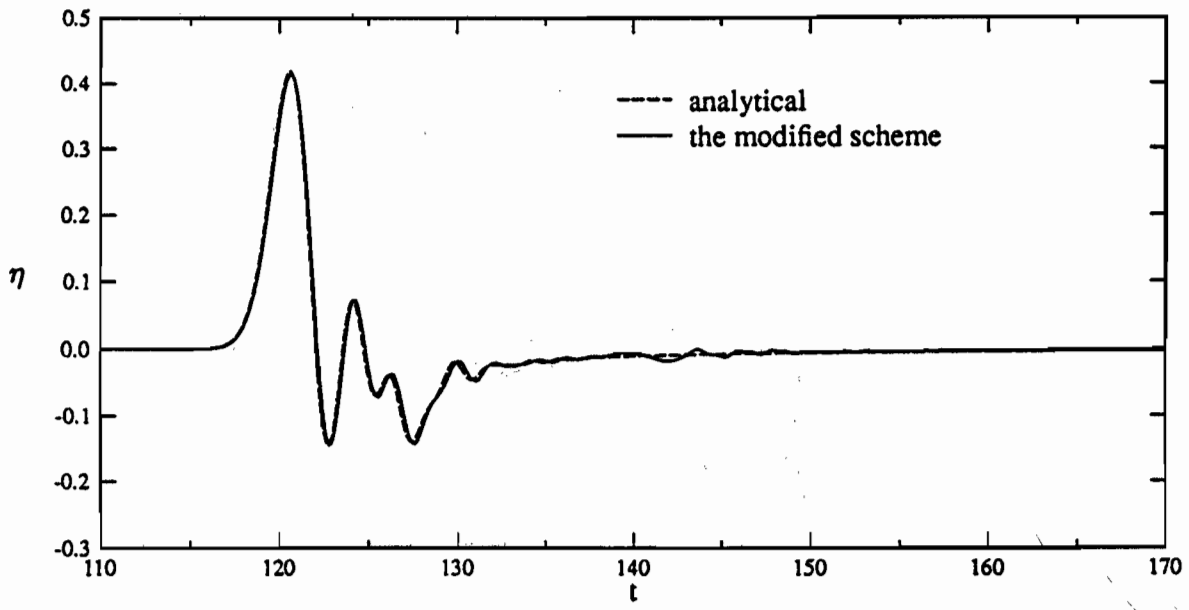

(b)

Figure 7 (a), (b).

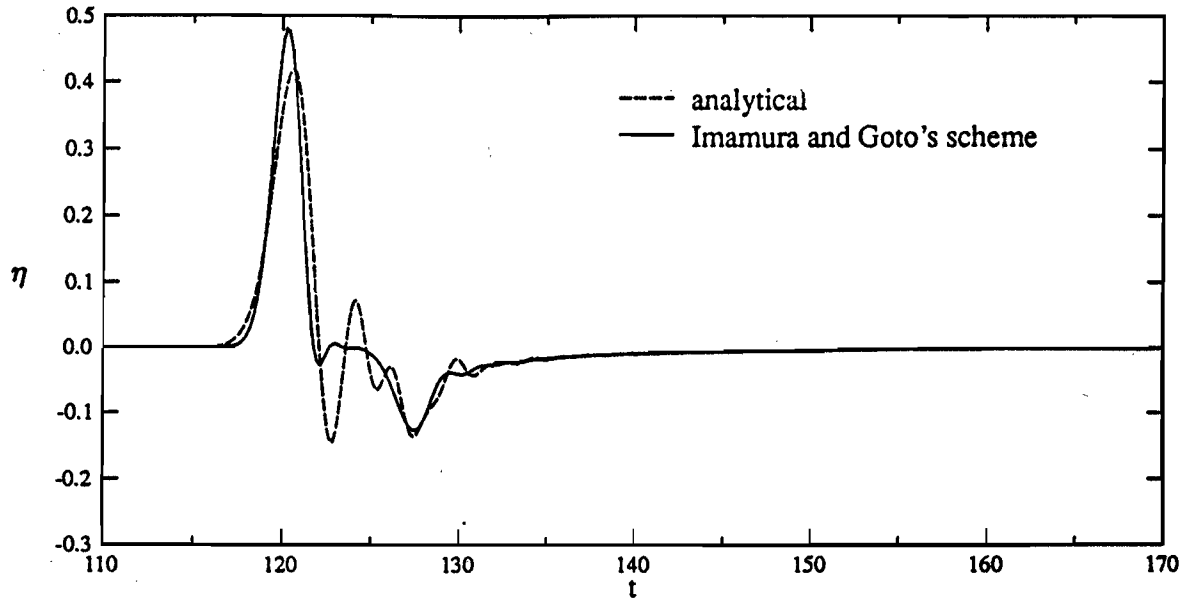

(c)

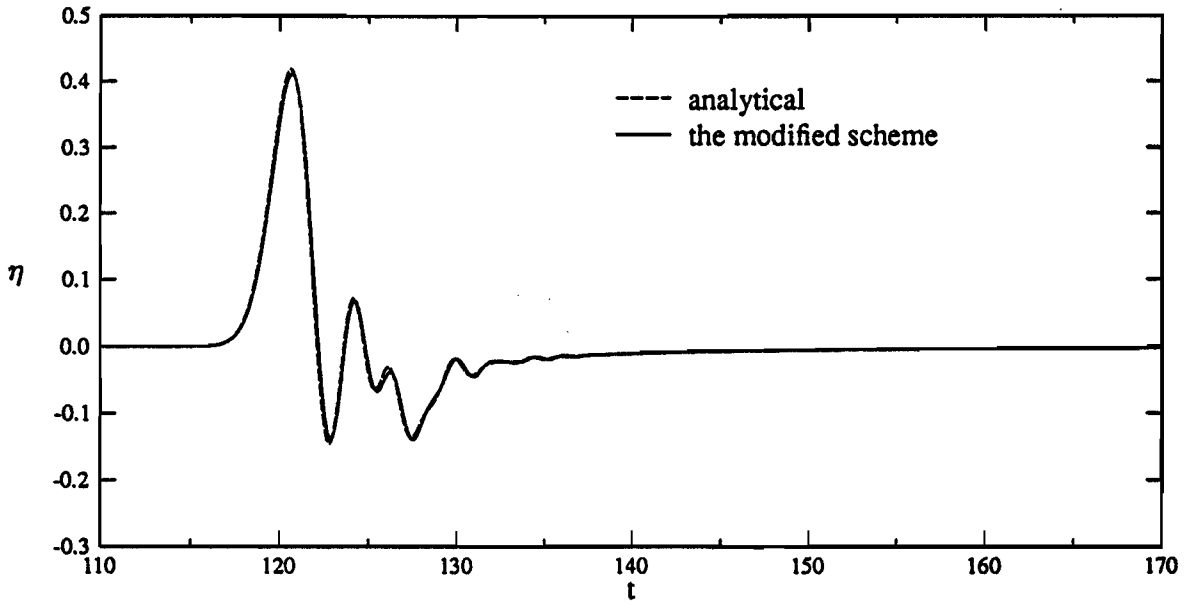

(d)

Figure 7 (c), (d).

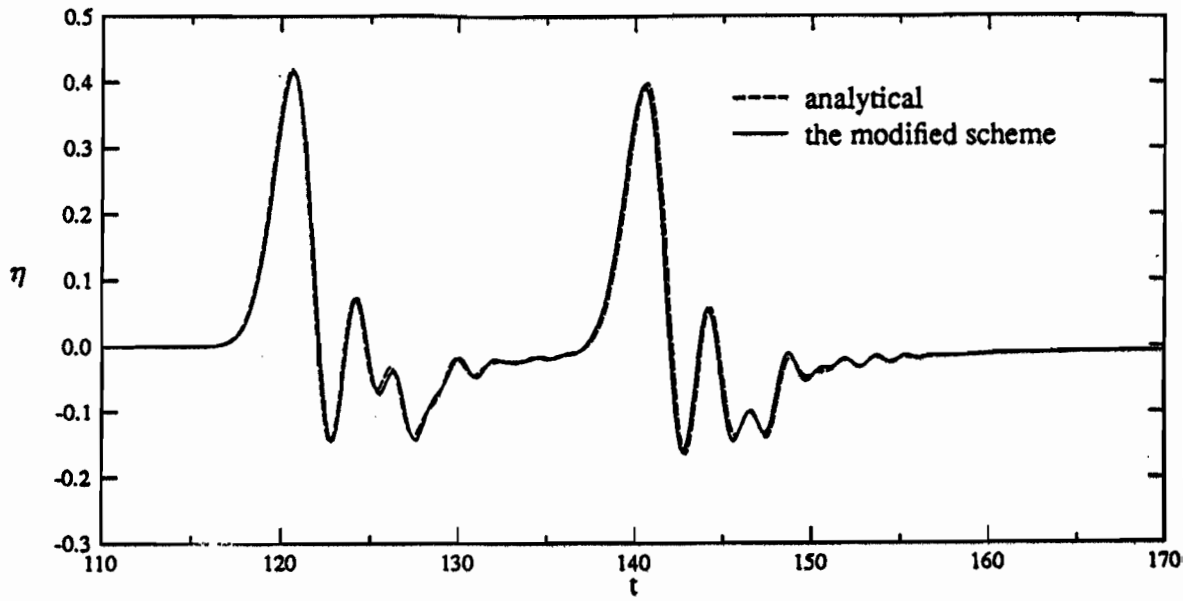
0.5
0.4
0.3
0.2
0.1
0.0
-0.1
-0.2
-0.3
η
110
120
130
140
150
160
170
t
analytical
the modified scheme

Figure 8.

Proceedings of the IUGG/IOC International Tsunami Symposium

NUMERICAL SIMULATIONS OF TSUNAMI INUNDATION AT HILO, HAWAII

PHILIP L.-F. LIU
Professor, School of Civil and Environmental Engineering
Cornell University, Ithaca, NY 14853, USA

SUNG B. YOON
Assistant Professor, Department of Civil Engineering
Hanyang University, Ansan 425-791, KOREA

SEUNG N. SEO
Principal Researcher, Korea Ocean Research and
Development Institute, Ansan 425-600, KOREA

YONG-SIK CHO
Graduate Student, School of Civil and Environmental Engineering
Cornell University, Ithaca, NY 14853, USA

ABSTRACT

A leap-frog finite difference model is used to simulate the transoceanic propagation of 1960 Chilean tsunami and the associated inundation in Hilo bay, Hawaii. In computing the transoceanic tsunami propagation, the linear shallow-water equations with Coriolis force are solved. However, grid sizes and time step sizes are selected in such a way that the numerical dispersion introduced by the leap-frog method is almost the same as the frequency dispersion in the Boussinesq equations. Because the grid size and the time step size depend on the local depth, a nested multiple grid system is developed for the simulation model. In the inundation model, nonlinear shallow-water equations including bottom friction are used. A moving boundary condition scheme is developed to track the movement of shoreline. The maximum inundation area is calculated and compared with the field record.

1. INTRODUCTION

The 1960 Chilean tsunami was one of the largest tsunamis that occurred in the Pacific Ocean. It caused devastating damages not only along the Chilean coast (over 1000 people were killed and the total property damage from the combined effects of the earthquake and tsunami was $417 million) but also at Hilo, Hawaii, where 61 deaths and $23 million in damage occurred. The epicenter of the earthquake was located about 100 km offshore. The fault zone was roughly 800 km long and 200 km wide and the displacement of the fault was 24 m. The orientation of the fault was $N10°E$. The focal depth of the slip was estimated at 53 km with a 90° slip angle and a 10° dip angle [3,4]. Using these estimated fault parameters, one can calculate the initial free surface displacement [6]. The wavelength of the initial tsunami wave form was roughly 1000 km and the wave height was roughly 10 m. The leading trough of the tsunami arrived 10 to 15 minutes after the earthquake, along more than 500 m of the Chilean coast.

The distance between Hilo, Hawaii and the source region of the Chilean tsunami is about 10,000 km. Because the average depth in the Pacific Ocean is 4 km and tsunami travels at a speed of $\sqrt{gh} \approx 200\ m/sec$, it takes roughly 14 hours for the leading wave of the tsunami to arrive at the Hawaii island chain. Because of the dispersion and the spreading of wave energy, the wave height of the leading tsunami became smaller as it reached the Hawaii island chain; the wave height was about 2 m (see Figure 4). However, due to shoaling and focusing effects, significant inundation occurred in the Hilo bay (see Figure 6).

It is the objective of this paper to simulate the propagation of the 1960 Chilean tsunami from the source region to the Hawaii island chain and beyond. The inundation in the Hilo bay is then calculated. Although numerical results simulating the 1960 Chilean tsunami have been reported in literature [2,5], our numerical results provide much finer resolution in the vicinity of Hawaii island chain. In Imamura and Shuto's study [2], their main interest was the tsunami run-up along the Japanese coastline, therefore, high resolution solutions near Hawaii islands were not necessary; they employed 10 min ($\approx$ 18 km) grids in the area. On the other hand, Mader and Curtis [5] used 5 min ($\approx$ 9 km) grids to calculate the arriving tsunami at the Hilo bay. The tsunami run-up in the bay was then calculated by using a 100 meter grid system. Therefore, there was an abrupt change from the large grid system to the small grid system in their simulation model. The offshore boundary of the small grid system was represented by a single point in the large grid system. Hence, the boundary condition was always uniform along the offshore boundary [5]. In the present model, a nested multiple grid system is introduced for the transoceanic propagation computations. The smallest grid size is 114 m. An inundation model with 100 m grid is then used to investigate the tsunami run-up.

2. GOVERNING EQUATION

2.1 Transoceanic Propagation

Since the tsunami has an initial wavelength of 1000 km and the typical water depth is around 4 km, tsunami propagation can be adequately described by a set of shallow-water equations. Using a typical wave height of 5 m, Imamura [1] estimated the relative importances of inertia forces, Coriolis force and pressure force and concluded that nonlinear inertia force is relatively insignificant and may be neglected. Because the 1960 Chilean tsunami traveled a long distance from the source region to the Hawaii island chain, the Coriolis force is important. Furthermore, the frequency dispersion also becomes significant after a tsunami travels a long distance. Hence, in terms of the spherical coordinate system, the linear long wave equations for transoceanic tsunami propagation can be expressed as

$$\frac{\partial \eta}{\partial t} + \frac{1}{R\cos\phi}\left[\frac{\partial P}{\partial \lambda} + \frac{\partial}{\partial \phi}\left(Q\cos\phi\right)\right] = 0 \tag{1}$$

$$\frac{\partial P}{\partial t} + \frac{gh}{R\cos\phi}\frac{\partial \eta}{\partial \lambda} - fQ = \frac{1}{R\cos\phi}\frac{\partial}{\partial \lambda}\left(\frac{h^3 F}{3}\right) \tag{2}$$

$$\frac{\partial Q}{\partial t} + \frac{gh}{R}\frac{\partial \eta}{\partial \phi} + fP = \frac{1}{R\cos\phi}\frac{\partial}{\partial \phi}\left(\frac{h^3 F}{3}\right) \tag{3}$$

where

$$F = \frac{1}{R\cos\phi}\left[\frac{\partial^2}{\partial t \partial \lambda}\left(\frac{P}{h}\right) + \frac{\partial^2}{\partial t \partial \lambda}\left(\frac{Q}{h}\cos\phi\right)\right] \tag{4}$$

$\eta(\phi, \lambda, t)$ is the free surface displacement, (ϕ, λ) denote the latitude and the longitude of the earth, R measures the radius of the earth, P and Q are the discharges per unit width in the $\phi-$ and $\lambda-$direction, respectively. The right-hand side terms of Eqs.(2) and (3) represent the frequency dispersion of the wave propagation.

2.2 Tsunami Run-up

In the coastal zone, depth becomes shallower and the nonlinear convective force becomes increasingly important, while the Coriolis force becomes insignificant because of the small horizontal length scale involved. Furthermore, the bottom friction becomes a dominating force in determining run-up heights. The governing equations in terms of Cartesian coordinates (x, y) can be expressed as:

$$\frac{\partial \eta}{\partial t} + \frac{\partial P}{\partial x} + \frac{\partial Q}{\partial y} = 0 \tag{5}$$

$$\frac{\partial P}{\partial t} + \frac{\partial}{\partial x}\left(\frac{P^2}{D}\right) + \frac{\partial}{\partial y}\left(\frac{PQ}{D}\right) + gD\frac{\partial \eta}{\partial x} + \tau_x D = \frac{gD^3}{6}\left[\frac{\partial^3 \eta}{\partial x^3} + \frac{\partial^3 \eta}{\partial x \partial y^2}\right] - \frac{gD^2}{2}\left[\frac{\partial^2}{\partial x^2}\left(D\frac{\partial \eta}{\partial x}\right) + \frac{\partial^2}{\partial x \partial y}\left(D\frac{\partial \eta}{\partial y}\right)\right] \tag{6}$$

$$\frac{\partial Q}{\partial t} + \frac{\partial}{\partial x}\left(\frac{PQ}{D}\right) + \frac{\partial}{\partial y}\left(\frac{Q^2}{D}\right) + gD\frac{\partial \eta}{\partial y} + \tau_y D = \frac{gD^3}{6}\left[\frac{\partial^3 \eta}{\partial x^2 \partial y} + \frac{\partial^3 \eta}{\partial y^3}\right] - \frac{gD^2}{2}\left[\frac{\partial^2}{\partial x \partial y}\left(D\frac{\partial \eta}{\partial x}\right) + \frac{\partial^2}{\partial y^2}\left(D\frac{\partial \eta}{\partial y}\right)\right] \tag{7}$$

in which $D = h + \eta$ is the total depth and τ_x and τ_y denote the $x-$ and $y-$component of bottom frictional force per unit mass, which can be written in terms of either the Manning's formula or the Chezy's formula, i.e. for Manning's formula

$$\tau_x = \frac{gn^2}{D^{10/3}} P\sqrt{P^2 + Q^2} \tag{8}$$

$$\tau_y = \frac{gn^2}{D^{10/3}} Q\sqrt{P^2 + Q^2} \tag{9}$$

where n is the Manning's relative roughness coefficient, and for Chezy's formula

$$\tau_x = \frac{g}{C^2 D^3} P\sqrt{P^2 + Q^2} \tag{10}$$

$$\tau_y = \frac{g}{C^2 D^3} Q\sqrt{P^2 + Q^2} \tag{11}$$

in which C is the Chezy's frictional coefficient. The right-hand side terms in Eqs.(6) and (7) denote the frequency dispersion. The shoreline is defined as the location of zero total depth, i.e. $D = 0$.

3. NUMERICAL SCHEME

A staggered leap-frog finite difference scheme is used to solve both linear and nonlinear versions of the shallow-water equations, Eqs.(1) to (3) and Eqs.(5) to (7). In both cases, the frequency dispersion terms are ignored. Because of numerical discretization, numerical results obtained from the leap-frog scheme are only approximated solutions to the shallow-water equations without frequency dispersion terms. The error terms introduced by the leap-frog method are more or less the same as those of frequency dispersion terms in Eqs.(1) to (3) and Eqs.(5) to (7), if the time step size and the grid size are properly chosen. For a square grid, Imamura [1] suggests that the grid size, $\Delta x = \Delta y$, is determined by

$$\Delta x = \sqrt{4h^2 + gh(\Delta t)^2} \tag{12}$$

Therefore, as water depth changes grid size and time step size need to be adjusted in order to include the frequency dispersion properly. In choosing Δt and Δx other considerations must be taken. For instance, to avoid the numerical instability, the Courant number must be less or equal to unity, i.e.

$$\frac{\sqrt{gh}\Delta t}{\Delta x} \leq 1 \tag{13}$$

and to avoid numerical damping at least twenty nodes should be included within one local wavelength. Employing the linear dispersion relation for long waves, one find that the grid size must be

$$\Delta x \leq \frac{L_f}{20}\sqrt{\frac{gh}{gh_f}} \tag{14}$$

where L_f is the length of the short axis of a fault and h_f is the water depth at the fault. It is clear that if Eq.(12) is satisfied, so will be Eq.(13). From Eqs.(13) and (14) we can determine a condition for choosing the time step size, i.e.

$$\sqrt{4h^2 + gh(\Delta t)^2} \leq \frac{L_f}{20}\sqrt{\frac{h}{h_f}} \tag{15}$$

Once Δt is determined for a local depth, Δx can be estimated from Eq.(12).

According to Eqs.(12) and (15), we have designed a nested multiple grid system to calculate the propagation of the 1960 Chilean tsunami. As shown in Table 1, the entire Pacific Ocean is divided into six subregions; within each subregion different time step size and grid size are used.

The staggered leap-frog method is a standard numerical scheme and will not be repeated here. However, the scheme for exchanging information between two regions of different grid sizes requires a brief discussion. As shown in Figure 1, a smaller grid system is nested in a larger grid system. The arrows represent the discharges, P and Q, across each grid cell, while circles and dots indicate the locations where the free surface displacement is evaluated.

Table 1. Grid System for Numerical Simulation of Tsunami Inundation at Hilo, Hawaii

region	O	A	B	C	D	E
grid size	$10min$	$5min$	$10sec$	$33.3sec$	$11.1sec$	$3.7sec$
	$18,468m$	$9,234m$	$3,078m$	$1,026m$	$342m$	$114m$
time step (sec)	20	10	5	2.5	1.25	0.625
no. of grid points (771,842)	1020x738 (752,760)	85x61 (5,185)	37x37 (1,369)	55x55 (3,025)	55x55 (3,025)	79x82 (6,478)
lower left coordinate	$129°E$ $60°S$	$161°W$ $18°N$	$155°30'W$ $19°15'N$	$155°15'W$ $19°30'N$	$155°83'W$ $19°41.7'N$	$155°6.1'W$ $19°42.2'N$
upper left coordinate	$90°W$ $60°N$	$154°W$ $23°N$	$154°30'W$ $20°15'N$	$154°45'W$ $20°N$	$154°58.3'W$ $19°51.7'N$	$154°1.3'W$ $19°47.2'N$

At a certain time level, discharges in both large and small grid systems are determined from the momentum equations, with the exception of discharges for the smaller grid system along the boundaries between two grid systems. These data are determined by interpolating the neighboring discharges from the large grid system. The free surface displacement at the next time level for the small grid system can be calculated from the continuity equation. Usually the time step size for the smaller grid system is smaller than that used in the larger grid system. Therefore, the discharges along the boundary of the small grid system at the next time level must be obtained by interpolating the neighboring discharges obtained from the large grid system over a larger time interval. After the free surface displacements in the small grid system are calculated up to the next time level of the large grid system, the free surface displacements in the large grid system are updated.

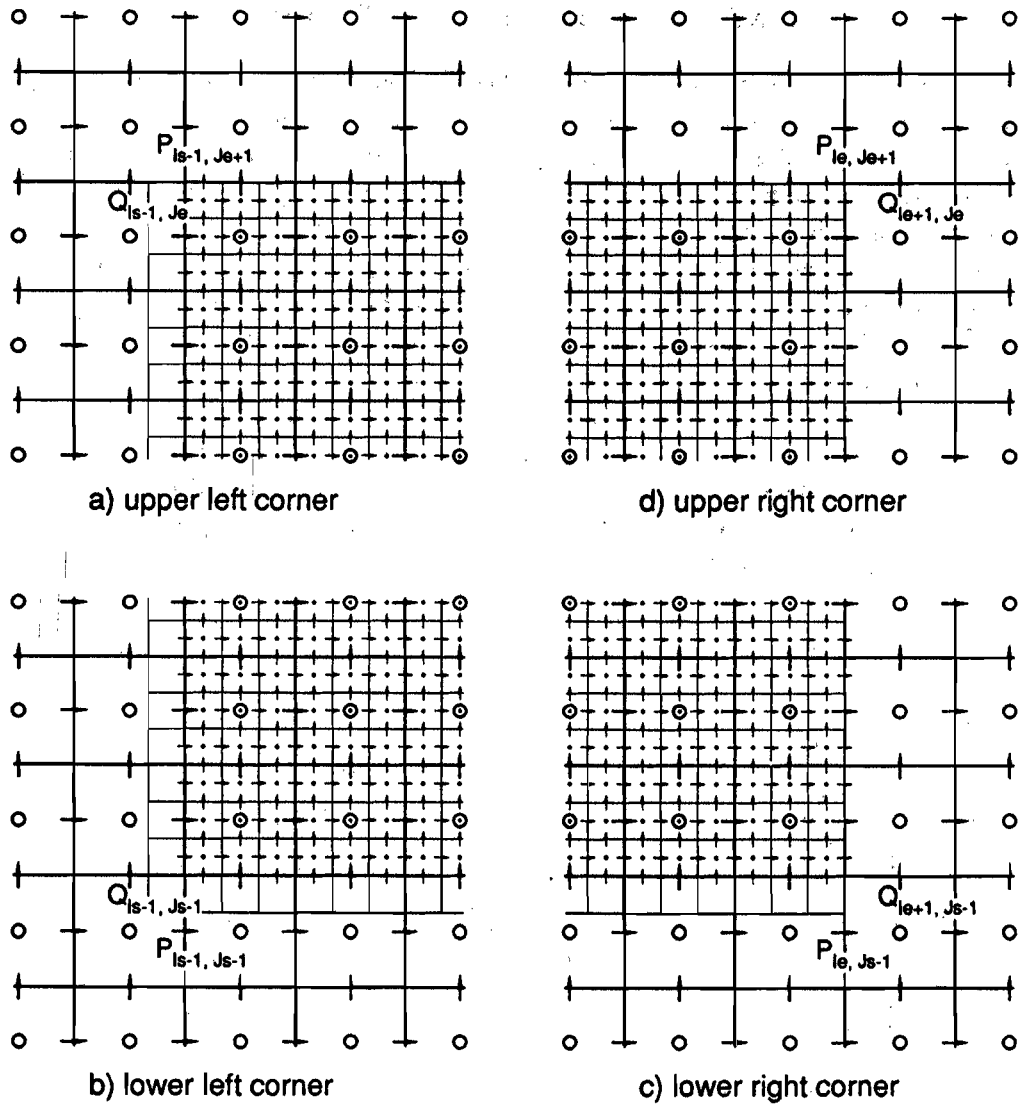

Figure 1. The nested grid system.

To estimate inundation area in the Hilo bay, a grid system with a 100 m x 100 m mesh is used to cover an area 9.9 km by 16.0 km. Not only the bathymetry of the bay but also the land topography are digitized and stored for each mesh. The offshore boundary and the right-hand side lateral boundary conditions are the time series of free surface displacement obtained from the transoceanic propagation model (region D in Table 1). No-flux boundary conditions is used along the left-hand side lateral boundary. A moving boundary condition is implemented along the shoreline.

4. NUMERICAL RESULTS AND DISCUSSION

The transoceanic propagation of the 1960 Chilean tsunami was calculated using the numerical scheme described in the previous section. Numerical solutions have been animated and a videotape showing the propagation of the tsunami has been made. Here we only show the results at selected locations (see Figure 2 and Table 2). The comparison between numerical solutions and theoretical estimation based on linear wave theory for the arrival time is given in Figure 3. The theoretical arrival time is calculated from $T = L/\sqrt{gh}$, where L is the distance between the source and the target. The agreement is very good. The time history of free surface displacement at each location is shown in Figure 4. Near the source region (location (a)) the leading wave looks like a solitary wave followed by a relatively long negative wave. As the tsunami propagates into the Pacific Ocean, the wave front spreads over a large area, reducing the leading wave amplitude. Because of the dispersion, the leading wave evolves into two solitary waves (location (b) to location (g) in Figure 4) and the negative wave becomes shorter with large amplitude.

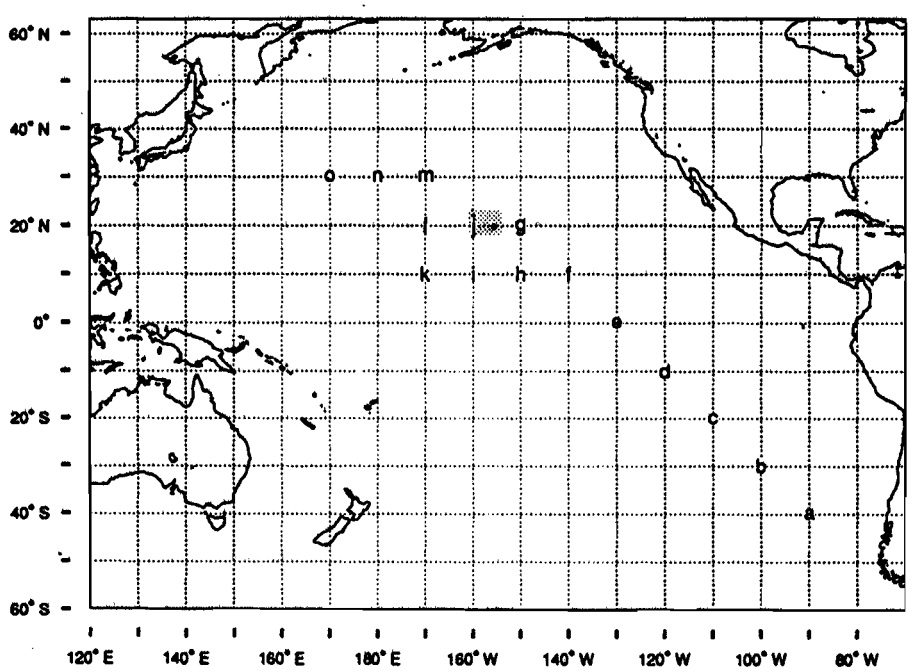

Figure 2. The locations of computed time history.

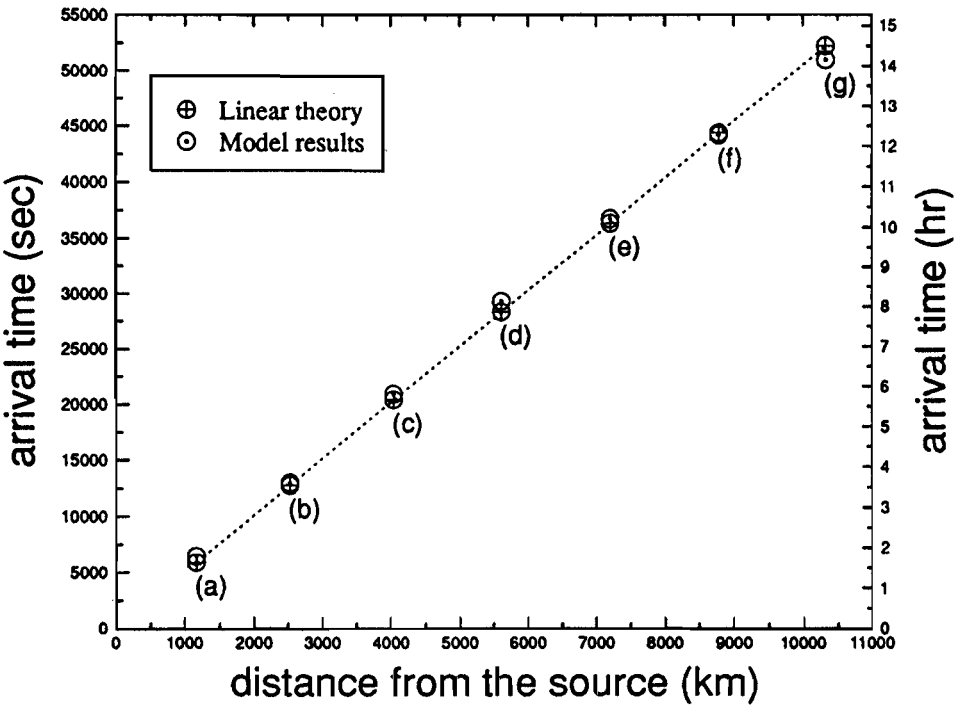

Figure 3. Arrival time of the leading wave front.

Table 2. The coordinates of the locations where numerical results are shown in Figures 2 and 3

a	b	c	d	e	f	g	h
$40°S$	$30°S$	$20°S$	$10°S$	$0°$	$10°N$	$20°N$	$10°N$
$90°W$	$100°W$	$110°W$	$120°W$	$130°W$	$140°W$	$150°W$	$150°W$

i	j	k	l	m	n	o	p
$10°N$	$20°N$	$10°N$	$20°N$	$30°N$	$30°N$	$30°N$	$19°40'N$
$160°W$	$160°W$	$170°W$	$170°W$	$170°W$	$180°E$	$170°E$	$155°W$

The boundary conditions along the offshore boundary and the right-hand side lateral boundary for the nonlinear run-up models are obtained from the transoceanic

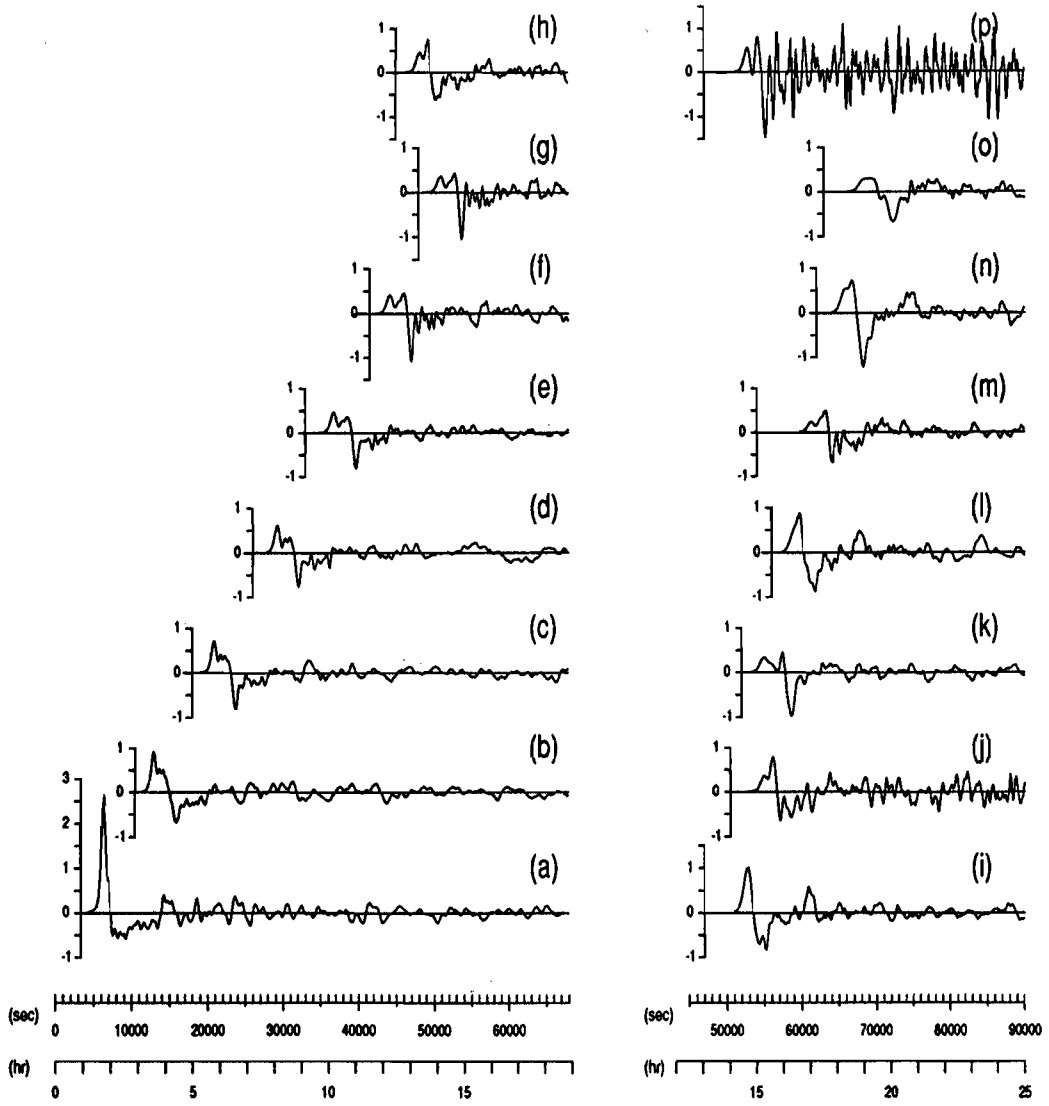

Figure 4. The time history of Chilean tsunami results of multiple grids (O-E).

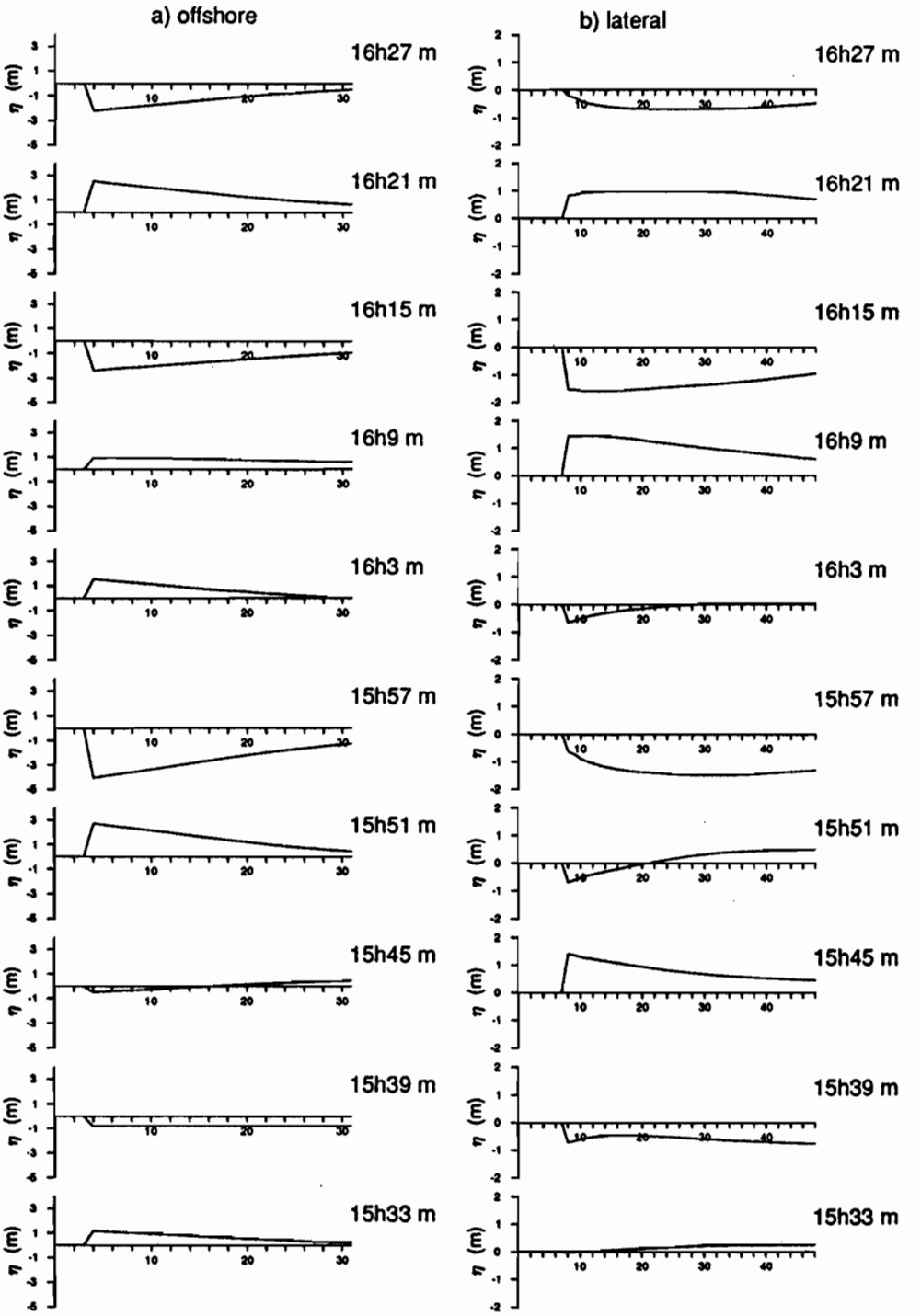

Figure 5. The time history of free surface displacement along the offshore boundary and the lateral (right-hand side) boundary.

propagation model in region D. Because the grid size in region D is 342 m while the grid size for the run-up model is 100 m, a linear interpolation scheme is used to transfer the information. In Figure 5, the time histories of the free surface elevation at several locations along the offshore boundary and the right-hand side lateral boundary are shown. They are not uniform along the boundary and imply that the direction of wave propagation is not normal to the boundary. The maximum inundation area in the Hilo bay is calculated by using variable Chezy's frictional coefficients [5]. The maximum inundation area is shown in Figure 6. The field record is also plotted for comparison. Figure 6 shows only 5 km by 5 km area. In Figure 7 numerical result for the maximum inundation area using no-flux conditions along both lateral boundaries is shown. The maximum inundation area is smaller than that prescribed in Figure 6 and agrees better with the observed data. However, the no-flux boundary condition on the right-hand side lateral boundary is not physically correct. Further research on the appropriate boundary condition is needed.

ACKNOWLEDGEMENT

The research is supported by grants from the National Science Foundation (BCS-9024965 and BCS-9115552) and by a grant from the New York Sea Grant Institute (#NA90AA-D-SG078) to Cornell University.

REFERENCES

1. Imamura, F., Possibility of Tsunami Numerical Forecasting, Doctoral dissertation, Tohoku University (in Japanese), (1989).

2. Imamura, F. and Shuto, N., Numerical Simulation of 1960 Chilean Tsunami, Proc. Japan-China (Taipei) Joint Seminar on National Hazard Mitigation, Kyoto, pp.515-524, (1989).

3. Kanamori, H. and Ciper, J.J., Focal Process of the Great Chilean Earthquake, May 22, 1960. Phy. Earth Planet, Vol.9, pp.128-136, (1974).

4. Kanamori, H. and Anderson, K.L., Amplitude of the Earth's Free Oscillations and Long-Period Characteristics of the Earthquake Source, J. Geophy. Res., Vol.80, No.8, pp.1075-1078, (1975).

5. Mader, C.L. and Curtis, G.D., Numerical Modeling of Tsunami Inundation of Hilo Harbor, JIMAR Contribution No. 91-251, University of Hawaii, (1991).

6. Mansinha, L. and Smylie, D.E., The Displacement Fields of Inclined Faults, Bull. of the Seismological Soc. of America, Vol.61, No.5, pp.1433-1440, (1971).

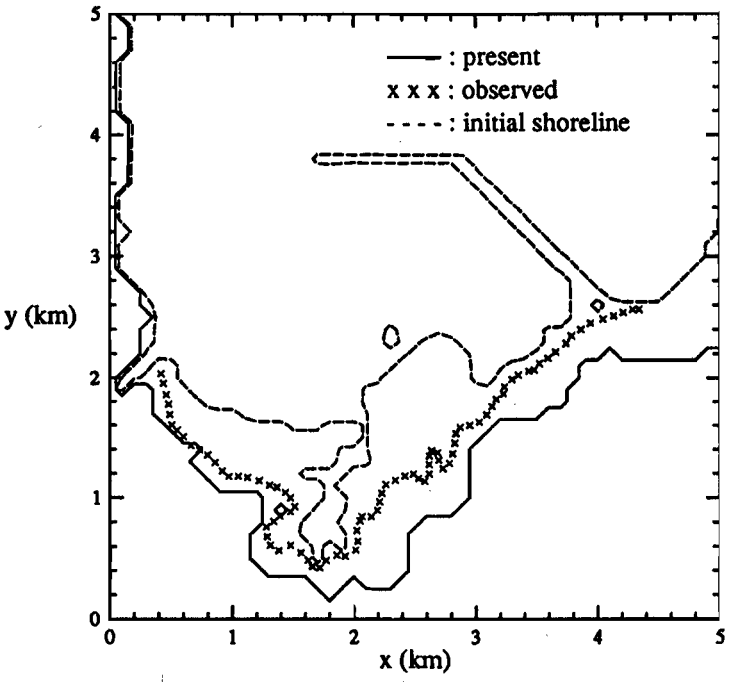

Figure 6. The calculated maximum inundation area of Hilo Bay, Hawaii.

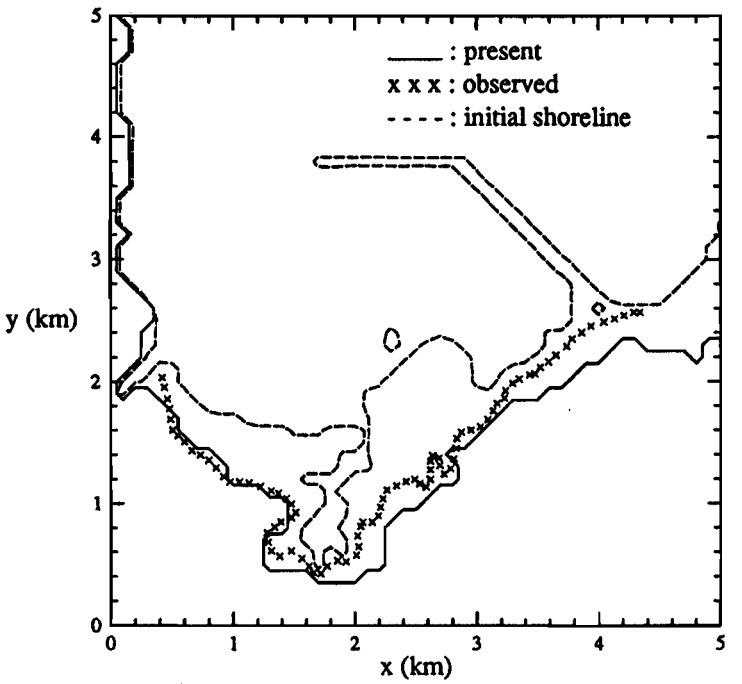

Figure 7. The calculated maximum inundation area of Hilo Bay, Hawaii.

Marine Geodesy, Volume 16, pp. 87–100
Printed in the UK.

0149-0419/93 $10.00 + .00

Numerical Simulation of Two-Dimensional Tsunami Runup

Z. KOWALIK

Institute of Marine Science
University of Alaska
Fairbanks, Alaska 99775-1080

T. S. MURTY

Institute of Ocean Sciences
Department of Fisheries and Oceans
Sidney, British Columbia
Canada V8L 4B2

Abstract *The hydrodynamic and mathematical problems connected with discontinuity between wet and dry domains, nonlinearity, friction, and computational instability are the main problems that have to be sorted out in the runup computation. A variety of runup models are analyzed, including the boundary conditions used to move the shoreline. Based on the initial experiments one-dimensional and two-dimensional algorithms are constructed. These models are tested against analytical solutions obtained by others. The extent of inundation along Alaska, British Columbia, Washington, and Oregon coasts caused by the 1964 Alaska earthquake tsunami is well documented. The data gathered at Alberni Inlet, British Columbia, Canada, is used to test the numerical model and the boundary conditions set at the mouth of the inlet. The computed extent of flooding turned out to be in satisfactory agreement with the data obtained from the observations.*

Introduction

In the ocean wave spectrum, tides, storm surges, and tsunamis belong to the class of long gravity waves. There have been several studies involving analytical and numerical simulation of storm surge and tsunami runup on a beach for the one-dimensional case. While there are a few studies available on numerical simulation of two-dimensional runup due to storm surges (e.g., Flather and Heaps, 1975), similar two-dimensional tsunami runup simulations are rare (Mader, 1988; Kim and Shimazu, 1982).

In this study we developed a numerical model for tsunami runup over smooth and discontinuous bathymetry and calibrated it at first through comparison with the known one-dimensional and two-dimensional analytical solutions. Then we used this model to simulate runup of the Alaska earthquake tsunami at Port Alberni in British Columbia, Canada. Reasonable agreement was found between observed inundation and simulated results.

Correspondence should be addressed to Z. Kowalik

Literature Review and Identification of Problems

To study tsunami runup the vertically integrated set of equations of motion and continuity is usually used:

$$\frac{\partial u}{\partial t} + u\frac{\partial u}{\partial x} + v\frac{\partial u}{\partial y} = -g\frac{\partial \zeta}{\partial x} - \frac{ru\sqrt{u^2 + v^2}}{D} \tag{1}$$

$$\frac{\partial v}{\partial t} + v\frac{\partial v}{\partial y} + u\frac{\partial v}{\partial x} = -g\frac{\partial \zeta}{\partial y} - \frac{rv\sqrt{u^2 + v^2}}{D} \tag{2}$$

$$\frac{\partial \zeta}{\partial t} = -\frac{\partial (Du)}{\partial x} - \frac{\partial (Dv)}{\partial y} \tag{3}$$

All notations are standard, with u directed along the x direction and v along the y direction; ζ is the sea-level variation and D is the total water depth, $D = H + \zeta$.

Numerical models constructed by Reid and Bodine (1968), Sielecki and Wurtele (1970), and Flather and Heaps (1975) were able to simulate the extent of inundation, but not the actual processes of wave propagation, breaking, and interaction with the coastal structures. This approach was quite successful in predicting flooding due to a major tsunami in Chile (Hebenstreit et al., 1985). A very extensive and thorough study by Lewis and Adams (1983) resulted in a complicated numerical solution for the one-dimensional problem only. Kowalik and Bang (1987) derived a solution using a different numerical algorithm, but again, only for the one-dimensional case. The boundary point between dry and wet domains is a singular point. Its position can be calculated from the equation of motion and continuity by directional derivatives only. One has to suggest a tsunami "predictor" which will move the boundary between dry and wet grid points. The best-known approach was proposed by Sielecki and Wurtele (1970). They applied an extrapolation of the sea level to the first dry point based on the continuity equation (3). Denoting m as an index of time integration and j as an index of space integration along the x direction, the extrapolated level can be found as

$$\zeta_j^{m+1} = (\zeta_j^m)_{\text{ext}} - \frac{T}{h}\{[(uD)_{j+1}^m]_{\text{ext}} - (uD)_j^m\} \tag{4}$$

Here

$$(\zeta_j^m)_{\text{ext}} = 2\zeta_j^m - \zeta_{j-1}^m \tag{4a}$$

$$[(uD)_{j+1}^m]_{\text{ext}} = 2(uD)_j^m - (uD)_{j-1}^m \tag{4b}$$

where T is time step and h is space step of numerical integration. Kim and Shimazu (1982), on the other hand, applied an equation of transport neglecting friction and inertia.

Observations of the tsunami in shallow water suggest that it behaves like a bore and not like the long waves on the gently sloping beaches. Hibberd and Peregrine (1979) studied the runup and backwash by considering the long wave equations together with the wave-front condition represented by a bore. Their condition is based on the fact that total depth equals zero at the boundary and $\zeta = -H$. To find velocity at the shoreline this condition can be incorporated into the equation of motion. Considering frictionless motion along the x direction one can write from (1),

$$\frac{\partial u_s}{\partial t} + u_s \frac{\partial u_s}{\partial x} = g \frac{\partial H}{\partial x} \tag{5}$$

The next step, which made the wave-front prediction more realistic, was an inclusion of the dissipative effects. Matsutomi (1983) proposed a new wave-front condition which depends on the time-varying friction parameter. Mader (1988) suggested a somewhat different and very simple approach to the moving boundary proposed. The movement of the boundary follows from the equation of continuity written for the upwind–downwind form. Thus, if velocity is positive in point j, the depth differences are considered between points $j + 1$ and j; for the negative velocity the differences are taken between points j and $j - 1$.

The final choice of the boundary condition will depend on the comparison of analytical or numerical computations and observations. The experiments carried out in a wave tank by Yeh (1987) did show discrepancies between observed bore front and the proposed analytical or numerical solution. Such experiments are helpful in searching for the realistic wave-front condition.

Along with the hydrodynamical problems, the mathematical problems connected with discontinuity and nonlinearity make the runup problem very difficult. Strong nonlinearity and discontinuity are often sources of the computational instability which require sophisticated filtering techniques (Lewis and Adams, 1983). A small error near the boundary, due to the approximation of a different order from the general set of equations, will generate the short wave oscillations that rapidly propagate into the whole computational domain (Marchuk et al., 1983). To delete the short period oscillations three approaches are feasible:

(1) Shapiro's space filter constructed on nine grid points (Shapiro 1970; Lewis and Adams, 1983). The filtered value is calculated as

$$\bar{F}_j = \frac{1}{256}[186F_j + 56(F_{j-1} + F_{j+1}) - 28(F_{j-2} + F_{j+2}) + 8(F_{j-3} + F_{j+3}) - (F_{j-4} + F_{j+4})] \tag{6}$$

(2) High-order upstream derivative method. The high-order finite difference formulas constructed on the seven-point stencil (Kowalik and Bang, 1987) and applied to the advective term also generate stable solution.

(3) Filtering by the additional horizontal friction term. By proper tuning this term can be used as a short-wave filter without distorting the long-period harmonics.

Along with the line of research described above, a second approach has been evolving. In this approach, a transformation of variables is applied and the independent variables x, t are transformed as

$$X = \frac{x}{l(t)} \quad \text{and} \quad T = t \tag{7}$$

where $l(t)$ is the distance from the origin of coordinate to a shore line. Through this transformation the variable region $0 \leq x \leq l(t)$ is transformed into a fixed region $0 \leq X \leq 1$, and no special boundary condition is required. The method has been extensively applied

in USSR by L'atkher et al. (1978), in England by Johns (1982), and in Japan by Takeda (1984).

To check numerical results the comparison against the exact solutions can be performed. Here an analytical solution for the wave running up the beach without friction, given by Carrier and Greenspan (1958), may be used. The solution derived by Thacker (1981) for two-dimensional oscillation in the parabolic basic is useful in predicting the extent of inundation.

Numerical Scheme Construction and Testing

To construct a numerical scheme, a space-staggered grid is applied which requires either sea level or velocity as a boundary condition. The first-order scheme is applied in time and in space. An integration is performed along the x and y directions separately. For this purpose the set (1)–(3) is split in time into two subsets. Denoting m as an index of numerical integration in time, the method can be explained through the following difference–differential equations.

First, these equations are solved along the x direction,

$$\frac{u^{m+1} - u^m}{T} + \left(u\frac{\partial u}{\partial x}\right)^m + \left(v\frac{\partial u}{\partial y}\right)^m = -g\left(\frac{\partial \zeta}{\partial x}\right)^m - \left(\frac{ru\sqrt{u^2 + v^2}}{D}\right)^m \tag{8a}$$

$$\frac{1}{2}\frac{\zeta^* - \zeta^m}{0.5T} = \frac{\partial(D^m u^{m+1})}{\partial x} \tag{8b}$$

and next along the y direction,

$$\frac{v^{m+1} - v^m}{T} + \left(v\frac{\partial v}{\partial y}\right)^m + \left(u\frac{\partial v}{\partial x}\right)^m = -g\left(\frac{\partial \zeta}{\partial x}\right)^m - \left(\frac{rv\sqrt{u^2 + v^2}}{D}\right)^m \tag{9a}$$

$$\frac{1}{2}\frac{\zeta^{m+1} - \zeta^*}{0.5T} = -\frac{\partial(D^m v^{m+1})}{\partial y} \tag{9b}$$

In this algorithm the calculation of the sea level starts from time step m, and along the x direction a preliminary value ζ^* is obtained. Afterward, this value is carried over to the y direction to derive sea level at the $m + 1$ time step.

To apply boundary conditions at the water–land boundary, first the boundary must be located at each time step. This was done by a simple algorithm proposed by Flather and Heaps (1975) for the storm surge computations and explained in Fig. 1 for the x direction only. To answer whether u_j is a dry or wet point (see Fig. 1), the sea level is tested at this point:

$$\begin{aligned} &u_j \text{ is a wet point if } 0.5(D_{j-1} + D_j) \geq 0 \\ &u_j \text{ is a dry point if } 0.5(D_{j-1} + D_j) < 0 \end{aligned} \tag{10}$$

It is obvious that total depth is positive at the wet points and equals zero at the boundary because here $\zeta = -H$. The small negative value of the total depth set at the dry points allows identification of the location of all dry regions in the computational process. Next, Sielecki and Wurtele's (1970) extrapolation (4–4b) of the sea level to the first dry point was used. The velocity in the first dry point was extrapolated linearly from the two last

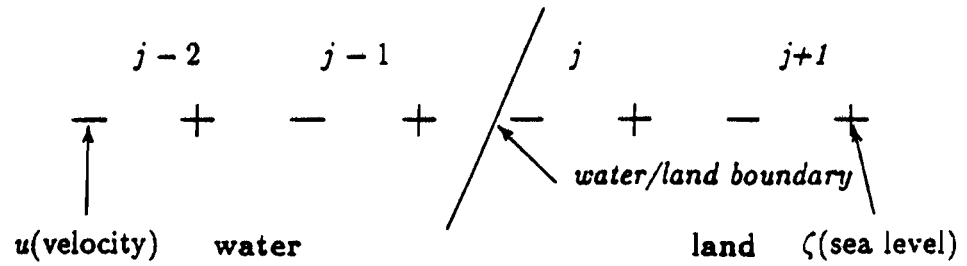

Figure 1. One-dimensional space-staggered grid for the runup calculations. Velocity points (−) and sea level points (+) are set at the different locations.

points. Linear extrapolation is easy to program but caution should be used in the case of a rough beach.

To test the above numerical method, we simulated a case that was solved analytically by Carrier and Greenspan (1958). The wave running up the beach without friction was considered and the problem was solved in the dimensionless coordinates. The distribution of the sea level along the sloping beach at the various times given both by analytical (dotted line) and numerical (continuous line) solutions is plotted in Fig. 2.

One can see that the numerical method has reproduced the analytical solution quite well, but for time $t = 0.2$ and 0.3 the short-period oscillations occur in the numerical

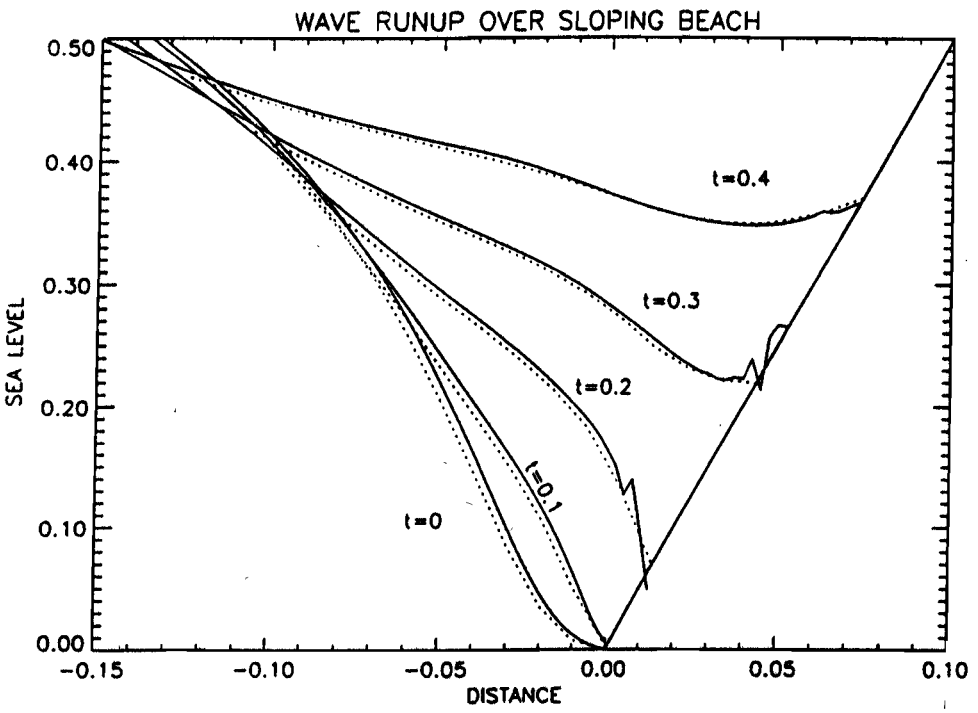

Figure 2. Numerical simulation of Carrier and Greenspan's (1958) problem. All variables, i.e., sea level time and horizontal distance, are dimensionless. The numbers represent time from the onset of the runup. The dotted line represents the analytical solution and the continuous line depicts the numerical solution.

results. Small errors near the boundary, due to the different order of approximation of the general set of equations and boundary conditions, are causing these oscillations. These oscillations were eliminated by a filter (6).

Besides, an analytical solution for the sloping beach, the solution derived by Thacker (1981) for the parabolic basin may serve well to test the frictionless motion. The initial

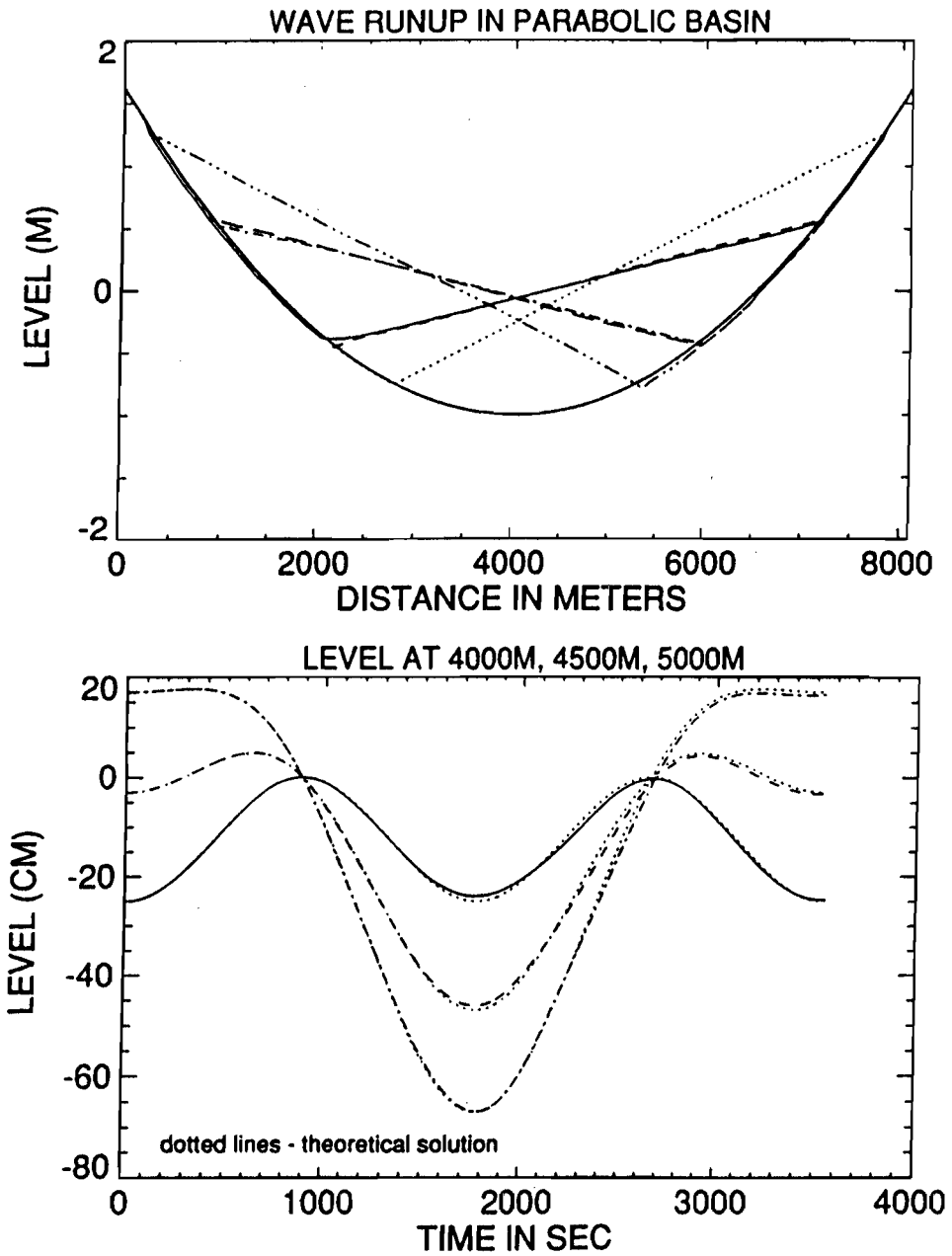

Figure 3. Numerical simulation of Thacker's (1981) solution in parabolic basin. Free surface in the frictionless motion, given initial surface distribution is planar (top portion, dotted line), will oscillate and remain planar at any time. In the bottom portion the water level oscillations are depicted at 4, 4.5, and 5 km from the left edge of the parabolic basin.

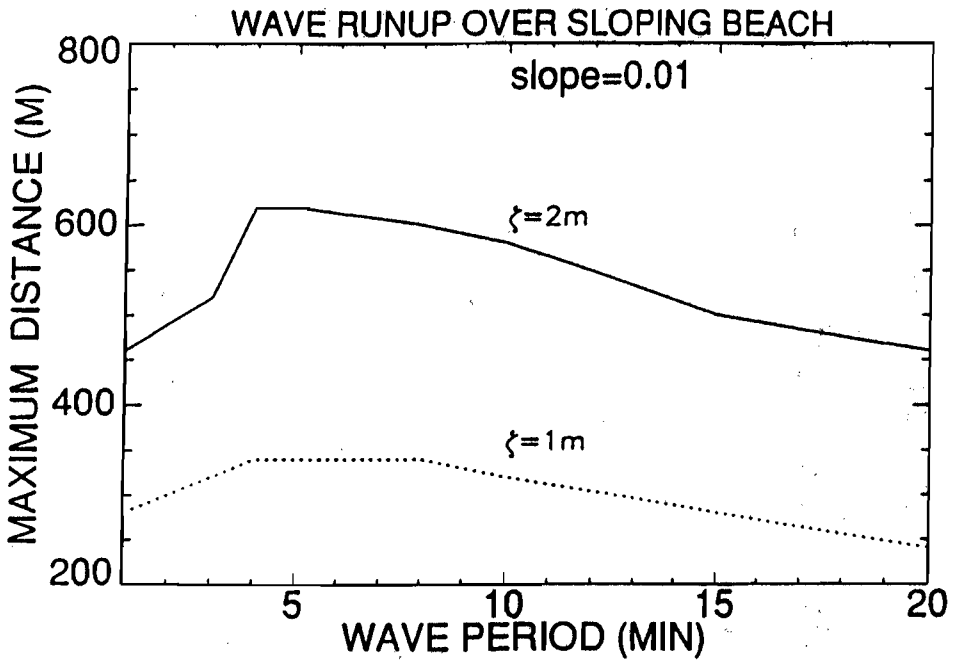

Figure 4. Maximum distance of wave penetration over dry land as a function of the wave period and wave amplitude for the constant bottom slope. The wave of given amplitude and period (e.g., 1 m and 5 min) is generated at 1 km from the shoreline. Propagation of the first wave over sloping beach of 0.01 slope is monitored and maximum travel distance from the shoreline is recorded. The dotted and continuous lines were constructed by repetition of above experiment for the various periods and two wave amplitudes (1 and 2 m).

planar free surface motion will continue to be a planar with a seiche period, depending on the depth and horizontal distance. The motion in cross section along the x axis is reproduced in the upper portion of Fig. 3 (initial position is given by dotted line). In the lower portion of Fig. 3 the sea level computed both analytically and numerically is given at a few locations.

A constructed numerical algorithm has been applied to study a response of the coastal domain to the incoming sinusoidal wave. A sloping beach with the bottom slope equal to 0.01 is considered. At the open ocean boundary, located 1 km from the shoreline, a sinusoidal wave is given as a boundary condition. Two experiments were carried out. In the first experiment, at the open boundary a 1-m wave amplitude is prescribed and the wave period is varied from 1 to 20 min. In the second experiment, the 2-m amplitude is considerd. Figure 4 depicts the maximum distance of wave penetration over dry land as a function of the wave period. This is runup calculated from the first incoming wave. Since the wave at the open boundary pumps water in a continuous fashion, it is interesting to see if this pumping mode influences runup distance. Two experiments were performed with bottom friction coefficient $r = 0$ and $r = 0.03$. The results for the 1-m amplitude are depicted in Fig. 5. For the high friction case the runup does not change in time, but frictionless motion displays runup increase for the second and third wave. This runup stays almost constant after the third wave.

Realistic motion in two-dimensional space often takes place over discontinuous bathymetry where a simple extrapolation scheme for the moving boundary fails to produce

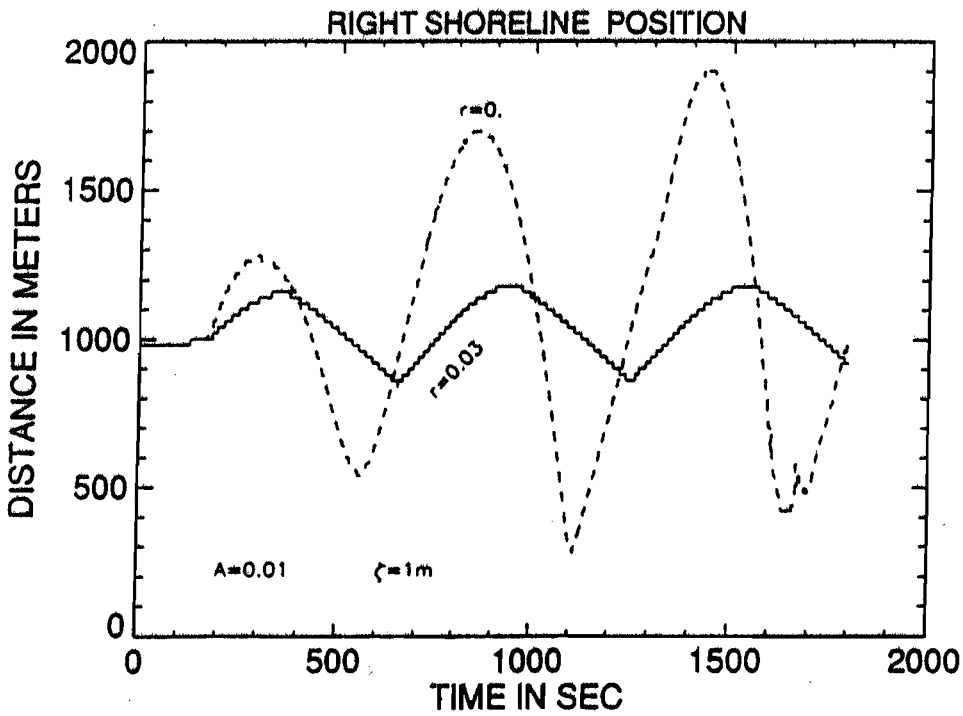

Figure 5. Computed runup distance for two cases of bottom friction ($r = 0$ and $r = 0.03$). The wave of 1-m amplitude and 10-min period is generated 1 km from the shoreline. Propagation of the several waves in the wave train is monitored by recording position of the shoreline in time. In the frictionless motion ($r = 0$) the second and third waves generate larger runup than the first wave. If the bottom friction is introduced ($r = 0.03$) the runup decreases and differences in the runup of the first, second, and third waves are very small.

the right answer. To account for the various cases of overtopped, submerged, or exposed barriers, special boundary conditions have been introduced. For example, for the overtopped barrier the velocity is calculated by

$$u = \pm\sqrt{gD} \tag{11}$$

Here D is depth of the water over the barrier. The water is transported from the top of the barrier to the foot by the above velocity. When water flows across a submerged barrier the velocity is calculated by the formula for a submerged weir, Reid and Bodine (1968).

To illustrate a two-dimensional motion with discontinuous topography, two cases of waves running up the beach are considered. The channel, which comprises a sloping beach along the x direction, is 200 wide along the y direction. As in the previous experiments, the open boundary is located 1 km from the shoreline and a 1-m amplitude sinusoidal wave is set at the open boundary. In the first experiment a depression in the beach profile is considered (Fig. 6). The water running up the beach will flow into the depression from the various directions and eventually fill it up completely (Fig. 6). The second experiment demonstrates wave interaction with an obstacle located on the beach (Fig. 7). The obstacle reflects the wave and divides the flow into two branches; finally, the divided flow joins beyond the obstacle and runs up the beach.

Simulation of Tsunami Runup at Port Alberni

We constructed a grid for the head of the Alberni Inlet and the Somass River with the grid size of 50 m. The total number of grid points along the length of the inlet is 135 and there are 75 points along the width. Figures 8 and 9 respectively show the water depth in the inlet and river and the surrounding land elevations. At time $t = 0$ a tsunami wave with amplitude of 3.8 m and period of 95 min enters the head of the inlet. Figure 10 shows the computed tsunami inundation (the computed inundation boundary (heavy line) and observed inundation boundary (broken line) (White 1966)). The overall comparison seems to be satisfactory, although in the region located around $x = 5000$ m, $y = 500$ m the model depicts higher inundation than the observed values. This can be explained only

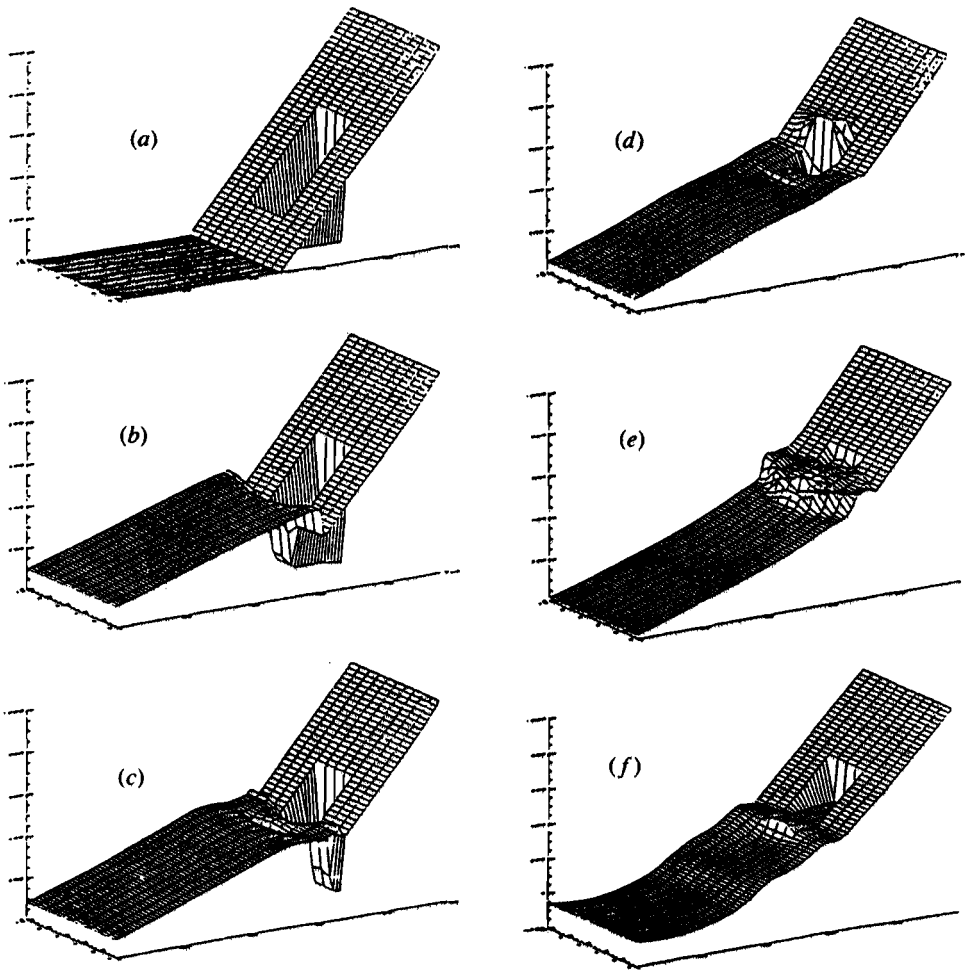

Figure 6. Simulation of two-dimensional motion with discontinuous topography: a depression in the beach profile. A sloping bottom chanel of 1 km long and 200 m wide continues as a sloping beach of 1 km long with depression of 80 m wide and 400 m long located 180 m from the shoreline (a). The wave enteres the depression and climbs the shores around it (b, c). Further progress in filling up the depression with the multiple reflections and confused sea level distribution is depicted in Fig. 6d and e. The wave recedes down-slope leaving water in the depression (f).

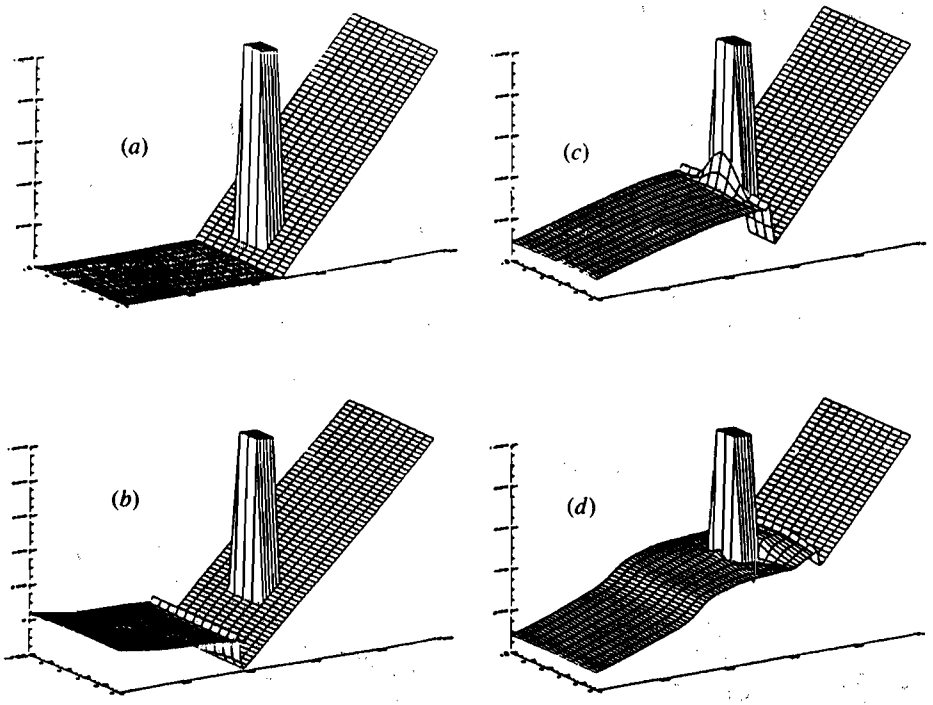

Figure 7. Simulation of two-dimensional motion with discontinuous topography: an obstacle located on the beach. A sloping bottom channel of 1 km long and 200 m wide continues as a sloping beach of 1 km long with an obstacle located 60 m from the shoreline (a). The obstacle is 80 m wide, 120 m long, and 10 m high. The wave of 1-m amplitude travels up the beach (b), impinges on the obstacle and reflects from it (c), and displays a curved front behind the obstacle (d).

by the small land slopes in this region. Here terrain raises from 5 to 10 m at a distance of 500 to 800 m.

There are hills on the north side of the inlet and there was little tsunami inundation. On the west side, the agreement between the observed and computed inundation is quite satisfactory. The disagreement between the computed and observed inundation in the southwest corner was somewhat reduced (Fig. 11) when the topography was improved by including the location of the hugh MacMillan-Bloedel pulpmill in the computation.

Figure 12 shows the observed (broken line) and computed (solid line) data of the first few waves at Port Alberni (Dunbar et al., 1991). According to Dunbar et al. the simulation at Port Alberni shows that the first wave is modeled well, but thereafter the predicted wave lags the measured wave. The modeled third wave has the largest amplitude (6 m); observations by Wigen and White (1964) suggest that the third wave was, in fact, the highest at about 4.2 m above the tidal water level. However, the modeled wave lags observations by about one-half a wave period ($1\frac{1}{4}$ h). White (1966) recognized that the Port Alberni observations are imprecise, since the gauge at the townsite had broken and these high-water values are a synthesis made up from data collected up the Somass River and from eyewitness accounts at the town.

The differences in height and timing between the modeled and observed data reflect the fact that Alberni Inlet is nearly resonant with the initial wave (100- to 110-min period), and the treatment of the reflecting boundary conditions at Port Alberni. Modeled water

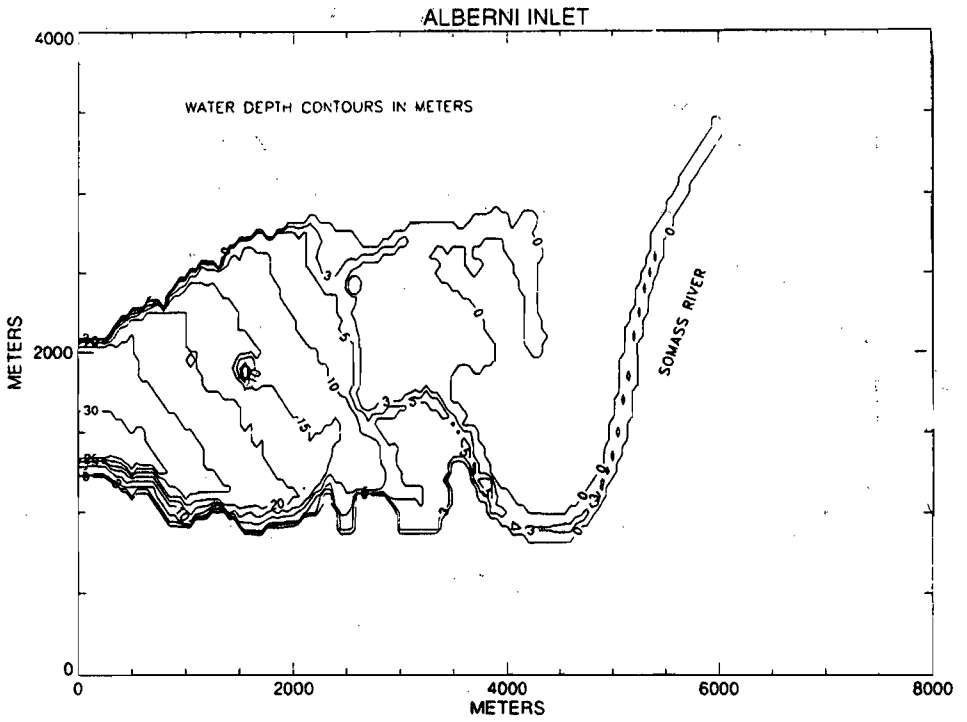

Figure 8. Head of the Alberni Inlet and Somass River; water depth in m.

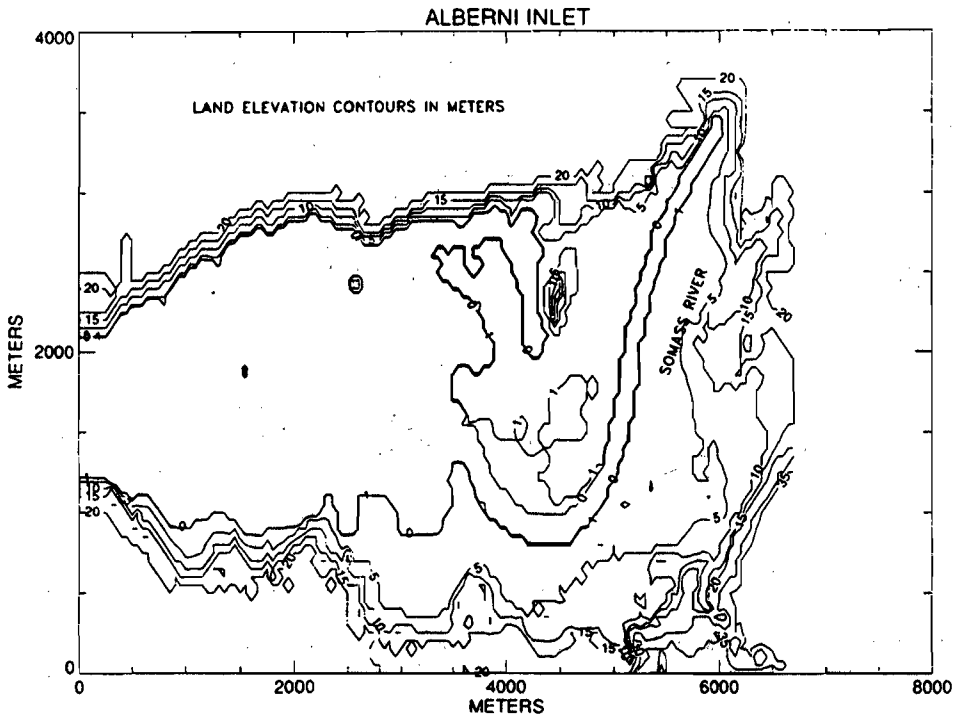

Figure 9. Head of the Alberni Inlet and Somass River; land elevation in m.

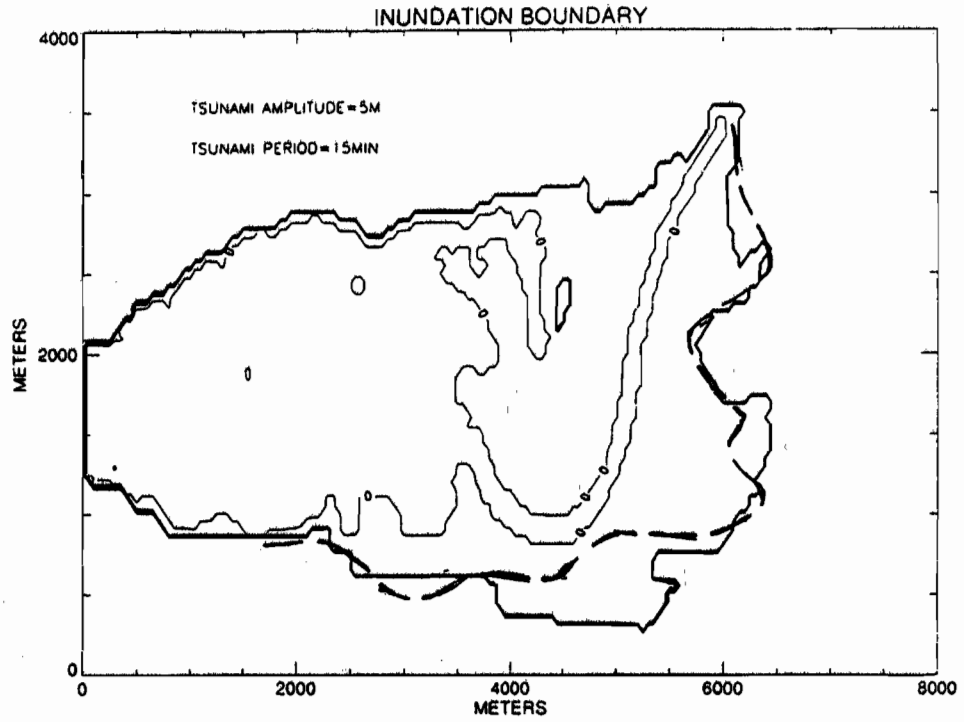

Figure 10. Computed (solid line) and observed (broken line) inundation of Port Alberni.

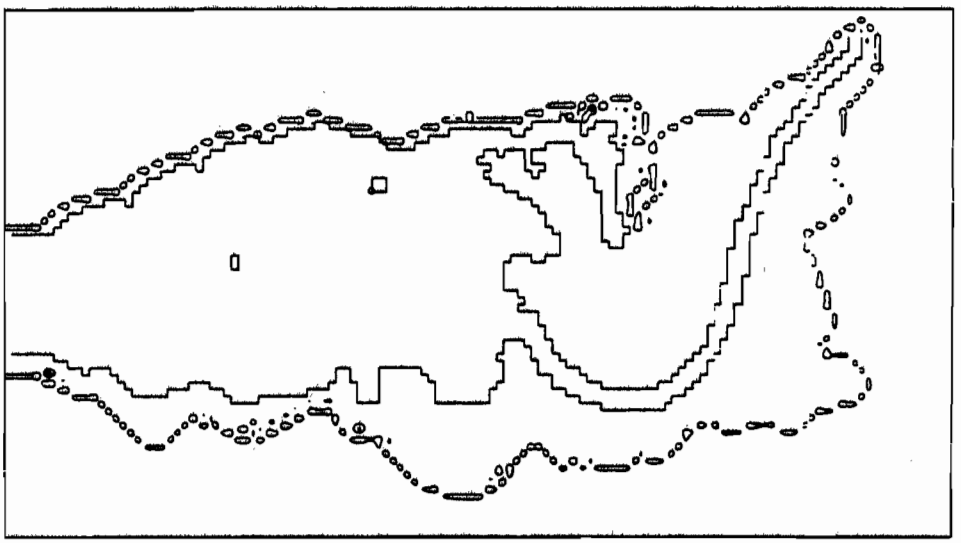

Figure 11. Computed inundation of Port Alberni, after proper inclusion of the pulpmill in the computations.

levels at the head of the inlet could be improved by incorporating a high-resolution model of the flood-dry area in the Somass River valley that allows the tsunami to dissipate some energy by inundating the surrounding land.

This has been done in the present work and, as can be seen from Fig. 13, the modeled waveforms agree with the observed waveforms quite well, in both phase and amplitude. We hope to improve the results even more in future work, by including structures on the land that was inundated in the computations.

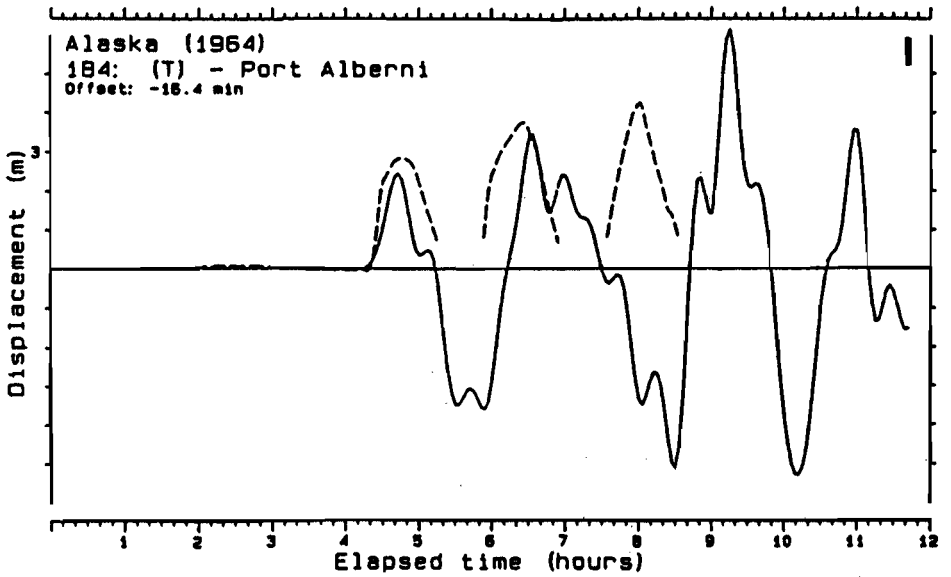

Figure 12. Observed (broken line) and computed (solid line) tsunami wave forms at Port Alberni (Dunbar et al., 1991) without including land flooding.

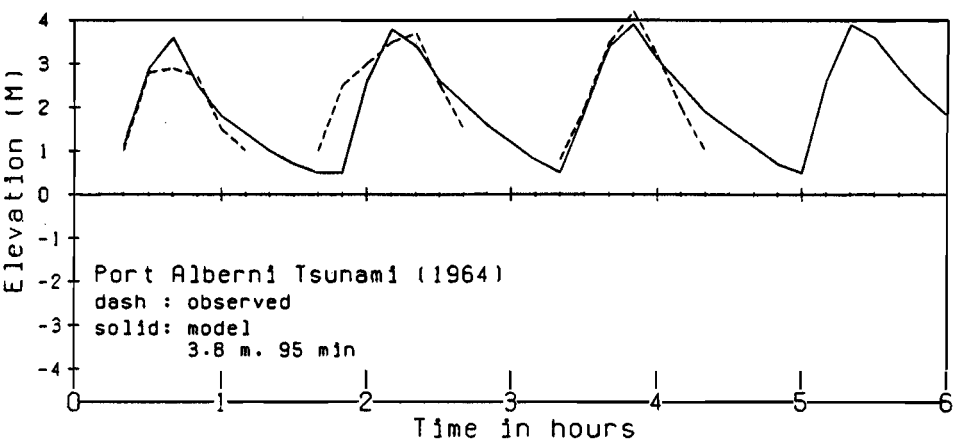

Figure 13. Observed (broken line) and computed (solid line) tsunami wave forms at Port Alberni with the inclusion of inundation.

References

Carrier, G. F., and H. P. Greenspan. 1958. Water waves of finite amplitudes on a sloping beach. *J. Fluid Mech.* 4:97–109.

Dunbar, D. S., P. H. LeBlond, and T. S. Murty. 1991. Evaluation of tsunami amplitudes for the Pacific coast of Canada, *Progress in Oceanogr.* 15:115–177.

Flather, R. A., and N. S. Heaps. 1975. Tidal computations for Morecambe Bay. *Geophys. J. R. Astron. Soc.* 42:489–517.

Hebenstreit, G. T., F. I. Gonzalez, and A. F. Morris. 1985. Near-source tsunami simulation of Valparaiso Harbor, Chile. In T. S. Murty and W. J. Rapatz, eds. *Proc. Int. Tsunami Symp.* Sidney, BC: Inst. Ocean Sciences.

Hibberd, S., and D. H. Peregrine. 1979. Sur and run-up on a beach: A uniform bore. *J. Fluid Mech.* 95:323–345.

Johns, B. 1982. Numerical integration of the shallow water equations over a sloping beach. *Int. J. Numerical Methods Fluids* 2:253–261.

Kim, S. K., and Y. Shimazu. 1982. Simulation of tsunami runup and estimate of tsunami disaster by the expected great earthquake in the Tokai District, Central Japan. *J. Earth Sci. Nagoya Univ.* 30:1–30.

Kowalik, Z., and I. Bang. 1987. Numerical computation of tsunami run-up by the upstream derivative method. *Sci. Tsunami Hazards Int. J. Tsunami Soc.* 5(2):77–84.

L'atkher, V. M., A. N. Militev, and S. Ya. Shkol'nikov. 1978. Calculation of the tsunami run-up. In *Tsunami research in the open ocean*, pp. 48–55. Moscow: Nauka.

Lewis, C. H., III, and W. M. Adams. 1983. Development of a tsunami-flooding model having versatile formulation of moving boundary conditions. *The Tsunami Society Monograph Series*, No. 1.

Mader, L. Ch. 1988. *Numerical modeling of water waves.* Berkeley: University of California Press.

Marchuk, A. G., L. B. Chubarov, and Iu. I. Shokin. 1983. *Numerical modeling of tsunami waves.* Novosibirsk: Id. Nauka, English translation, Los Alamos, 1985.

Matsutomi, H. 1983. Numerical analysis of the run-up of tsunamis on dry bed. In K. Iida and T. Iwasaki, eds. *Tsunamis: Their science and engineering*, pp. 479–493. Tokyo: Terra Sci.

Reid, R. O., and B. R. Bodine. 1968. Numerical model for storm surges in Galveston Bay. *J. Waterway Harbour Div.* 94(WWI):33–57.

Shapiro, R. 1970. Smoothing, filtering and boundary effects. *Rev. Geophys. Space Phys.* 8:359–387.

Sielecki, A., and M. G. Wurtele. 1970. The numerical integration of the nonlinear shallow-water equations with sloping boundaries. *J. Comput. Phys.* 6:219–236.

Takeda, H. 1984. Numerical simulation of run-up by the variable transformation. *J. Oceanogr. Soc. Japan* 40:271–278.

Thacker, W. C. 1981. Some exact solutions to the nonlinear shallow-water wave equations. *J. Fluid Mech.* 107:499–508.

White, W. R. H. 1966. The Alaska earthquake: Its effect in Canada. *Can. Geophys. J.* 72(6).

Yeh, H. 1987. Tsunami action on a beach: summary. In E. N. Bernard, ed. *Proc. International Tsunami Symp., Vancouver, BC*, pp. 206–211. Seattle: NOAA/PMEL.

TSUNAMI '93
Proceedings of the IUGG/IOC International Tsunami Symposium
Wakayama, Japan, August 23-27, 1993, pp. 627-635

Appendix J

A numerical study of wave runup of the September 1, 1992 Nicaraguan tsunami

Vasily Vladimirovitch Titov

Research assistant, School of Engineering , University of Southern California
Los Angeles, California, 90089-2531

Costas Emmanuel Synolakis

Associate Professor, School of Engineering , University of Southern California
Los Angeles, California, 90089-2531

ABSTRACT

This is a study of the coastal effects of the Nicaraguan tsunami of September 1, 1992. A two dimensional nonlinear model is used for modeling the generation and propagation of the wave and then a one dimensional nonlinear runup model is used for studying the wave runup. The model uses the splitting method and a variable space grid to improve the accuracy of the computations, consistently. The revised source parameters estimated by Imamura et al [1] are applied to the generation mechanism and this model's predictions appear in good agreement with the field data. These results suggest that for simple plane-beach type bathymetries -like the Pacific Coast of Nicaragua- a combination of two-dimensional and one-dimensional models may be adequate for predicting tsunami runup.

1. INTRODUCTION

On September 12, 1992 a catastrophic tsunami hit the Pacific coast of Nicaragua. The tsunami was triggered by an earthquake with an epicenter estimated about 100 km offshore with a surface wave magnitude M_S estimated in the range M_S = 7.0 - 7.3 ([2], [3], [4]). An extensive field survey was conducted two weeks after the event by an international scientific team which reported maximum runup heights up to 10 meters and penetration distances up to half-a-mile into the dry land. The tsunami caused 168 deaths, 489 casualties and extensive property damage.

[1], [2], [3] and [4] all reported a large discrepancy between the low surface wave magnitude (M_S) and the large measured tsunami runup heights. Satake et al [4] estimated a tsunami earthquake magnitude of M_t=8.0 and they characterized this earthquake as a tsunami earthquake in the sense of Kanamori [5].

Numerical modeling of the tsunami generation and propagation was carried out shortly after the event [1] and the international survey team actually used some of their predictions in planning the survey. The model used linear shallow-water-wave theory without directly calculating wave runup; the calculations stopped at the 10m contour and the wave runup was estimated by multiplying the wave height at the 10m contour by a factor of two. The numerical values of these predictions were considerably different than the field observations, even though the relative distribution of "runup" values along the shoreline was approximately correct, i.e., the model

predicted correctly the hardest hit areas, without predicting correctly the runup amplitudes. These computations suggested that perhaps the conventional method of estimating the source parameters from seismic data may not predict accurately the bottom displacement that generated the wave; any calculations using incorrect bottom displacements are unlikely to produce good agreement with the field data.

To improve their numerical predictions, Imamura et al [1] re-evaluated their source parameters by comparing the field observations with the model results. They found that they could obtain a satisfactory agreement if they multiplied the model results by a factor of 10 and they conjectured that -since they were solving a linear problem- the seismic moment which was used to obtain the source motion should also be multiplied by a factor of 10. Preliminary unpublished results suggested that their calculation with the "improved" seismic moment did not produce substantially better agreement between the model and the field data and the results still differed by large factors. Titov [6] used a nonlinear model -again stopping at the 10m contour- and the same technique of using the runup ratio of 2 to predicted measured data and he showed good agreement with field observations. The overall factor of 20 used in [1] suggest that perhaps the linear model stopping at the 10m contour is not an equally reliable method as the nonlinear model for calculating runup heights.

In this paper we will present a substantial improvement of the Titov [6] two-dimensional numerical model including a one-dimensional shoreline calculations. This model appears to predict satisfactorily the field observations of the Nicaraguan tsunami based on the revised seismic moment.

2. DESCRIPTION OF THE 2-D NUMERICAL MODEL

We use the two-dimensional shallow-water-wave equations to model tsunamis propagating over variable bottom. These equations are now believed to model most important physical characteristics of tsunami propagation, despite certain severe limitations [7].

The shallow water wave equations are

$$\begin{aligned} &h_t + (uh)_x + (vh)_y = 0 \\ &u_t + uu_x + vu_y + gh_x = gd_x \\ &v_t + uv_x + vv_y + gh_y = gd_y . \end{aligned} \tag{1}$$

where $h = \eta(x,y,t) + d(x,y,t)$, $\eta(x,y,t)$ is the amplitude, $d(x,y,t)$ is the undisturbed water depth, $u(x,y,t)$, $v(x,y,t)$ are the depth-averaged velocities in the x and y directions respectively.

Appropriate boundary and initial conditions should be specified for these equations. Here we solve the problem of tsunami generation due to bottom displacement, so we specify the following type of initial conditions

$$\begin{aligned} &d(x,y,t) = d_0(x,y,t), \quad t \le t_0 \\ &d(x,y,t) = d_0(x,y,t_0), \quad t > t_0 . \end{aligned} \tag{2}$$

Usually, t_0 is assumed to be small, so that the bottom movement is an almost instantaneous vertical displacement.

For arbitrary topography and bottom displacement the system of equations (1) has to be solved numerically. We will use finite-differences algorithm based on the splitting method. This method reduce the numerical solution of the 2-D problem into consecutive solution of two 1-D problems (containing only one space variable), as follows

$$
\begin{aligned}
&h_t + (uh)_x = 0 && h_t + (vh)_y = 0 \\
&u_t + uu_x + gh_x = gd_x && v_t + vv_y + gh_y = gd_y \\
&v_t + uv_x = 0 && u_t + vu_y = 0
\end{aligned} \qquad (3)
$$

Each system above can be written in characteristic form as

$$
\begin{aligned}
&p_t + \lambda_1 p_x = gd_x \\
&q_t + \lambda_2 q_x = gd_x \\
&v' + \lambda_3 v' = 0
\end{aligned} \qquad (4)
$$

where $p = u + 2\sqrt{gh}$, $q = u - 2\sqrt{gh}$ and $v' = v$ are the Riemann invariants of this system and $\lambda_{1,2} = u \pm \sqrt{gh}$ and $\lambda_3 = u$ are the eigenvalues.

The system of equations (3) has three families of characteristic lines with slopes λ_1, λ_2 and λ_3; λ_1 is positive, λ_2 is negative almost everywhere in the region, where the Froude number is less then 1, and λ_3 can be either positive or negative. One or two boundary conditions are necessary on each boundary depending on the sign of λ_3 on the boundary. The boundary conditions for a totally reflective left boundary are

$$p = -q, v' = 0, \qquad (5a)$$

and for the right boundary they are

$$q = -p, v' = 0. \qquad (5b)$$

Gustafsson and Kreiss [8] used this characteristic approach to develop an absorbing boundary conditions for time dependent problems. A totally absorbing boundary allows waves to go through (absorb) but it does not allow any waves to reflect back in the computation region, i.e. the invariant on outgoing characteristics does not carry any disturbances into the computational area. We assume that the water depth is constant outside the area of computation; then the absorbing boundary conditions for the left boundary become

$$p = 2\sqrt{gd_n}, v' = 0, \qquad (6a)$$

where d_n is water depth at the left boundary. For the right boundary they are

$$q = -2\sqrt{gd_n}, v' = 0 \qquad (6b)$$

where d_n is water depth at the right boundary.

These boundary conditions work well. Our computations show that there are no detectable waves reflected from this boundary.

The numerical solution uses the following explicit finite-difference scheme:

$$\frac{\Delta_t p_i^n}{\Delta t} + \frac{1}{2\Delta x}\left[\lambda_i^n(\Delta_{-x} + \Delta_x)p_i^n - \frac{\Delta t}{\Delta x}\lambda_i^n \Delta_x \Delta_{-x}(\lambda_i^n p_i^n)\right] = \frac{g}{2\Delta x}\left[(\Delta_{-x} + \Delta_x)d_i^n - \frac{\Delta t}{\Delta x}\lambda_i^n \Delta_x \Delta_{-x} d_i^n\right] \qquad (7)$$

where $f_i^n = f(x_i, t_n)$, $\Delta_t f_i^n = f(x_i, t_n + \Delta t) - f(x_i, t_n)$, $\Delta_x f_i^n = f(x_i + \Delta x, t_n) - f(x_i, t_n)$, $\Delta_{-x} f_i^n = f(x_i, t_n) - f(x_i - \Delta x, t_n)$

The condition of the stability for the scheme is the Courant-Friedrichs-Lewy criterion

$$\Delta t \le \frac{\Delta x}{|u| + \sqrt{gh}}. \tag{8a}$$

The finite-difference scheme (7) is used for the computation of the unknown variables p and q in the interior grid points of the computational area. However, these equations can't be used to compute boundary values. At those points, the boundary conditions (5) and (6) determine only one of the two invariants. The other value on the boundary (the value of the Riemann invariant on the incoming characteristic) is computed using one of the equations (3) by the upwind or the downwind finite-difference equations, depending on the boundary.

Good accuracy of numerical solutions of any hyperbolic equation is obtained whenever there are "enough" grid points per wave length. The qualification "enough" depends on the numerical method. The Lax-Wendroff technique, which is very often used for the solution of shallow-water-wave equation, requires at least twenty grid points in one wave length to avoid the decay of the modeling wave [9]. Our method only requires about ten points per wavelength.

During shoaling the wavelength becomes shorter; therefore calculations using a uniform grid throughout the computational domain suffer either loss of accuracy in the near-shore field or they require very fine grid; and then it does not produce consistent resolution. In our method we use a variable grid.

To allow for the variable grid, we modify equations (7) by replacing the first order derivative operator

$$\frac{(\Delta_{-x} + \Delta_x)}{2\Delta x} \tag{9a}$$

by

$$\frac{(\Delta_{-x} + \Delta_x)}{\Delta x_{i-1} + \Delta x_i}, \tag{9b}$$

while the second order derivative operator

$$\frac{\Delta_{-x}\Delta_x}{\Delta x^2} \tag{10a}$$

is replaced by

$$\frac{2}{\Delta x_{i-1} + \Delta x_i}\Delta_x\left(\frac{\Delta_{-x}}{\Delta x_i}\right). \tag{10b}$$

The stability criterion for this variable grid scheme becomes

$$\Delta t \le \min_i \frac{\Delta x_i}{|u_i| + \sqrt{gh_i}}. \tag{8b}$$

To model tsunami wave propagation areas with complex bottom profiles containing shorelines, two different numerical grids are used. One grid is for computing the deep sea propagation and it has larger space steps. The other grid has finer grid spacing for near-shore computation. Our algorithm provides a fairly good accuracy of computation, the number of points per wave length remaining consistent throughout the computational area.

3. DESCRIPTION OF THE 1-D RUNUP MODEL

The numerical modeling of the runup process using finite-difference method requires approximating the moving shoreline boundary. In the present study the modeling of the runup process uses the one-dimensional shallow-water-wave equations

$$h_t + (uh)_x = 0$$
$$u_t + uu_x + gh_x = gd_x \qquad (11)$$

A finite-difference scheme similar to the one described earlier has been used to solve the equations written in a characteristic form [10].

To simulate the runup of long waves on the dry bed, moving boundary conditions have been applied at the shoreline. Since it is not possible to solve (7) directly, approximations of the boundary values from previous space nodes are used. The variables used in shoreline scheme is described in Figure 1.

The objective is to keep the shoreline boundary point on the surface of the beach slope during the computation . To accomplish this the length of the last space step Δx is adjusted every time step. The values of the unknown variables on the shoreline node are extrapolated from the previous internal point, where these values are computed by equations (7). When the boundary point reaches the next fixed grid point (n-th grid point in Figure 1), a new internal node is introduced between the shoreline point and the previous internal node.

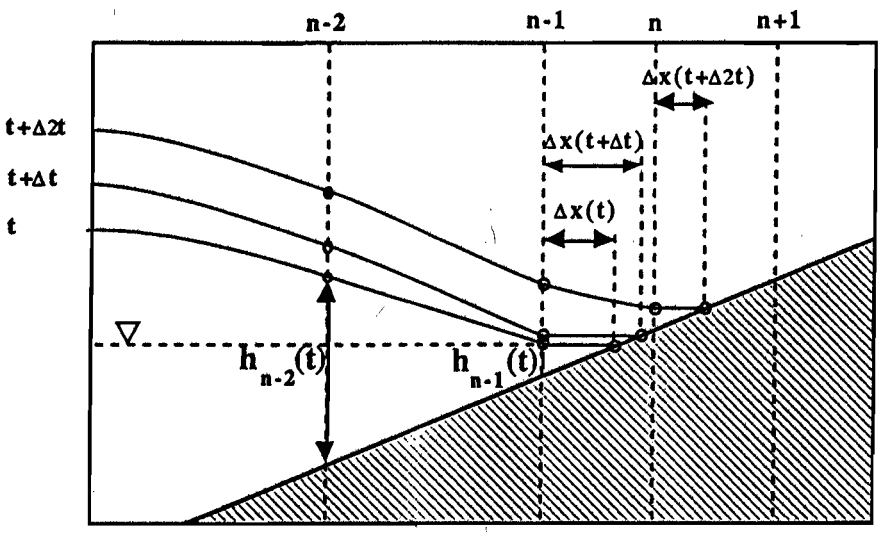

Figure 1. Definition sketch for the shoreline boundary computation

The method have been tested on the solution of solitary wave runup on sloping beach. The comparison with analytical solution and experimental results shows excellent agreement [10].

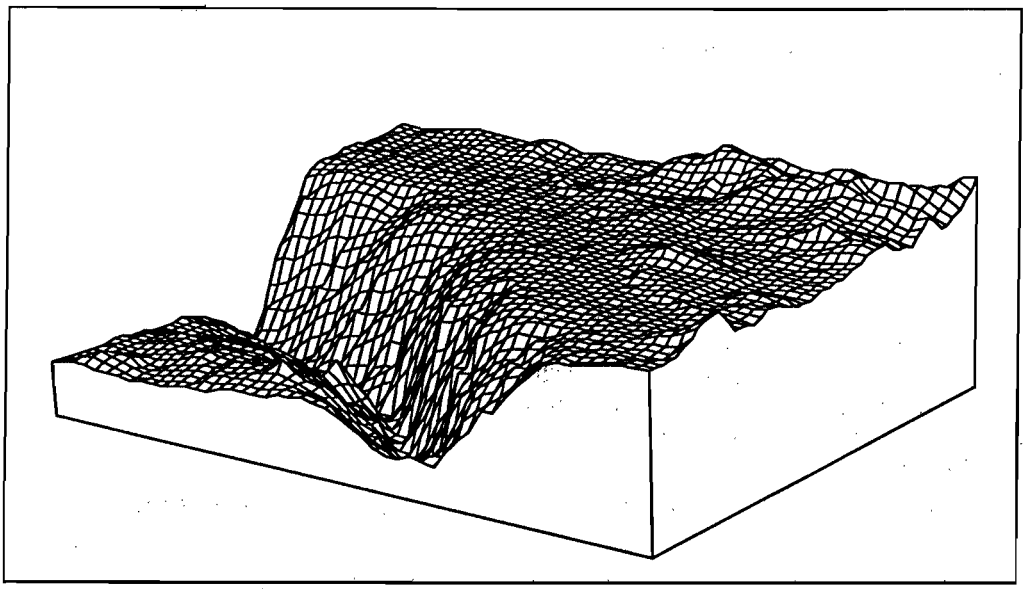

Figure 2. Bottom profile near the Nicaragua coast.

4. RESULTS OF THE RUNUP COMPUTATION

The objective of this paper is to predict the coastal effects of the Nicaraguan tsunami with the bathymetry data available at the time of the writing of this paper from hydrographic charts which -at best- can be digitized on a 1.5 km grid. This type of coarse grid cannot predict correctly the details of the runup motion on the shoreline which always is a strong function of the local features. For example, in the village of El Transito, Nicaragua, the international survey team measured runup heights ranging from 9.9m to 6.4m [2] and unpublished observations near the south side of the beach reported runup heights as low as 1.8m, all within a length of 1 km. Significantly lower runup heights were measured in beaches north and south of El Transito suggesting wave focusing at El Transito.

Therefore without detailed relief data it is unavailing to attempt to model the two-dimensional shoreline motion. Instead, we conjectured that since the shelf off the Nicaragua coast has a simple bathymetry similar to a plane beach (Figure 2), then perhaps we could use a one dimensional model beyond the offshore location where the wave crest was practically parallel to the coastline. We tested our hypothesis as follows.

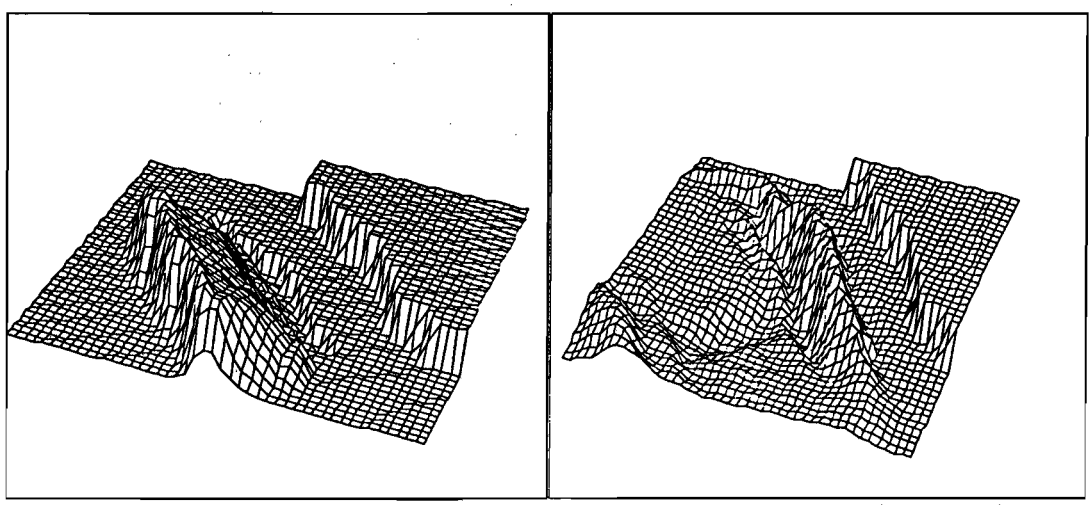

Figure 3a,b. Three dimensional wave profiles at 25 sec and at 4 min 20 sec after generation.

We calculated the static deformation of the bottom using the elastic model of the earthquake source [11] with source parameters ten times larger moment than estimated from the seismic data [3]. These parameters were 302°, the dip angle of 16°, the slip angle of 87° and the seismic moment of 3.0×10^{27} dyne-cm. The fault plane was estimated from the aftershocks-distribution to be about 200x100 km, and the average dislocation was estimated about 3.75m. Figure 3a,b shows the three-dimensional wave profiles at the initial instant of the earthquake and at 4 min 20 sec after generation.

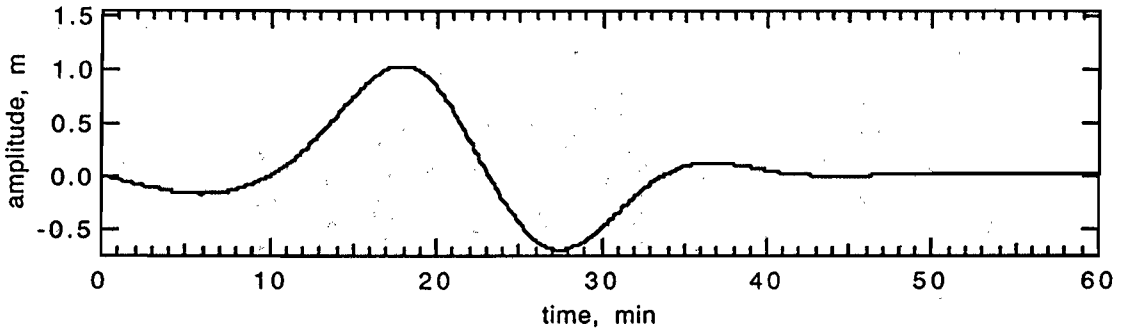

Figure 4a. The waveform computed by two-dimensional model at 200 m depth contour. This profile was used as an input for the runup computation at El Transito.

Figure 3b, shows that after 4 minutes of propagation -when the tsunami reaches the shelf area- the wave front becomes almost parallel to the shoreline and it is fairly straight-crested, suggesting that down to the resolution of this model, the wave reaches the coastline of Nicaragua as a plane wave on a plane beach. (See Figure 2). Assuming that there is little wave dispersion and diffraction at the north and south boundaries of the calculation, it is reasonable to treat the shoreline evolution as a one-dimensional problem, with initial data provided by the two dimensional model.

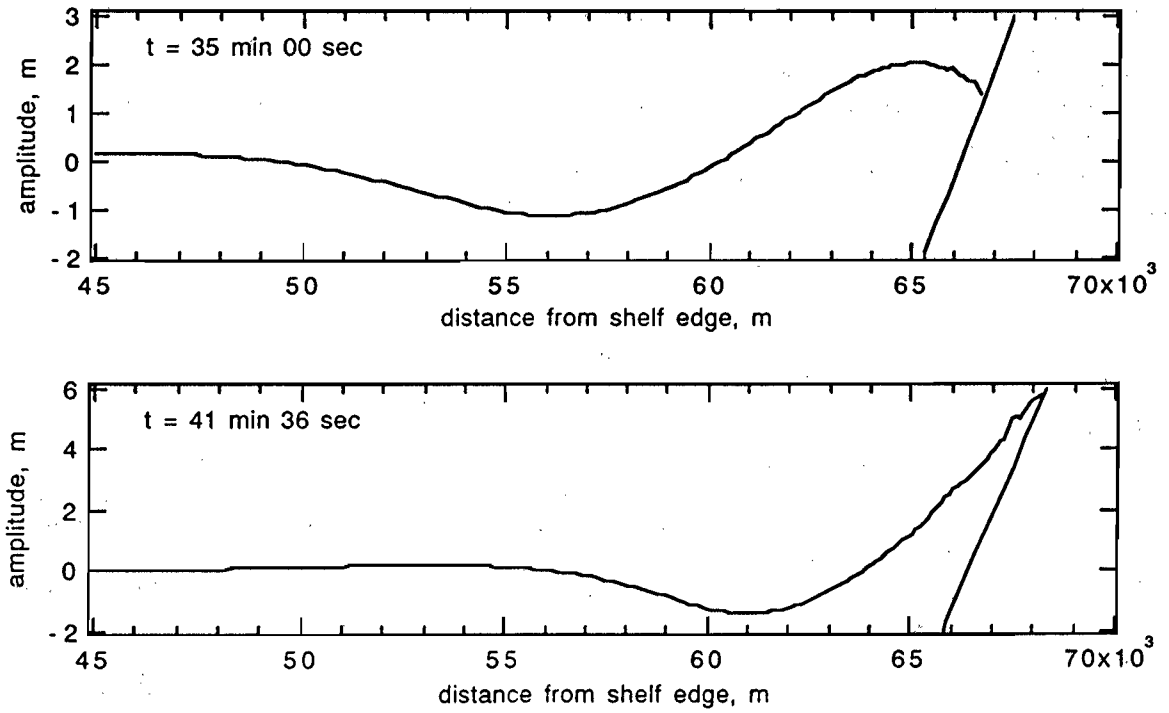

Figure 4b,c. The wave profiles for two different times computed by the one-dimensional model using waveform shown on figure 4a as an input.

As an example, Figure 4a shows the wave profile used as input for the one-dimensional model calculations for El Transito. This is the profile resulting from the two dimensional calculations from the 200m contour. Figure 4b shows the same wave 35min later, after breaking and figure 4c shows the wave profile near maximum runup. The comparison among computed and measured runup heights along the Nicaraguan shore using this procedure is shown in figure 5.

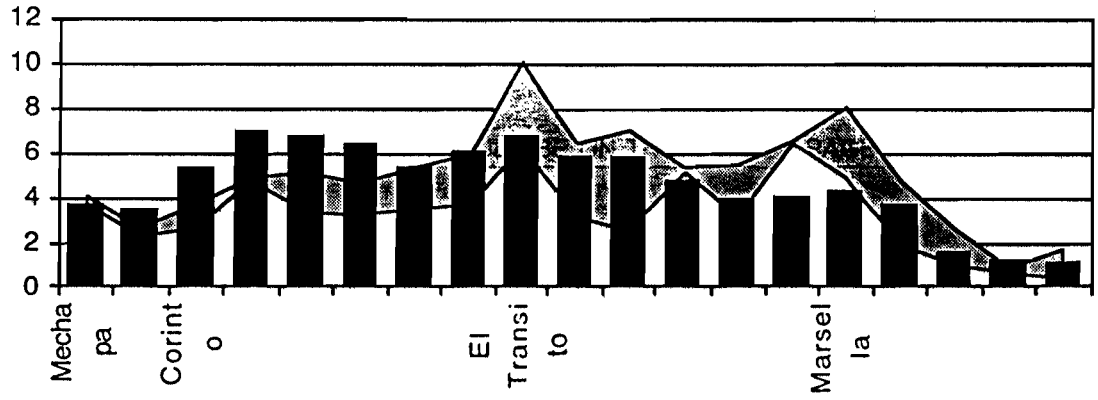

Figure 5. The comparison among the computed and measured runup heights along the Nicaragua coast. Black bars are computed results; two lines with a shadow area between them are maximum and minimum measurements at the site.

5. CONCLUSIONS

In this paper we calculated the generation, propagation and runup of the tsunami waves generated in the September 1, 1992 Nicaraguan tsunami. We used a combination of a two-dimensional nonlinear finite difference model for the wave generation and propagation calculations offshore and then a one-dimensional nonlinear model for calculating the wave runup. For the generation, we used the revised source parameters as estimated by Imamura et al (1992).

Our model results are in good agreement with the field observations, suggesting that for simple topographies like in the Pacific Coast of Nicaragua, a combination of two-dimensional and one-dimensional nonlinear models may be more effective method for estimating wave runup than simpler linear models which predict wave runup based on the wave height at the 10m contour.

REFERENCES

[1] Imamura, F., Ide, S., Yoshida, Y., Abe. K. and Shuto, N., Estimate of the tsunami source of the 1992 Nicaragua earthquake from tsunami data, Geoph. Res. Let., (submitted).

[2] Abe, K., Abe, K., Tsuji, Y., Imamura. F., Katao, H., Iio., Y., Satake, K., Bourgeois, J., Noguera, E. and Estrada, F., Survey of the Nicaraguan earthquake and tsunami of September 2, 1992, (in press).

[3] Ide, S., Imamura, F., Yoshida, Y. and Abe, K., Source characteristics of the Nicaraguan tsunami earthquake of September 2, 1992, Geoph. Res. Let., (submitted).

[4] Satake, K., Bourgeois, J., Abe, K., Abe, K., Tsuji, Y., Imamura, F., Iio., Y., Katao, H., Noguera, E. and Estrada, F., Tsunami field survey of the 1992 Nicaragua earthquake, EOS, Transactions, American Geophysical Union, Vol. 74, No. 13, (1993).

[5] Kanamori, H., Mechanism of tsunami earthquakes, Phys. Earth Planet. Inter., No 6, pp. 346-359, (1972)

[6] Titov, V. V., Numerical modeling of tsunami propagation by using variable grid, Tsunamis: their science and hazard mitigation, Proc. Intern. Tsunami Symposium, IUGG, Novosibirsk, USSR, pp. 46-51., (1989).
[7] Liu, P. L.-F., Synolakis C. E., Yeh, H. H., Report on International Workshop on Long-Wave Run-Up, J. Fluid Mech., No. 229, pp. 675-688., (1991)
[8] Gustafsson, B. and Kreiss, H.-O., Boundary conditions for time dependent problems with an artificial boundary, J. Comp. Phys., No. 30, pp. 333-351., (1979)
[9] Shuto, N., Suzuki, T., Hasegawa, K., Inagaki, K., A study of numerical technique on the tsunami propagation and runup, Proc. Intern. Tsunami Symposium, IUGG, Sydney, British Columbia, pp. 88-93, (1985).
[10] Titov, V. V. and Synolakis C. E., 1993, Numerical Modeling of Breaking and Nonbreaking Long Wave Propagation and Runup, ASCE, J. Waterways, Port, Coastal and Ocean Eng., (in review).
[11] Gusiakov, V.,K., Static displacement on the surface of an elastic space. Uslovno korrektnye zadachi matematicheskoi fisiki v interpretacii geofisicheskikh nabludenii, Novosibirsk, VC SOAN SSSR, pp. 23-51, (1978) (in Russian).

*U.S. GOVERNMENT PRINTING OFFICE:1995-673-018/00134